

**Combination Radiation Therapy and Oncolytic Vaccinia Virus
Therapy in Preclinical Models of Glioma**

by

Rachel Fung

A thesis submitted to the Faculty of Graduate Studies and Research in partial fulfillment of the
requirements for the degree of

Master of Science

in

Cancer Sciences

Department of Oncology

University of Alberta

© Rachel Fung, 2016

Abstract

Gliomas are the most common primary malignant brain tumour in adults, with glioblastoma multiforme (GBM), the most common and most deadly form of glioma, making up over half of all diagnosed cancers in the brain/central nervous system. The standard of care for gliomas has remained unchanged for the past decade: maximal surgical excision is the primary means of therapy, followed by post-operative radiotherapy and concurrent chemotherapy with the alkylating agent temozolomide (TMZ). Despite this, however, the prognosis for malignant gliomas, and in particular GBMs, is incredibly poor. As such, improved therapeutic options are sorely needed, especially those with a high safety profile and an ability to target tumour microextensions missed by surgery and radiotherapy.

Oncolytic virotherapy is an exciting new field in cancer therapeutics, with the first oncolytic virus approved by the Food and Drug Administration in 2015 and many more undergoing clinical trials currently. In our lab, a genetically engineered vaccinia virus (VACV) has been proposed as an addition to this expanding field of oncolytic virotherapy. A study performed by a group led by David Evans at the University of Alberta (PLoS Path., 2010) found that deletion of the vaccinia gene encoding the small subunit (R2, encoded by F4L) of the ribonucleotide reductase enzyme (a ubiquitous enzyme necessary for the generation of nucleotides to facilitate DNA synthesis) attenuated virus growth ~15-50 fold in HeLa cells. However, pancreatic cancer cells, naturally expressing high levels of cellular R2, could support F4L-deleted vaccinia virus growth at levels comparable to that of wild-type vaccinia virus. Further studies from our lab have demonstrated that this efficacy of F4L-deleted vaccinia virus growth, as well as cytotoxicity, extends to both bladder cancer and breast cancer. Here, we look to assess the efficacy of F4L-deleted vaccinia viruses in glioma.

With the many clinical trials currently underway for the use of oncolytic viruses, it is becoming increasingly apparent that oncolytic virotherapy will be most effective in combination with other therapeutic modalities. This holds especially true to gliomas, which are notoriously

heterogeneous and difficult to treat. As such, we propose that combining our F4L-deleted vaccinia virus mutants with radiotherapy, which is a standard of care in nearly all cases of glioma, may provide improved therapeutic benefit. Our results showed that human GBM cell lines that had been exposed to ionizing radiation (IR) remained supportive of infection with our mutant vaccinia virus deleted in both F4L and the thymidine kinase gene J2R ($\Delta F4L\Delta J2R$ VACV). We also saw upregulation of R2 and its p53-inducible form, p53R2, in irradiated U-87 MG xenografts. As our $\Delta F4L\Delta J2R$ VACV is dependent on cellular R2 for dNTP synthesis, this suggests that cells exposed to IR may become more susceptible to mutant VACV infection. Furthermore, early animal studies combining image-guided radiation therapy (IGRT) with $\Delta F4L\Delta J2R$ VACV treatment of U87 MG xenografts have suggested that there may be a survival benefit to treating gliomas with either $\Delta F4L\Delta J2R$ VACV alone or with the combination of $\Delta F4L\Delta J2R/IR$, when compared to IR alone or to no treatment. Though still in early stages, these results indicate that $\Delta F4L\Delta J2R$ VACV may be a promising alternative to TMZ in the treatment of gliomas, especially if used as an adjuvant to radiotherapy.

Dedication

I would like to dedicate this thesis to my father, Dr. Donald Fung; forever my role model and superhero; and to my mother, Sharon Fung; kindest and most loving person I know.

Acknowledgments

I would first like to thank my supervisor, Dr. Mary Hitt, for everything she has done for me over the past few years. She provided me the opportunity to complete my Masters degree under her supervision, and it is an experience that has proven both rewarding and invaluable to my personal and academic growth. I am forever grateful to Mary for her help, her kindness, her patience and understanding, and most importantly the constructive and welcoming environment she has created within her lab. I would like to extend my thanks to all the members of the Hitt laboratory; to Kate Agopsowicz, for training me in all the lab basics and for her help with animal work; to Kyle Potts, for all his mentorship, his help with procedures and trouble-shooting, and for always being available for discussion of relevant topics; to Shyam Chaurasiya, for his guidance and aid with various experiments; and to Powel Crosley for his friendship, his understanding, and his help within the lab; and to all past members of the lab for laying the foundations for this work. I would also like to thank our frequent collaborator Dr. David Evans, and the members of his lab, for all their contributions towards the completion of this thesis. I also wish to acknowledge the members of my supervisory committee, Dr. Armin Gamper and Dr. David Murray, for their guidance throughout the completion of this thesis. Finally, I would like to give thanks to all the members of the Department of Oncology for their help with various aspects of this thesis.

I would finally like to recognize my friends and family, without whom I could not have considered Edmonton my home for the last several years. I would especially like to recognize Michaela Eifler, for the endless support, motivation, commiseration, and, when all that failed, cheese. And of course, I would not be where I am today without the incredible support and love from my parents, Dr. Donald and Sharon Fung, my siblings, Alison and Nicholas, and my grandparents, Valerie Carbell and Ruby Fung.

TABLE OF CONTENTS

Abstract.....	ii
Dedication.....	iv
Acknowledgments.....	v
TABLE OF FIGURES.....	ix
LIST OF ABBREVIATIONS.....	xi
CHAPTER 1. <u>INTRODUCTION</u>	1
1.1. GLIOMA	2
1.1.1. Introduction to glioma.....	2
1.1.2. Standard of care and limitations.....	3
1.1.3. Experimental therapeutics.....	4
1.2. ONCOLYTIC VIROTHERAPY	5
1.2.1. Introduction to oncolytic virotherapy.....	5
1.2.2. Oncolytic vaccinia virus.....	7
1.3. RADIATION THERAPY	14
1.3.1. Biology of radiation therapy.....	14
1.3.2. Cellular response to radiation.....	17
1.3.3. Clinical radiation therapy in glioma.....	18
1.3.4. Mouse models of radiation therapy.....	18
1.4. ONCOLYTIC VIROTHERAPY AND RADIATION IN GLIOMAS	24
1.4.1. Oncolytic virotherapy and radiation.....	24
1.4.2. Glioma recurrence and resistance to standard therapies.....	25
1.4.3. Potential advantages of a combinatorial approach.....	26
1.4.4. Thesis objectives.....	27
CHAPTER 2. <u>IN VITRO VACCINIA GROWTH KINETICS AND CYTOTOXICITY IN COMBINATION WITH IONIZING RADIATION IN HUMAN GLIOMA CELLS</u>	31
2.1. MATERIALS/METHODS	32
2.1.1. Cell culture.....	32
2.1.2. Recombinant viruses.....	32

2.1.3. Virus titration	33
2.1.4. Virus infection and growth curves	34
2.1.5. Cell irradiation	35
2.1.6. Cell survival assays	35
2.1.7. Lysate collection and western blots	36
2.2. RESULTS	37
2.2.1. Yield of vaccinia virus (VACV) mutants is comparable to that of wild-type VACV in human GBM cells	37
2.2.2. Cell killing of human GBM cells by $\Delta F4L\Delta J2R$ VACV is comparable to that of wild-type VACV	38
2.2.3. U-87 MG and U-118 MG cells resistance to 8 Gy IR	43
2.2.4. Radiation increases ribonucleotide reductase small subunit expression in U87 MG (p53-wild-type) and U118 MG (p53-mutant) cell lines	43
2.2.5. Exposure to IR did not reduce $\Delta F4L\Delta J2R$ or wild-type VACV growth in human GBM cells.	44
2.2.6. Combining IR with $\Delta F4L\Delta J2R$ VACV infection increased cell killing in human GBM cells.	52
2.2.7. Single-replication round yield of $\Delta F4L\Delta J2R$ and wild-type VACV is not reduced by increasing time to infection post-irradiation in U-87 MG cells	53
CHAPTER 3. <u>ESTABLISHING PLATFORM FOR COMBINATION THERAPY USING VACV AND EXTERNAL BEAM RADIATION</u>	60
3.1. MATERIALS/METHODS	61
3.1.1. Cell preparation for <i>in vivo</i> injection	61
3.1.2. <i>In vivo</i> U-87 MG subcutaneous radiation marker study	61
3.1.3. Immunohistochemical staining of U-87 MG radiation markers	62
3.1.4. <i>In vivo</i> subcutaneous radiation and $\Delta F4L\Delta J2R$ VACV survival	62
3.2. RESULTS	64
3.2.1. Bilateral subcutaneous U-87 MG glioma flank model in immunocompromised NIH III mice	64
3.2.2. SARRP-mediated image-guided radiation therapy (IGRT) of bilateral subcutaneous U-87 MG tumours in immunocompromised NIH III mice	65

Table 3.1. Small Animal Radiation Research Platform (SARRP) treatment plans of U-87 MG bilateral flank tumours.....	67
3.2.3. DNA damage and radiation response in subcutaneous U-87 MG tumours treated with SARRP image-guided radiation therapy (IGRT).....	69
3.2.4. Combination 10 Gy IGRT and $\Delta F4L\Delta J2R$ VACV increased survival and time to tumour progression in pilot study of U-87 MG subcutaneous mouse model.....	79
3.2.5. $\Delta F4L\Delta J2R$ VACV replication in tumours is maintained up to 150 days post-injection.....	80
CHAPTER 4. . DISCUSSION	91
4.1. DISCUSSION	92
4.1.1 Oncolytic activity of F4L-deleted VACV in human GBM cells.....	93
4.1.2 R2/p53R2 upregulation in irradiated glioma cells: implication for $\Delta F4L\Delta J2R$ VACV infection.....	97
4.1.3 Combination radiotherapy and oncolytic VACV in <i>in vitro</i> and <i>in vivo</i> glioma models.....	99
4.2. FUTURE DIRECTIONS	104
4.2.1 $\Delta F4L\Delta J2R$ VACV kinetics in the brain.....	104
4.2.2 Radiation-mediated induction of senescence and susceptibility to vaccinia infection.....	105
4.2.3 Vaccinia virus and combination therapy kinetics in glioma stem cell populations.....	106
4.2.4 Furthering animal studies: xenograft and orthotopic models of combination therapy.....	108
4.3. CONCLUSIONS	110
REFERENCES	111

TABLE OF FIGURES

Figure 1.1. Nucleotide biogenesis pathway.....	10
Figure 1.2. Ribonucleotide reductase structure.....	11
Figure 1.3. F4L (R2) deletion attenuates vaccinia virus in Balb/C mice.....	13
Figure 1.5. Early model of X-Strahl Small Animal Radiation Research Platform (SARRP).	21
Figure 1.6. Interchangeable tertiary collimators for focal radiation beam delivery.	22
Figure 1.7. MuriPlan treatment planning for precise radiation delivery.	23
Table 1.1. Oncolytic viruses discussed in thesis.....	29
Figure 2.2. Yield of vaccinia virus (VACV) mutants comparable to that of wild-type VACV in human U-87 glioma cells.....	39
Figure 2.3. Yield of F4L-deleted vaccinia virus (VACV) mutants slightly reduced compared to wild-type and Δ J2R VACV in U-118 glioma cells.....	40
Figure 2.4. Δ F4L Δ J2R VACV induces comparable cytotoxicity to wild-type VACV in U-87 glioma cells.	41
Figure 2.5. Δ F4L Δ J2R VACV induces comparable cytotoxicity to wild-type VACV in U-118 glioma cells.	42
Figure 2.6. Resistance of U-87 and U-118 MG to treatment with 8 Gy IR.	46
Figure 2.7. Radiation effects on R2/p53-R2 levels in U-87 MG and U-118 MG glioma cells.	47
Figure 2.8. Exposure to IR does not reduce Δ F4L Δ J2R VACV yield in U-87 MG cells.....	48
Figure 2.9. Exposure to IR does not reduce wild-type VACV yield in U-87 MG cells.....	49
Figure 2.10. Exposure to IR does not reduce Δ F4L Δ J2R VACV yield in U-118 MG cells. .	50
Figure 2.11. Exposure to IR does not reduce wild-type VACV yield in U-118 MG cells.....	51
Figure 2.12. Combination IR with Δ F4L Δ J2R VACV infection increased cell killing of U87 cells.	54
Figure 2.13. Combination IR with Δ F4L Δ J2R VACV infection increased cell killing of U-118 MG cells.	55
Figure 2.14. Combining IR with wild-type VACV infection did not significantly increase cell killing in U-87 MG cells.....	56

Figure 2.15. Combination IR with $\Delta F4L\Delta J2R$ VACV infection did not significantly increase cell killing of U-118 MG cells, except at the lowest MOI.....	57
Figure 2.2. Increasing time to infection post-irradiation does not reduce $\Delta F4L\Delta J2R$ or wild-type virus yield in U-87 MG cells.....	59
Figure 3.1. Growth kinetics of untreated subcutaneous bilateral U87 xenograft tumours in NIH III mice.	66
Figure 3.2. SARRP treatment planning in subcutaneous bilateral flank model of human GBM.	68
Figure 3.3. γ -H2AX expression <i>in vivo</i> increased at 1 hour post-irradiation following treatment with 2 Gy or 10 Gy targeted IR.....	72
Figure 3.4. p21 expression <i>in vivo</i> increased relative to non-irradiated tumour at 6 to 48 hours following treatment with 10 Gy radiation.....	74
Figure 3.5. p53-R2 expression <i>in vivo</i> increased relative to non-irradiated tumour up to 48 hours following treatment with 10 Gy radiation.....	76
Figure 3.6. R2 expression <i>in vivo</i> following 10 Gy radiation compared to non-irradiated control.	78
Figure 3.7. Flow chart for combination image-guided radiation therapy (IGRT) and $\Delta F4L\Delta J2R$ VACV therapy of U-87 subcutaneous flank model.	83
Figure 3.8. Combination 10 Gy IGRT and $\Delta F4L\Delta J2R$ VACV increased time to tumour progression <i>in vivo</i> in pilot study.....	86
Figure 3.9. Combination treatment with 10 Gy IGRT and $\Delta F4L\Delta J2R$ VACV increased overall survival <i>in vivo</i> in pilot study of immunocompromised subcutaneous human GBM model.	88
Figure 3.10. mCherry-fluorescence in mCh- $\Delta F4L\Delta J2R$ VACV-treated animals was visible in tumours up to 150 days post-infection.....	90

LIST OF ABBREVIATIONS

ATM	Ataxia telangiectasia-mutated protein
C₁₂FDG	5-Dodecanoylamino fluorescein Di-β-D-Galactopyranoside
CBCT	Conebeam computed tomography
CCI	Cross Cancer Institute
CDK	Cyclin-dependent kinase
CNS	Central nervous system
CSC	Cancer stem cell
CT	Computed tomography
DAB	3'3'-Diaminobenzadine tetrahydrochloride
ddH₂O	Double-distilled water
ΔF4L	F4L-deleted VACV
ΔF4LΔJ2R	F4L-deleted J2R-deleted VACV
ΔJ2R	J2R-deleted VACV
DMEM	Dulbecco's Modified Eagle Medium
DSB	Double-strand DNA break
EDTA	Ethylenediaminetetraacetic acid
EEV	Extracellular enveloped virus
FACS	Fluorescence-activated cell sorting
FBS	Fetal bovine serum
FDA	Food and Drug Administration
FFPE	Formalin-fixed paraffin-embedded
GBM	Glioblastoma multiforme
GCV	Ganciclovir
γH2AX	Histone-variant 2AX phosphorylated at ser139
GM-CSF	Granulocyte colony macrophage stimulating factor
GTR	Gross total resection
h.p.i.	Hours post-infection
h.p.ir.	Hours post-irradiation
HRP	Horseradish peroxidase
HSLAS	Health Sciences Laboratory Animal Services
HSV-1	Herpes simplex virus -1
HSV-tk	Herpes simplex virus thymidine kinase
IGRT	Image-guided radiation therapy
IMV	Intracellular mature virion
IR	Ionizing radiation
IRES	Internal ribosomal entry site
IVIS	In Vivo Imaging System
MDM2	Mouse double minute 2 homolog (E3 ubiquitin-protein ligase)
MEM	Minimum Essential Medium
MOI	Multiplicity of infection
MRI	Magnetic resonance imaging

MRN	Mre11-Rad50-Nbs1 complex
NHEJ	Non-homologous end-joining pathway
ns	Not significant
NSG	NOD.Cg-Prkdc ^{scid} Il2rg ^{tm1Wjl} /SzJ
PBS	Phosphate-buffered saline
PBST	PBS with 0.1% Tween-20
pfu	Plaque-forming units
PMSF	Phenylmethanesulfanyl fluoride
Rb	Retinoblastoma
RIPA	Radioimmunoprecipitation buffer
RTK	Receptor tyrosine kinase
S.E.M.	Standard error of the mean
SA-β-gal	Senescence-associated β-galactosidase
SARRP	Small Animal Radiation Research Platform
SDS	Sodium dodecyl sulfate
SIPS	Stress-induced premature senescence
SSB	Single-strand DNA break
STR	Subtotal resection
T-vec	Talimogene laherparapvec
TBS	Tris-buffered saline
TIL	Tumour-infiltrating lymphocyte
TK	Thymidine kinase
TMZ	TMZ
VACV	Vaccinia virus
VGf	Vaccinia growth factor
vvDD	Double-deleted vaccinia virus
WR	Western Reserve

CHAPTER 1. INTRODUCTION

1.1. GLIOMA

1.1.1. Introduction to glioma

Gliomas, which arise from the supportive cells of the central nervous system (CNS), are the most common primary brain tumour diagnosed in adults [1, 2]. The cells from which gliomas arise can be of oligodendroglial, astrocytic, or mixed origin. Severity of the disease varies based on the originating cells, with gliomas containing an oligodendroglial component generally showing improved survival [3]. The World Health Organization has assigned a classification to the subtypes of astrocytomas, ranging from grade 2 astrocytomas through the more aggressive grade 3 anaplastic astrocytomas, and finally to the most aggressive grade 4 glioblastoma (also called glioblastoma multiforme, GBM), which is known to cause 3-4% of all cancer-related deaths in the United States each year [1, 4, 5]. Together GBMs and anaplastic astrocytomas comprise ~76% of all malignant gliomas [6] and both have incredibly poor prognoses. Anaplastic astrocytoma patients have a median survival of 3-5 years, while GBM patients have a median survival of only 15 months, with 5-year survival rates at under 5% [1, 3, 6].

GBMs have several defining molecular characteristics. One of the driver mutations of GBM is a mutated form of EGFR containing the variant III deletion of the extracellular domain, and is known as EGFRvIII [5, 7]. This mutation can be found in ~40% of GBM cases and can exert a transformative effect on neighbouring cells. GBMs, like many other cancers, also show high rates of alterations in the retinoblastoma (Rb) pathway, the p53 pathway, and receptor tyrosine kinase (RTK) signaling pathways [3, 7]. In a study of 91 GBM cases, mutations in the Rb, p53, and RTK pathways were found in 87%, 78%, and 88% of cases, respectively [7]. Interestingly, *de novo* versus secondary GBMs show different molecular signatures within the framework of these pathways. GBM arising *de*

novo, with no prior evidence of pathology, generally has alterations in p16, p19/p14, and EGFR, while secondary GBM arising from a lower grade glioma is typically mutated in p53 and CDK4 or PDGF [4, 8].

1.1.2. Standard of care and limitations

The current standard of care for malignant gliomas is based on several landmark studies evaluating the effects of radiation and temozolomide (TMZ), an alkylating chemotherapeutic agent, as additions to surgical resection [9-11]. In the majority of cases, surgical resection is the primary curative therapy, whether it be gross total resection (GTR) or subtotal resection (STR) [5]. A clinical trial study of 303 patients in 1978/1980 additionally established post-operative radiation therapy as a means to nearly double the median survival time, from 18.5 weeks with surgical resection alone to 34.5 weeks with the addition of radiation therapy [6, 11]. This study also established the ideal dosing schedule of fractionated doses of 1.8-2.0 Gy delivered 5 days a week for a total dose of 50-60 Gy [6]. Finally, a landmark study by Stupp *et al.* published in 2005 established TMZ as an adjuvant to post-operative radiation [5, 9]. TMZ works by crossing the blood-brain barrier and causing methylation of purines, which results in DNA damage and activation of apoptosis [5, 11]. A subsequent study by the same group found that TMZ given in addition to radiation therapy increase both median survival and long-term survival at 5 years [12].

Despite the advances in glioma therapy made with the final addition of adjuvant TMZ, the prognosis remains incredibly poor, with 18,000 deaths per year attributed to malignant gliomas in the United States [6]. In Canada, it was estimated that there would be 3000 newly diagnosed cases and 2100 deaths attributed to brain and spinal cord cancer; in 2015 of these, ~70% will be due to malignant gliomas [13]. There are several major barriers to

curative therapy, not least of which are characteristics of malignant glioma itself. Malignant gliomas by nature are highly invasive tumours, infiltrating the surrounding tissue and extending well beyond the tumour borders visible by magnetic resonance imaging (MRI) [4]. This high level of invasion renders complete surgical resection impossible [6], and also extends beyond the volume reached by radiation. Recurrence, therefore, invariably occurs, generally within one year of surgical resection of the primary tumour [2], and there is no current standard of care for recurrent malignant gliomas [6]. Additionally, resistance to TMZ can arise through overexpression of O⁶-methylguanine-methyltransferase, an enzyme that is able to repair the damage caused by TMZ, and there are few other chemotherapeutic agents that are able to pass the blood-brain barrier for systemic treatment of malignant glioma [6]. It has also been shown that TMZ is not well tolerated in some patients, with severe toxicities in the bone marrow and gastrointestinal tract, which limits its use in some patients [3, 14].

1.1.3. Experimental therapeutics

As the prognosis for malignant gliomas remains so poor, there are several options that are being studied as alternatives to the current standard of care. Delivering chemotherapeutic agents directly to the surgical site is one such option, as local delivery can limit the systemic toxicity of the drug [6]. Carmustine, a nitrosourea alkylating agent, is one such drug being studied for local delivery. Biodegradable wafers impregnated with the drug can be implanted at the surgical site, and the controlled release of carmustine by the wafer has been shown to increase survival by several months without demonstrating any adverse effects when compared to a placebo group [6, 15]. Other options include local gene therapy, an example of which is implantation of neural stem cells transduced with herpes

simplex virus thymidine kinase (HSV-tk) gene; given with a prodrug form of ganciclovir (GCV). HSV-tk can convert the nontoxic GCV to its active form killing the adjacent tumour via a bystander effect. This strategy has demonstrated safety in early clinical trials, albeit with limited therapeutic benefit [16].

In addition to therapies directly targeting cancer cells, studies are being undertaken to assess therapies that improve immune responses to gliomas. While the blood-brain barrier, which limits transport through intracerebral capillaries, was long thought to also prevent immune infiltration, increasing evidence has demonstrated that the brain is an immune-distinct but not immune-inaccessible location [4, 17]. Malignant gliomas, additionally, are typically characterized by highly disrupted vasculature and deterioration of the blood-brain barrier. In fact, serum antibodies to distinct glioma antigens are detectable in glioma patients, while activated tumour-infiltrating lymphocytes (TILs) and macrophages have also been detected in glioma tissues [18, 19]. Immunotherapies such as dendritic cells, which are activated *ex vivo* using patient biopsy material and then re-introduced into tumour for patient tumour specificity, have been shown to induce anti-tumour immune responses and prolong survival [5, 20]. Perhaps a more effective way of stimulating an anti-tumour immune response, however, is through use of replicative oncolytic viruses, which in addition to direct cell lysis can provide an immunogenic benefit.

1.2. ONCOLYTIC VIROTHERAPY

1.2.1. Introduction to oncolytic virotherapy

Oncolytic viruses are a promising new field of experimental cancer therapeutics, with over 30 oncolytic viruses currently in clinical trials [21]. There are several inherent or genetically engineered traits of oncolytic viruses that provide several benefits to traditional

therapies: oncolytic viruses have demonstrated selective killing of tumour cells due to either a natural or genetically-engineered tropism for tumour sites, as well as through restriction of replication to specific molecular alterations present in tumour cells [21]. Oncolytic viruses are also of particular interest in the growing field of cancer immunotherapy, as they have the potential to be highly immunogenic and to increase anti-tumour immune responses [21]. Talimogene laherparapvec (T-vec), a herpes simplex virus -1 (HSV-1) expressing granulocyte macrophage colony stimulating factor (GM-CSF), was the first Food and Drug Administration (FDA)-approved oncolytic virus, and is currently used in the treatment of advanced melanoma [22, 23]. Several other oncolytic viruses, including but not limited to reovirus, coxsackievirus, adenovirus, and vaccinia virus (VACV), are currently undergoing clinical trials for a variety of different cancers, with those in early phases showing high tolerability and no adverse effects, often with no maximum tolerated dose reached [24-27].

Of the cancer types that could particularly benefit from the immune-stimulatory effects of oncolytic virotherapy, malignant gliomas in particular are an ideal target due to their highly immunosuppressive nature [14]. Virus-based therapies, which have demonstrated low toxicity and high immunogenicity, could therefore provide an exciting breakthrough as novel glioma therapeutics, and indeed patient benefit has already been seen in several early clinical trials. DNX-2401, a replication-competent, tumour-selective oncolytic adenovirus, has demonstrated induction of a specific anti-tumour immune response in preclinical studies, with a survival benefit seen in Phase I trials [28]. G207, a conditionally-replicative HSV-1, has also been shown in a Phase I trial to offer some prolonged survival and no serious adverse effects, in particular, showing no induction of intracerebral edema following intratumoural injection [29]. H-1PV, an oncolytic parvovirus, has been shown to be highly cytopathic to glioma cells, while also inducing tumour regression in orthotopic rat models following systemic delivery [30, 31]. In May 2016, the FDA granted breakthrough status to a conditionally replicating poliovirus type-1 containing an internal ribosomal entry site (IRES)

from human rhinovirus type 2 (PVS-RIPO), following evidence of increased survival benefit for patients with recurrent GBM in early clinical trials [32, 33].

1.2.2. Oncolytic vaccinia virus

1.2.2.1. *Vaccinia virus*

VACV is a large (~200 kilobase pair), double-stranded DNA virus belonging to the family *Orthopoxvirus*, which are distinguished from most other DNA viruses by their cytoplasmic replication [34, 35]. VACV, which is perhaps most famous as the virus used in smallpox vaccinations, is well characterized, with a genome encoding virulence genes targeting a variety of pathways in host cells, from cell cycle to apoptosis to immune responses [36]. Infection by VACV is characterized by rapid virus replication, with the generation of 100-200 plaque-forming units (pfu)/cell at 20-40 hours following infection, as well as by its dual means of cellular spread [37, 38]. The primary method of VACV spread is through a double-enveloped form known as the extracellular enveloped virus (EEV), which allows release from the cell without immune-detection, thus enabling long-range spread of the virus [39, 40]. Interestingly, the virus is also able to utilize the cellular actin cytoskeleton to enable direct cell-cell spread through propulsion of a second form of the virus, the intracellular mature virion (IMV), from the cytoplasm directly into the neighbouring cell, which again provides a mechanism of evading exposure to the host immune system [41]. Virus spread is further enhanced by virus-induced formation of actin tails that not only prevent superinfection, but also propel extracellular virus particles from cell to cell until they reach an uninfected cell [42].

1.2.2.2. *Oncolytic vaccinia virus*

VACV exhibits several traits that make it an ideal candidate for oncolytic virotherapy. The large genome enables genome manipulation and transgene insertion for increasing tumour selectivity [34, 35], while its rapid and efficient replication and spread enables high levels of oncolysis. Its capacity as an immunogenic potentiator aligns with the increasing focus on immunotherapy in cancer therapeutics [36]. The first oncolytic VACV agents emerged several years ago, having in common a deletion of the J2R gene encoding thymidine kinase (TK) (Figure 1.1). This deletion renders the virus reliant on cellular dNTP pools for virus replication, limiting virus replication to actively dividing cells and sparing normal, non-dividing cells [43]. Additional anti-viral mechanisms further protect normal tissues from damage by J2R-deleted viruses. Currently, TK-inactivated VACV is in clinical trials as JX-594, additionally expressing GM-CSF, and as GL-ONC1, with inactivation of J2R and A56R (encoding hemagglutinin) genes (Table 1.1) [26, 27]. Preclinical studies with these viruses have demonstrated induction of anti-tumour immunity in animal models and the subsequent resistance to tumour re-challenge [38, 43]. Early clinical trials of another TK-deleted VACV, vvDD, expressing vaccinia growth factor (VGF) have demonstrated high tolerability and safety without evidence of dose-limiting toxicities, even with systemic delivery (Table 1.1) [37, 44]. In clinical trials JX-594 did, however, result in some development of lesions that tested positive for the virus [45, 46], suggesting that increased safety and tumour selectivity of the oncolytic VACV could be beneficial.

1.2.2.3. *Ribonucleotide reductase*

Ribonucleoside diphosphate reductase (also called ribonucleotide reductase) is an enzyme that catalyzes the reduction of ribonucleoside diphosphates (rNDPs) to deoxyribonucleoside diphosphates (dNDPs) for the *de novo* synthesis of nucleotides, with both mammalian and viral homologs (Figure 1.1) [39]. It is a tetrameric protein composed of dimers of each of two subunits; the large R1 subunit and the small R2 subunit (Figure 1.2) [47]. R1, while only transcribed during S-phase, has a long half-life that renders its levels essentially constant throughout the cell cycle [48]. R2, however, is expressed only in S-phase and is rapidly degraded by the anaphase-promoting complex (APC). R2 transcription in S-phase is thus the rate-limiting step for nucleotide biogenesis and subsequent cellular proliferation [47, 48]. Cells additionally encode a p53-dependent form of R2, p53-R2, which can form active tetramers with R1 [49]. P53-R2 is elevated in response to DNA damage and otherwise retains a relatively constant low-level expression because it lacks the KEN-box recognized by the APC-ubiquitin ligase complex which would otherwise target p53-R2 for degradation [47, 49].

1.2.2.4. Ribonucleotide reductase and vaccinia tumour selectivity

Of the viruses in the *Chordopoxvirinae* subfamily, only two viruses (Suipox- and Orthopoxvirus) encode both large and small subunits of the ribonucleotide reductase enzyme, with all others showing conservation of only the small subunit R2 [47]. VACV, which is an Orthopoxvirus, encodes I4L (large subunit, 87 kDa) and F4L (small subunit, 37 kDa), both of which are able to combine with each other or with human subunits to form functional complexes [47]. While deletion of I4L only mildly attenuates VACV, inactivation of F4L was shown to greatly attenuate the virus, reducing virus production

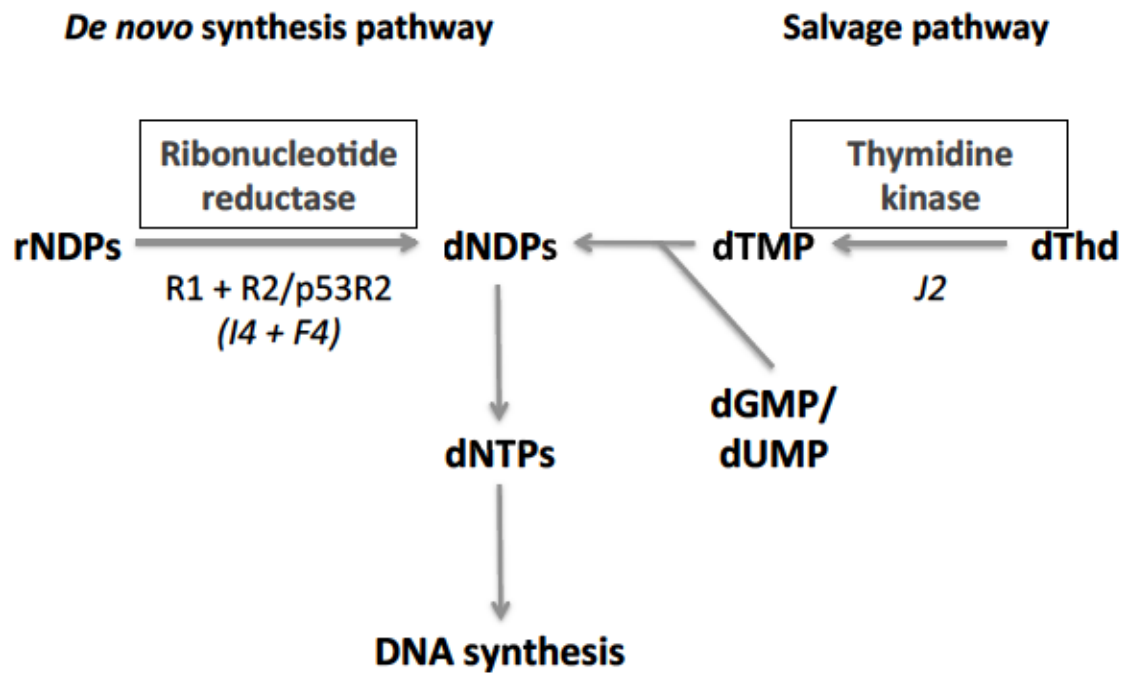


Figure 1.1. Nucleotide biogenesis pathway.

De novo synthesis of nucleotides relies on reduction of rNDPs to dNDPs; a reaction catalyzed by the ribonucleotide reductase enzyme. Ribonucleotide reductase consists of two subunits, a large (R1) subunit and small (R2) subunit. A separate salvage pathway is required for generation of thymidine, and relies on the enzyme thymidine kinase. VACV encodes homologs to both ribonucleotide reductase subunits as well as to thymidine kinase, which are denoted in italics. Figure adapted from Dr. David Evans, University of Alberta, Department of Medical Microbiology and Immunology.

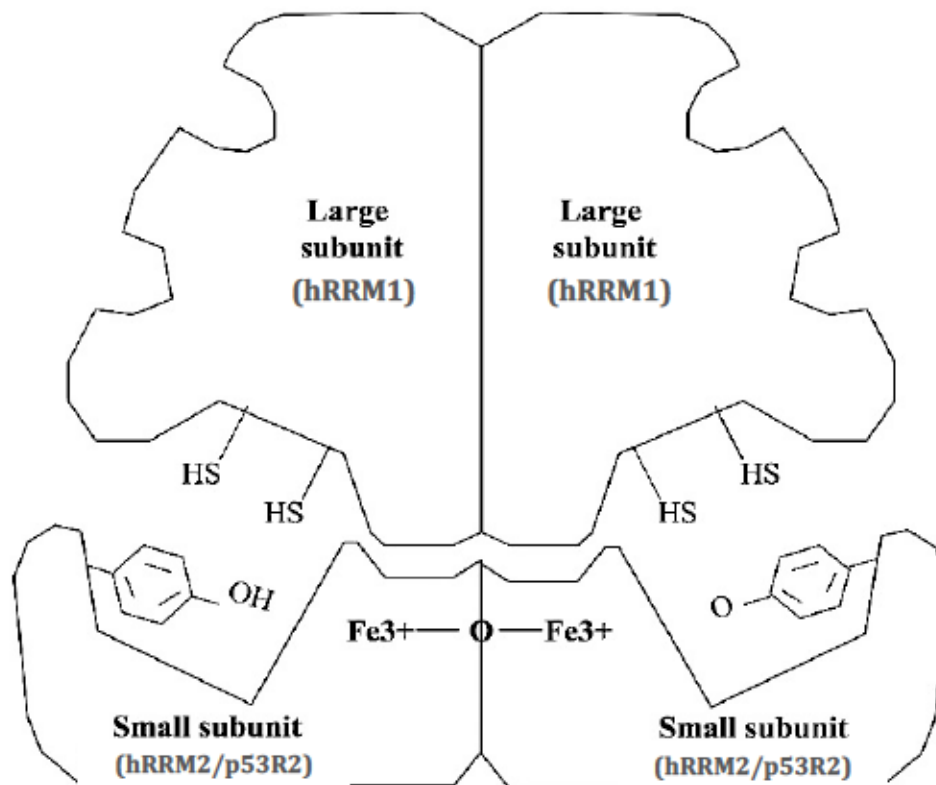


Figure 1.2. Ribonucleotide reductase structure.

Ribonucleotide reductase is a tetrameric holoenzyme composed of dimers of each of two subunits; a large (R1, or hRRM1 in humans) subunit of 80-100 kDa, and a small (R2, or hRRM2 in humans) subunit of 37-44 kDa. A p53-dependent form of R2, p53-R2, is constitutively present in very low levels and upregulated in a p53-dependent manner in response to genotoxic stress. The rNDP reduction is catalyzed in an oxygen-dependent manner. Figure from Yen, 2003 [50].

~1000 fold compared to wild-type [47]. When inoculated into mice, F4L-deleted virus showed virus infection indistinguishable from mock-infected mice, while I4L-deleted viruses caused a drop in weight and adverse effects comparable to a wild-type infection (Figure 1.3) [47]. Further studies demonstrated that VACV lacking F4L results in conditional replication, where virus replication is possible only in cycling host cells expressing high levels of R2 [47]. Importantly, this suggests that many tumour cell lines would be hosts for such mutant viruses due to the highly replicative nature of cancer cells, but not normal tissues which generally have low R2 expression [51]. VACV deleted in F4L, or possessing a double deletion in both F4L and J2R (encoding thymidine kinase), is therefore being tested in multiple models of cancer in the Evans and Hitt labs (Table 1.1) either as a standalone treatment or in combination therapies. In glioma models, however, it is likely that oncolytic VACV would have limited efficacy as a standalone treatment due to the highly heterogeneous nature of malignant gliomas, and would therefore benefit from a combination strategy approach [14] [52].

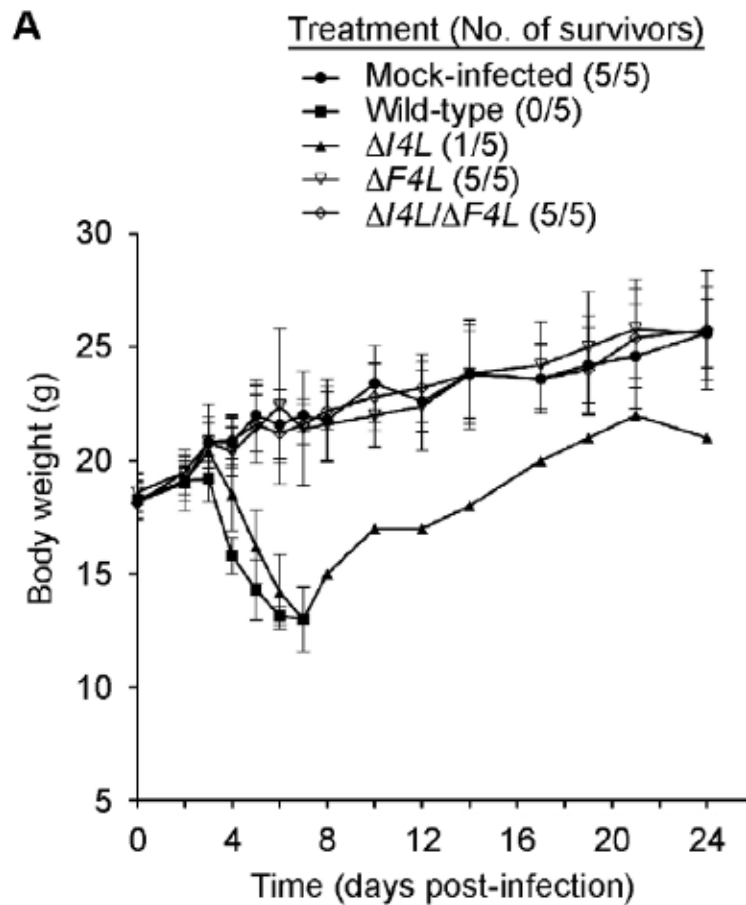


Figure 1.3. F4L (R2) deletion attenuates vaccinia virus in Balb/C mice.

Balb/C mice were intranasally inoculated with wild-type VACV as well as VACV mutants encoding deletions in F4L (R2), I4L (R1), or both genes. No difference was seen in mice infected with F4L-deleted VACV mutants when compared to mock-infected controls, while 5/5 mice infected with wild-type vaccinia and 4/5 mice infected with I4L-deleted vaccinia succumbed to disease and were euthanized. Figure from Gammon et al. 2010 [47].

1.3. RADIATION THERAPY

1.3.1. Biology of radiation therapy

Radiation therapy is one of the most common modalities of cancer treatment, used to treat over 50% of cancer patients as either a curative or adjuvant therapy [43]. While there are numerous different types of radiotherapy, gliomas are treated primarily by external beam radiotherapy, where ionizing radiation (IR) is delivered as γ -rays or X-rays [53, 54]. The IR can induce damage to cellular DNA in two ways: it can either directly disrupt the DNA, although this accounts for only ~30% of IR-induced DNA lesions; or more commonly the energy from the IR causes radiolysis of water molecules, forming the highly reactive oxygen species and nitrogen species that then induce DNA lesions through oxidative damage [53, 55-57]. The reactive oxygen species can induce a variety of DNA lesions [58, 59], however the most lethal and therefore most relevant to radiotherapy is the induction of double-strand DNA breaks (DSBs) [58, 60], minimally consisting of two single-strand breaks (SSBs) occurring within one helical turn on opposing DNA strands [58]. DSB formation is also influenced by the number of complex lesions, wherein multiple DNA lesions occur within 10 base pairs of each other and are improperly repaired [59]. The number of DSBs produced is cell-cycle-dependent, with the most DSBs generated in S-phase; however the number of unrepaired DSBs is more predictive of cellular lethality following radiation exposure [60, 61].

Following radiation, there are several possible cellular fates, the major three of which are mitotic catastrophe, apoptosis, and radiobiological cell death, or stress-induced premature senescence (SIPS) (Figure 1.4) [61, 62]. Apoptosis, or programmed cell death, is prevalent mode of cell death following IR-exposure, and is largely mediated by tumour suppressor proteins, the most well known of which is p53, although Rb has also been implicated [63]. P53-independent forms of apoptosis have also been identified, although p53-independent

apoptosis is generally delayed compared to p53-dependent apoptosis. Secondary to apoptosis, mitotic catastrophe accounts for a large proportion of IR-mediated cell death, and is thought to be responsible for late apoptosis following IR-induced damage. Mitotic catastrophe occurs when there is unregulated entry into the cell cycle, whether by p53-deficiency or loss of checkpoint control. Premature entry into mitosis and subsequent chromosome aberrations lead to cell death through apoptosis or necrosis (Figure 1.4) [63]. In some cases, however, and especially in cases with lower dose radiation that is not sufficient to induce direct cell death, cells will undergo irreversible growth arrest, or senescence; these cells may eventually undergo apoptotic death [63]. Response is also tissue-dependent: early responding tissues, which are typically highly proliferative tissues, are highly radiosensitive, whereas late-responding tissues are generally able to repair sublethal damage [55]. One major way through which clinical radiation delivery has taken advantage of these differential responses is through fractionated radiation therapy, whereby multiple fractions of radiation are given at a sublethal radiation dose at varying angles such that radiation beams converge on the tumour for a cumulative lethal dose to the more proliferative tumour, while surrounding normal tissue only receives a single fraction [55]. Additionally, by giving the fractions over a 6-week schedule to achieve the cumulative dose, the late-responding normal tissues are able to repair the sublethal damage largely minimizing radiation side effects [55].

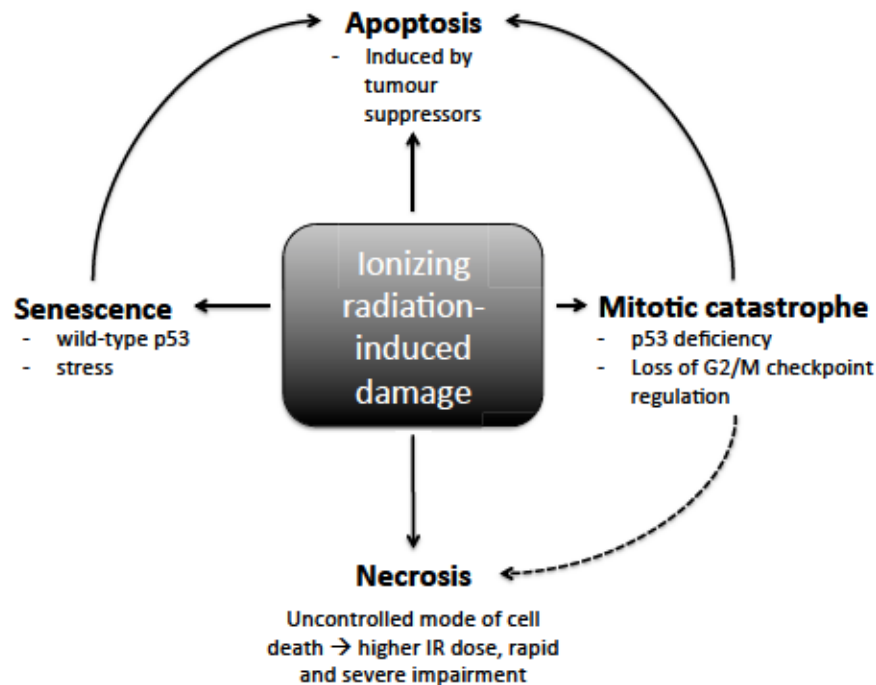


Figure 1.4. Cellular fates following IR-induced damage.

Following IR exposure, cells can undergo various forms of cell cycle arrest or cell death. Most commonly, cell death is induced directly through tumour suppressor-mediated induction of apoptosis, or through unregulated entry into the cell cycle and subsequent premature mitosis leading to mitotic catastrophe. Mitotic catastrophe can then result in cell death through apoptosis or necrosis, although necrosis is more commonly seen with higher radiation doses. While mitotic catastrophe is more common in p53-deficient cells, p53-proficient cells are more likely to undergo stress-induced premature senescence (SIPS), which typically leads to eventual apoptosis. Figure adapted from Kim *et al.* 2015 [63].

1.3.2. Cellular response to radiation

DSB repair can occur through two separate pathways, dependent on the stage of the cell cycle. If a sister chromatid is present, such as in late S and G2 phase, homologous recombination can be used as an error-free means of repair [59]. In G1 phase, the main repair pathway used to repair IR-induced DNA damage is non-homologous end-joining (NHEJ) which religates the ends of DSBs, however, this method is error-prone [59, 61, 64]. In both cases, in order to repair DNA, the DNA damage is first recognized by the Mre11-Rad50-Nbs1 (MRN) complex [58]. Ataxia telangiectasia-mutated (ATM) proteins are recruited to sites of MRN clusters, where they phosphorylate histone-variant H2AX at ser 139 (γ H2AX) [58]. γ H2AX clusters form at sites of DNA damage within 10-30 minutes post-irradiation, and can be used as a marker of radiation-induced DSBs [58, 65]. ATM is additionally responsible for phosphorylation of p53 and MDM2, disrupting the inhibitory interaction of MDM2 and stabilizing p53 [64, 65]. This activation of p53 induces subsequent transcription of target genes involved in senescence and apoptosis [66]. Of particular note is the p53-mediated transcription of p21, a senescence-associated cyclin-dependent kinase (CDK) inhibitor that blocks cell cycle progression and promotes growth arrest [55, 65]. Due to the anti-apoptotic effects of p21, the fate of cells treated with less than 10 Gy of radiation is generally directed towards SIPS and DNA repair rather than apoptosis [65, 66].

To facilitate DNA repair, however, there must first be *de novo* synthesis of nucleotides, which requires ribonucleotide reductase activity [67]. While initially DNA damage results in a p53-dependent increase in the levels of p53-R2 [68], there is also an induction of R2 transcription and a corresponding increase in R2 protein levels seen following radiation. In studies of cervical carcinoma lines, R2 expression following irradiation was elevated up to 30 hours post-irradiation, while there was no corresponding elevation in R1 [67, 69]. The post-irradiation upregulation of R2 was also shown to have some p53-

dependence, with a somewhat reduced upregulation seen in p53-mutant cell lines compared to p53-wild-type cell lines. In contrast, p53-R2 was only upregulated in p53-wild-type cell lines [49, 51]. As R2 is regulated independently of p53 (whereas p53-R2 is not), R2 is therefore able to complement the lack of p53-R2 upregulation in p53-mutant cells, facilitating DNA repair in these cells [51].

1.3.3. Clinical radiation therapy in glioma

Radiotherapy has been established as a key aspect of glioma treatment since 1976 when it was shown to nearly double survival time compared to chemotherapy alone [10, 64]. Post-surgery radiotherapy with concomitant TMZ was established in 2005 as providing the best survival benefit, and is still the standard of care today [9, 70]. Clinically, gliomas are treated by radiotherapy delivered in 2 Gray (Gy) fractions (where 1 Gy is equivalent to the absorption of 1 joule of energy per kilogram of matter), to a total of 60 Gy over a period of six weeks, with no further survival benefit seen by increased radiation dose [71]. TMZ is delivered at a dose of 75 mg per square meter of body surface per day concurrently with radiation, and then 4 weeks following radiation a second cycle of TMZ begins at an elevated dose of 150 mg per square meter [9]. This treatment regime has, however, been shown to increase toxic effects when compared to radiation alone, with some hematologic toxic effects, neutropenia, and thrombocytopenia observed in concurrent and adjuvant TMZ therapy [9].

1.3.4. Mouse models of radiation therapy

While radiation therapy is one of the most commonly used treatment modalities in the clinic, preclinical studies using external beam radiation therapy have often been hindered by the absence of a mode of radiation delivery comparable to that seen in the clinic. The majority of animal studies using external beam radiation used a single radiation field with lead shielding to protect the non-irradiated areas [72, 73]. This simple, uniform approach, while not only deviating from the conformal, multi-beam radiation delivery seen in the clinic [74], also resulted in unwanted side effects due to the unavoidable exposure of surrounding normal tissues [73], and as such necessitated a more clinically relevant model. The X-Strahl Small Animal Radiation Research Platform (SARRP) is a radiation delivery system developed at John Hopkins University that employs conebeam computed tomography (CBCT)-guided, highly targeted radiation delivery to small animal models, to better mimic the radiation treatment seen clinically [74, 75]. The SARRP combines CBCT image acquisition with advanced Muriplan treatment planning software with 360° delivery of isocentric radiation beams or arcs, for submillimetric precision delivery in any plane [75]. The SARRP system itself consists of an electronic imager, used for CBCT acquisition at high or low resolution, as well as a collimator system mounted on a rotational gantry for optimal precision delivery (Figure 1.5). The radiation beam is further focused through exchangeable tertiary collimators, with diameters ranging from 0.5 mm to 10 cm to allow manipulation of the size of the radiation beam (Figure 1.6). Muriplan treatment planning software allows for high precision of radiation delivery to manually-identified tumour isocentres, with isodose calculations demonstrating a dose highly targeted to the tumour with little radiation exposure of normal tissue (Figure 1.7). Previous studies have demonstrated that there is a high accuracy of dose delivery when using the SARRP as evidenced by γ H2AX expression localized within the irradiated area [72, 76]. The accuracy and reproducibility of the SARRP radiation delivery has been validated on several models of

intracranial GBM, using both MRI and bioluminescence imaging for visualization of tumour borders [72, 77].

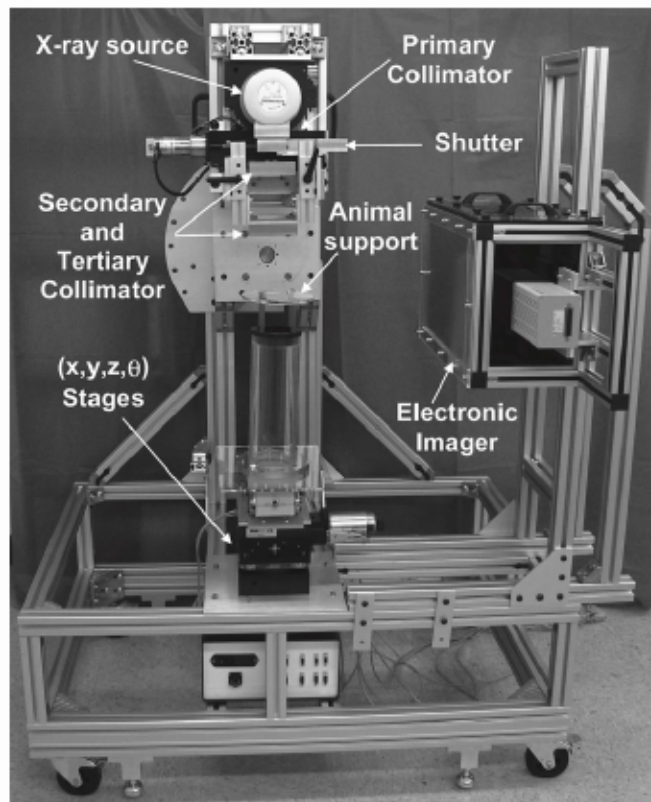


Figure 1.5. Early model of X-Strahl Small Animal Radiation Research Platform (SARRP).

Internal set-up of an early model of the X-Strahl SARRP. High or low resolution CBCT images are acquired through the electronic imager, while isocentric radiation delivery (beam or arc) is delivered through the primary, secondary and tertiary collimators to target the radiation beam for more precise delivery. The collimators are mounted on a rotational gantry, and the animal support bed is able to move submillimetrically in any plane for highly targeted radiation delivery. Figure from Wong *et al.* 2008 [75].



Figure 1.6. Interchangeable tertiary collimators for focal radiation beam delivery.

The X-Strahl SARRP is equipped with interchangeable tertiary collimators ranging in size from 0.5 mm to 10 cm (not pictured), to further increase precision of radiation delivery through manipulation of the size of the radiation beam.

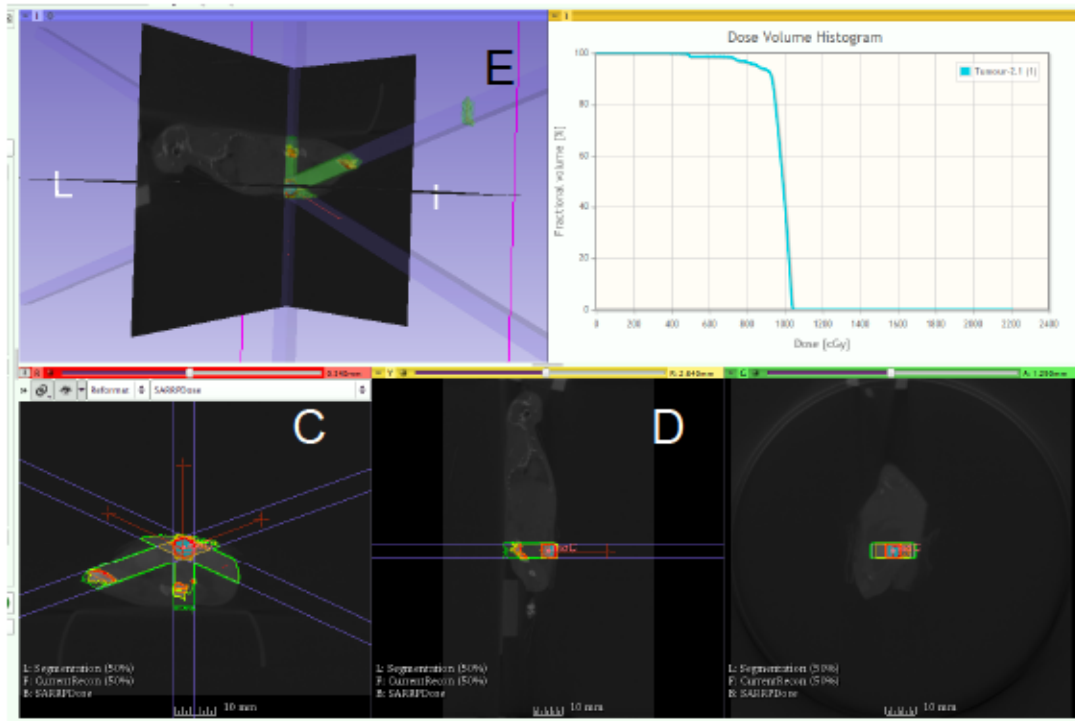


Figure 1.7. MuriPlan treatment planning for precise radiation delivery.

Computed tomography (CT) images scanned using the SARRP are uploaded into MuriPlan treatment planning software. Tumour is identified and tumour contours manually defined (not pictured). Tumour isocentre(s) are manually selected, with radiation beams (or arcs) targeted to selected isocentres. (A) Three converging beams targeted to defined tumour, with isodose to tumour and surrounding tissue shown as: green [0% - 20% target dose), yellow [60% - 70% target dose], orange [70% - 80% target dose], and red [80% - 100% target dose. (B), (C), (D) are transverse, sagittal, and frontal views of mouse CT, radiation beams, and isodoses. (E) Dose volume histogram (DVH) showing radiation dose (cGy) per fractional volume of tumour. Images from Kim Rans (Faculty Service Officer, Department of Oncology, University of Alberta) and Brittany Umer (Graduate student from the laboratory of Dr. David Evans, Department of Medical Microbiology and Immunology, University of Alberta).

1.4. ONCOLYTIC VIROTHERAPY AND RADIATION IN GLIOMAS

1.4.1. Oncolytic virotherapy and radiation

While many virotherapies in clinical trials have been used as standalone treatments, there have been several studies that have demonstrated improved cytotoxicity when oncolytic viruses were combined with chemotherapy or radiation [78]. In a study combining oncolytic VACV GLV-1h51 (Table 1.1) with radiation therapy for the treatment of pancreatic cancer, *in vitro* there was enhanced apoptosis of cells previously shown to be relatively radioresistant, while a xenograft mouse model showed a survival benefit when using combination therapy [79]. Another *in vitro* study combining oncolytic VACV GLV-1h68 with radiation to treat head and neck cancer cell lines showed no decreased virus replication following radiation, as well as improved cell killing even at a very low multiplicity of infection (MOI) [80].

A particularly significant combination effect was seen by combining reovirus with radiation therapy to treat relatively reovirus-resistant cell lines, demonstrating a strong induction of apoptotic pathways compared to either therapy alone, as well as a significant increase in survival in xenograft models [81]. Of particular interest was a study in human colorectal cancer cells treated with radiation therapy and oncolytic HSV-1 containing an insertional inactivation of R1. They found that the combined modalities demonstrated an increase in viral replication by a factor of 4.3, and increased cell death. Relevant to this thesis, they reported a significant increase in ribonucleotide reductase activity following exposure to IR [82].

To the best of our knowledge, there is currently one reported clinical trial of combination radiation therapy and oncolytic virotherapy in malignant glioma; G207, an oncolytic HSV-1, was given in combination with radiation for recurrent GBM. In a Phase I trial of intratumorally

administered G207 followed by a single 5 Gy radiation dose, the combination was well tolerated, with no development of encephalitis and some partial responses observed [29]. A second Phase I trial was also undertaken to assess the safety of multiple doses of G207 administered intratumorally prior to radiation delivery; in this completed trial, there was similarly no development of HSV encephalitis and only one patient developed adverse effects (fever, delirium) which resolved with steroid medication [83]. Although there have been no Phase II trials undertaken following completion of the Phase I trials, a Phase I trial of G207 in combination with radiation therapy for pediatric brain tumours is currently enrolling (<http://www.clinicaltrials.gov>, NCT02457845).

1.4.2. Glioma recurrence and resistance to standard therapies

The biggest barrier to curative therapy in the treatment of malignant glioma is the high propensity for recurrence, with median survival of 25 weeks from the time of recurrence [71, 84]. Interestingly, 70%-90% of GBMs recur within 2-3 cm of the original tumour [71], suggesting that the highly diffuse and infiltrative nature of gliomas may lead to incomplete surgical removal and/or extension beyond radiographic margins, thereby resulting in localized recurrence [55].

There are several characteristics of malignant glioma that render them resistant to many treatment options. Due to the locality and infiltration of the tumours, surgical resection presents a high risk of morbidity. Furthermore, the blood-brain barrier prevents systemic delivery of many chemotherapeutic agents to the brain [55, 71]. Additionally, malignant gliomas are inherently radioresistant, with even high doses failing to control tumours, while also inducing acute side effects [55]. Furthermore, with a time to recurrence of less than one

year, second-line radiation therapy is often not a possibility due to the late radiation effects and radionecrosis seen several months after initial treatment, increasing the risk of permanent brain injury with continued radiation therapy [6]. A means of eliminating the micro-extensions of the primary tumour would therefore be a viable approach to reducing tumour recurrence and thereby improving patient survival.

1.4.3. Potential advantages of a combinatorial approach

1.4.3.1. *Spatial cooperation*

As discussed above, malignant gliomas are one of the most deadly forms of cancers with a high propensity for recurrence. The infiltrative nature of malignant glioma renders it particularly resistant to curative therapies, with recurrence generally recurring within 2-3 centimetres of the original tumour mass [71]. We propose a combination strategy wherein the bulk of the tumour is treated with radiation therapy, while the tumour infiltrations are targeted by our replication-competent oncolytic VACV. This would allow the oncolytic VACV to spread through the tumour margins and microextensions that extend beyond the radiation target volume, thus providing a means of eliminating the tumour infiltrations, increasing tumour clearance and reducing possibility of recurrence to improve long-term survival.

1.4.3.2. *Additivity/synergy*

Additionally, we propose that cellular changes induced by IR exposure could benefit the virus for additive or synergistic effects. It has been demonstrated that radiation exposure results in DNA damage and leads to upregulation of DNA repair pathways, including an

increase in ribonucleotide reductase small subunit expression (both R2 and p53-R2). This induction of DNA repair also results in an increase in cellular dNTP pools and/or dNTP synthesis, which we hypothesize will provide an environment conducive to the growth of our R2-deleted VACV.

As malignant gliomas are known to be radioresistant, we additionally propose that our oncolytic VACV will be able to replicate in and induce cellular death in those tumour cell populations that are not killed by radiotherapy alone, for increased tumour killing. Additionally, several studies have shown that increasing immune responses to the tumour could have therapeutic effects. Radiation alone can activate inflammatory cell pathways [53], however the immunogenic effects of radiation therapy are often hampered by the immunosuppressive environment of the tumour [85] [86]. It has thus been proposed that radiation therapy could be improved through stronger induction of anti-tumour immunity [86]. As VACV has demonstrated high immunogenic potential, both in preclinical studies as an oncolytic virus as well as through its use in smallpox vaccinations, we hypothesize that combining radiation therapy with oncolytic VACV therapy could promote reactivation of an immune response to the tumour cells, further increasing tumour clearance by the immune system.

1.4.4. Thesis objectives

The objectives of this thesis were to provide the preclinical foundations for testing efficacy of the combination of our double-deleted oncolytic VACV $\Delta F4L\Delta J2R$ VACV (Table 1.1) with SARRP image-guided radiation therapy. To this end, we first assessed whether cells treated with IR would permit virus replication, and whether cell killing was enhanced by combination oncolytic VACV and radiation treatment. Our next step was to establish a

platform for testing combination treatment in a mouse GBM model, and initiate the assessment of the combination treatment in a small pilot study.

We hypothesized that, due to the efficient, tumour-selective spread of the virus and its immune-stimulatory potential, as well as the high safety profile and minimal adverse effects of other oncolytic VACVs seen in clinical trials, our oncolytic virus could provide an ideal alternative to TMZ in the treatment of malignant gliomas. Additionally, we hypothesized that the cellular changes induced by exposure to IR therapy, which is already a key component in the treatment of malignant glioma, could provide an environment that could further enhance virus replication and cytotoxicity. Combined, we believe that these advantages of oncolytic vaccinia virotherapy with radiation therapy could improve tumour response, reduce the rate of recurrence through virus spread in tumour microextensions, and improve survival in a cancer that has remained largely resistant to the therapies currently in use clinically.

Table 1.1. Oncolytic viruses discussed in thesis

Virus	Backbone	Mutation(s)	Mechanism of action	Stage of clinical trial
Talimogene laherparepvec (T-vec) [22,23]	HSV-1	ICP34.5 (deletion)	Tumour-selectivity	FDA approved (2015)
		ICP47 (deletion)	Antigen presentation	
		US11 (insertion)	Increased replication, oncolysis	
		GM-CSF (insertion)	DC recruitment and stimulation	
Ad5-Delta 24RGD mutant E1A (DNX-2401) [28]	Adenovirus	E1A (deletion)	Selectivity for retinoblastoma (Rb)-deficient cells	Phase I
		RGD-4C (insertion)	Integrin binding, for adenovirus receptor-independent infection	
G207 [29]	HSV-1 strain F	γ 34.5 (deletion)	Attenuation of neurovirulence	Phase I
		UL39 (inactivation)	Disruption of viral ribonucleotide reductase	
H-1PV [30,31]	Parvovirus	None	Wild-type rat virus, oncolytic, non pathogenic in normal cells	Phase I/II
PVS-RIPO [32,33]	Poliovirus	Internal ribosomal entry site (IRES) from human rhinovirus type 2	Attenuation of neurovirulence, entry restricted to poliovirus receptor CD155-expressing cells (oncofetal adhesion molecule and tumour antigen)	Phase I, FDA-granted breakthrough status
JX-594 [26]	Vaccinia virus (Wyeth strain)	J2R (deletion)	Thymidine kinase deletion - conditional replication	Phase III, FDA-granted orphan drug designation for HCC
		GM-CSF (insertion)	DC recruitment and stimulation	

GL-ONC1 (GLV-1h68) [27]	Vaccinia virus (Lister strain)	F14.5 L (inactivation)	Renilla luciferase Aequorea green fluorescent protein (RUC-GFP) insertion for visualization	Phase I/II
		J2R (inactivation)	Thymidine kinase deletion - conditional replication	
		A56R (inactivation)	Hemagglutinin deletion - virus attenuation	
Vaccinia virus vvDD [37,44]	Vaccinia virus (Western reserve strain)	J2R (deletion)	Thymidine kinase deletion - conditional	Preclinical
		Vaccinia growth factor (VGF) (deletion)	Virus attenuation, conditional replication	
Δ F4L Δ J2R VACV [47]	Vaccinia virus (Western reserve strain)	F4L (inactivation)	Disruption of viral ribonucleotide reductase - conditional replication	Preclinical
		J2R (inactivation)	Thymidine kinase deletion - conditional replication	
Δ F4L VACV [47]	Vaccinia virus (Western reserve strain)	F4L (inactivation)	Disruption of viral ribonucleotide reductase - conditional replication	Preclinical
GLV-1h51 [79]	Vaccinia virus (Lister strain)	F14.5 L (inactivation)	RUC-GFP insertion for visualization	Preclinical
		J2R (inactivation)	Thymidine kinase deletion - conditional replication	
		A56R (inactivation)	Hemagglutinin deletion - virus attenuation	

**CHAPTER 2. IN VITRO VACCINIA GROWTH KINETICS AND
CYTOTOXICITY IN COMBINATION WITH IONIZING
RADIATION IN HUMAN GLIOMA CELLS**

2.1. MATERIALS/METHODS

2.1.1. Cell culture

U-87 MG cells (ATCC #HTB14, from Dr. Roseline Godbout, Department of Oncology, University of Alberta) and U-118 MG cells (ATCC #HTB15, from Dr. David Evans, Department of Medical Microbiology and Immunology, University of Alberta) were maintained in Dulbecco's Modified Eagle Medium (DMEM) supplemented with 10% fetal bovine serum (FBS), 2 mM L-glutamine, 0.1 mg/mL penicillin, 100 U/mL streptomycin, and 250 µg/mL Amphotericin B. BSC40 cells (ATCC #CRL-2761, from Dr. Evans) were maintained in Minimum Essential Medium (MEM) supplemented with 5% FBS, 2 mM L-glutamine, 0.1 mg/mL penicillin, and 100 U/mL streptomycin. All cell lines were maintained at 37°C and 5% carbon dioxide (CO₂). Cells were passaged using 0.25% trypsin diluted in versene. All reagents were obtained from Gibco, Thermofisher Scientific.

2.1.2. Recombinant viruses

ΔF4LΔJ2R VACV, ΔF4L VACV, ΔJ2R VACV, and wild-type VACV were generated in the laboratory of Dr. David Evans. All viruses were constructed from a Western Reserve (WR) backbone (ATCC), with recombinant viruses containing an inserted mCherry gene for fluorescence imaging of viral replication (Figure 2.1). Viruses in this thesis were amplified by Kyle Potts and identities were confirmed by polymerase chain reaction (PCR) [87]. Viruses were re-titred immediately before use in experiments described in this thesis.

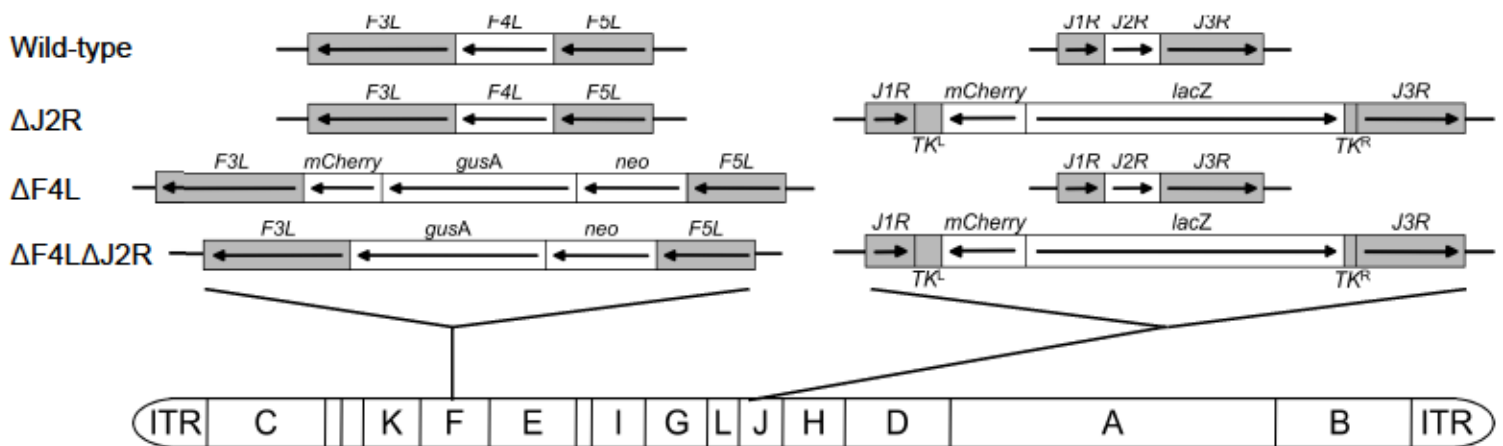


Figure 2.1. Recombinant vaccinia virus mutants.

Recombinant vaccinia mutants constructed from a Western Reserve (WR) backbone. $\Delta J2R$ VACV contains an *mCherry/lacZ* insertion in the *J2R* locus. $\Delta F4L$ VACV contains *mCherry* and *NeoGusA* insertions in the *F4L* locus. $\Delta F4L\Delta J2R$ VACV contains both insertional inactivations; the *mCherry/lacZ* *J2R* insertion and the *mCherry/NeoGusA* *F4L* insertion.

Figure from Kyle Potts (Graduate student of Dr. Mary Hitt, Department of Oncology, University of Alberta).

2.1.3. Virus titration

Confluent BSC40 cells on 150 (mm) plates were trypsinized and split into nine 6-well plates (54 wells total). 48 hours later, virus was serially diluted in phosphate-buffered saline (PBS). BSC40 plates were aspirated and 0.5 mL virus dilution in PBS (10^{-7} or 10^{-8} for high titre stocks, or as indicated below for lysates from growth curve experiments) was added in triplicate to 6-well plates. Plates were incubated at 37°C and 5% CO₂ for 1 hour, shaking plates every 15 minutes. Following the 1 hour incubation period, 2 mL of warmed medium (MEM) was added to each well and plates were incubated at 37°C and

5% CO₂. At 48 hours post-infection (h.p.i.), wells were aspirated and stained with crystal violet, and plaques were counted for each well. Titres of virus stocks (in plaque-forming units (pfu)/microlitre (µl)) were calculated as:

$$\text{Titre (pfu/}\mu\text{l)} = \frac{\text{Average (plaques/well)} \times \text{(dilution factor)}}{0.5 \frac{\text{ml}}{\text{well}} \times 1000 \text{ ul/ml}}$$

2.1.4. Virus infection and growth curves

Immediately prior to infection, a representative well or plate was trypsinized and cells counted with Trypan blue diluted 1:1 in PBS using a hemocytometer. The amount of virus required for the appropriate MOI was calculated. For each virus, cultures were aspirated, then infected with virus at an MOI of 0.03 pfu/cell (1 mL virus dilution in PBS for 60 mm plates, 20 µl per well of 96-well plates). In some cases, a t=0 plate was harvested by scraping and cells and medium were collected into a conical tube and stored at -80°C. For other time points, cells were incubated at 37°C and 5% CO₂ for 1 hour, shaking plates every 30 minutes. Following the 1-hour incubation, growth medium was added to plates and plates were incubated for the times indicated.

For virus growth curves, after the desired incubation time, each plate was scraped and medium and cells collected into conical tube and stored at -80°C. Collected cells underwent three freeze-thaw cycles of incubation in a 37°C water bath followed by freezing at -80°C, and were titred on BSC40 cells. Virus titres for each time point were calculated in pfu/cell:

Virus titre (pfu/cell)

$$= \frac{\frac{\text{Average plaques (pfu/well)}}{0.5 \text{ mL/well}} \times (\text{dilution factor}) \times (\text{total volume collected cells + medium})}{\text{Initial cell count}}$$

2.1.5. Cell irradiation

To minimize disruption of cells due to transportation across campus, cells were seeded at uniform density in 60 mm or 96-well plates as indicated and incubated at the Cross Cancer Institute (CCI). 24 hours post-seeding, cells were irradiated as indicated using a GammaCell cesium-source irradiator located at the CCI. Cultures were then transported to the Katz Building in an insulated container where they were incubated for the remainder of the experiment. At the indicated times post-irradiation (h.p.ir.), cells were infected with virus as described in section 2.1.4.

2.1.6. Cell survival assays

At 24 hours post-seeding, or 6 hours post-irradiation(h.p.ir), of cultures in 96-well plates, one well of each treatment plate was trypsinized and cells counted using a Trypan blue dye and a hemocytometer. Wells were infected in triplicate with 20 μ l of serial dilutions of virus at 0.001 pfu/cell to 10 pfu/cell in PBS, with negative and positive controls for cell killing of PBS (mock-infected) and 10% Triton X-100 in double-distilled water (ddH₂O), respectively. Plates were incubated for 1 hour, shaken at 15-minute intervals. Following the incubation period, 80 μ l of growth medium was added to each well and plates were incubated for 72 hours. At 72 h.p.i., 11 μ l of 440 μ M resazurin in sterile ddH₂O was added to each well and plates were incubated for 2-3 hours until fluorescence

developed. Fluorescence was measured using a microplate reader with excitation and emission wavelengths of 544 nm and 590 nm, respectively. Values in triplicate were averaged and background fluorescence (Triton X-100 treated wells) was subtracted from the sample fluorescence value. Cell survival was calculated as:

$$\% \text{ cell survival} = \frac{\text{fluorescence (experimental)}}{\text{fluorescence (mock infected)}} \times 100$$

2.1.7. Lysate collection and western blots

Cells were seeded at uniform density in 60 mm plates and 24 hours later were irradiated. At indicated time points, one plate each of irradiated and non-irradiated control was harvested for whole cell lysate. Lysates were collected by aspirating media from plates and rinsing twice with cold PBS, followed by treatment with radioimmunoprecipitation (RIPA) buffer (150 mM NaCl, 1% Triton X-100, 0.5% sodium deoxycholate, 0.1% SDS and 50 mM Tris pH 8.0) supplemented with 1% 100X Protease Inhibitor Cocktail (Halt™, ThermoFisher Scientific) and 1 mM phenylmethanesulfonyl fluoride (PMSF). Collected lysates were centrifuged and pelleted genomic material was removed. Lysates were stored at -80°C. Protein concentration of each sample was calculated against a standard curve of albumin using a BCA protein assay (Pearce™, ThermoFisher Scientific #23225).

For western blot, 20 µg of protein (in RIPA buffer) was separated on a SDS-12% polyacrylamide gel using a vertical electrophoresis cell. Proteins were wet-transferred to a nylon membrane using a transfer buffer containing 24 mM Tris base, 293 mM glycine, and 20% methanol. The membrane was blocked with Odyssey blocking buffer (LI-COR) and probed overnight at 4°C with primary antibodies for R2 (Santa Cruz Biotech, sc-

10846), p53R2 (Abcam, ab-8105), and p21 (Abcam, ab109199) diluted 1:1000 in 1:1 Odyssey blocking buffer:PBS. β -tubulin (detected with Abcam antibody ab-6046) was used as a loading control. Membranes were rinsed with PBS, 0.1% Tween-20 (PBST) and stained for 1 hour at room temperature with secondary antibodies (goat α -mouse IgG (H+L) IRDye 680 RD, donkey α -rabbit IgG (H+L) IRDye 680 LT, donkey α -rabbit IgG (H+L) IRDye 800 CW, donkey α -goat IgG (H+L) IRDye 800 CW) (all secondary antibodies obtained from LI-COR) diluted 1:20 000 in PBST + 0.01% sodium dodecyl sulfate (SDS). Membranes were rinsed in PBST followed by PBS, and scanned using a LI-COR Odyssey and the Image Studio™ software.

2.2. RESULTS

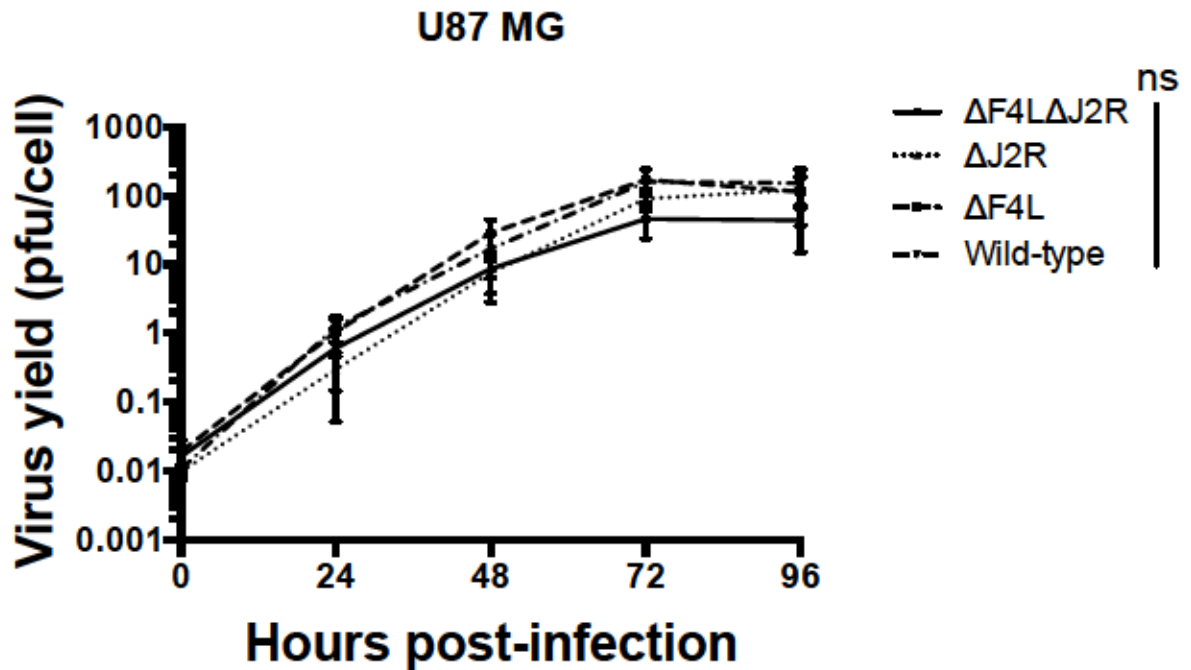
2.2.1. Yield of VACV mutants is comparable to that of wild-type VACV in human GBM cells

We first determined whether our human glioma cell lines supported F4L-deleted (Δ F4L or Δ F4L Δ J2R) VACV infection, and whether there was any reduction in replication compared to wild-type VACV or other VACV mutants used commonly in the Evans and Hitt labs. Growth curves of VACV mutants Δ F4L Δ J2R, Δ F4L, and Δ J2R as well as wild-type VACV were carried out on the human GBM cell lines U-87 MG and U-118 MG to determine whether replication of VACV mutants was hindered compared to wild-type VACV. Cells were infected with virus at an MOI of 0.03 pfu/cell and harvested up to 96 h.p.i. such that multiple rounds of replication would take place within the assay time period. In U-87 MG cells, Δ F4L VACV, Δ F4L Δ J2R VACV, and Δ J2R VACV grew to yields comparable to that of wild-type VACV, with final virus yields at 96 hours showing

no significant difference between wild-type VACV and the three mutant viruses (Figure 2.2). When U-118 MG cells were infected with mutant or wild-type VACV, $\Delta F4L\Delta J2R$ VACV showed no significant difference in final virus yield compared to wild-type and $\Delta J2R$ VACV; however there was an ~ 1 log reduction in final virus yield of $\Delta F4L$ VACV at 96 hours (Figure 2.3). As we saw no significant difference between $\Delta F4L\Delta J2R$ VACV and $\Delta F4L$ VACV infection in U-87 MG cells, and a lower $\Delta F4L$ VACV yield compared to $\Delta F4L\Delta J2R$ VACV in U-118 MG cells, we chose to continue with $\Delta F4L\Delta J2R$ VACV only for the rest of the study.

2.2.2. Cell killing of human GBM cells by $\Delta F4L\Delta J2R$ VACV is comparable to that of wild-type VACV

After confirmation that our glioma cell lines supported infection with our mutant viruses, we next assessed the cytotoxicity of $\Delta F4L\Delta J2R$ VACV compared to wild-type VACV in human GBM cells. To this end, we used a resazurin-based cell viability assay. Cells were treated with PBS (mock-infected) or with $\Delta F4L\Delta J2R$ or wild-type VACV at serial dilutions of 10 pfu/cell to 0.001 pfu/cell. A resazurin metabolic dye, which is converted to the fluorescent substrate resarufin by metabolically active cells, was added at 72 h.p.i. Fluorescence was assayed using a microplate reader, with cell viability expressed as percent fluorescence emitted by the infected wells compared to that of mock- (PBS-) infected cells. Both U-87 MG cells and U-118 MG cells showed no significant difference in sensitivity between $\Delta F4L\Delta J2R$ VACV and wild-type VACV at any MOI (Figure 2.4, Figure 2.5). Both cell lines also appeared to be relatively resistant to virus-mediated cell killing below an MOI of 1 pfu/cell.

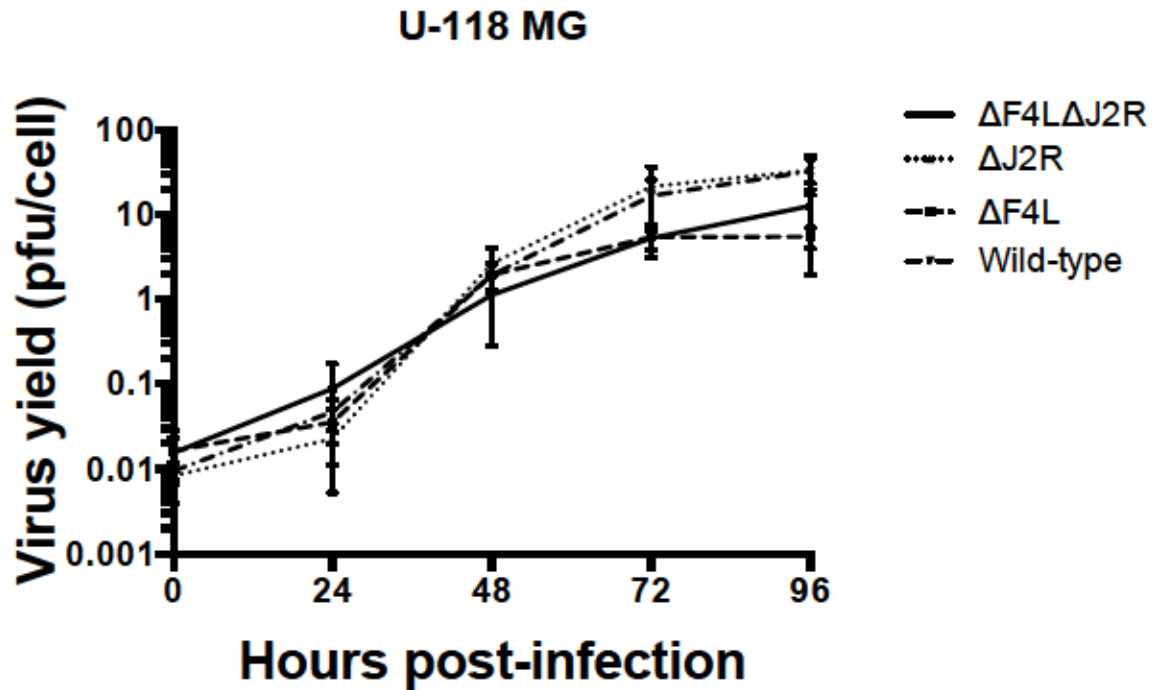


At 96 hours post-infection:

	Wild-type	ΔF4LΔJ2R	ΔF4L	ΔJ2R
Mean (pfu/cell)	159	44	46	123
P-Value (compared to wild-type VACV)	N/A	0.11	0.11	0.64

Figure 2.2. Yield of VACV mutants is comparable to that of wild-type VACV in human U-87 glioma cells.

Subconfluent cultures of U-87 glioma cells were infected with wild-type or mutant VACV at an MOI of 0.03 plaque-forming units (pfu)/cell. Cells were harvested at the indicated time points. Virus and cell lysates were titred on BSC40 cells. Mean titres +/- standard error of the mean (S.E.M). from three independent experiments are shown. At the 96-hour time point, virus yields were not significantly different between groups (t-test, $p > 0.05$) (ns = not significant).

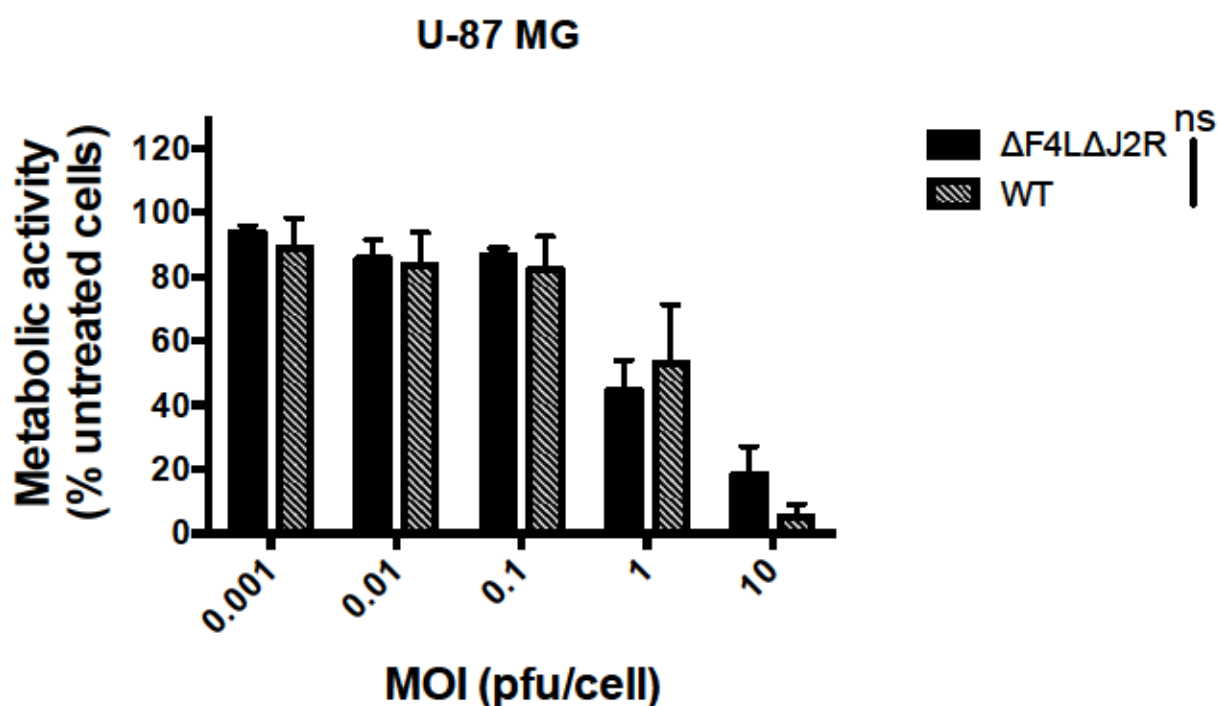


At 96 hours post-infection:

	Wild-type	$\Delta F4L\Delta J2R$	$\Delta F4L$	$\Delta J2R$
Mean (pfu/cell)	32	13	5.5	33
P-Value (compared wild-type VACV)	N/A	0.11	0.02	0.94

Figure 2.3. Yield of F4L-deleted VACV mutants is slightly reduced compared to wild-type and $\Delta J2R$ VACV in U-118 glioma cells.

Subconfluent cultures of U-118 glioma cells were infected with wild-type or mutant VACV at an MOI of 0.03 pfu/cell. Cells were harvested at the indicated time points. Virus and cell lysates were titred on BSC40 cells. Mean titres +/- S.E.M. from three independent experiments are shown. At the 96-hour time point, virus yield was reduced only in the $\Delta F4L$ VACV group when compared to yield of wild-type VACV (t-test, $p=0.02$).



MOI (pfu/cell)	0.001	0.01	0.1	1	10
P-value (wild-type versus $\Delta F4L\Delta J2R$)	0.44	0.78	0.52	0.51	0.08

Figure 2.4. $\Delta F4L\Delta J2R$ VACV induces comparable cytotoxicity to wild-type VACV in U-87 glioma cells.

U-87 glioma cells seeded in 96-well plates were infected in triplicate with $\Delta F4L\Delta J2R$ or wild-type VACV at serial dilutions of 10 pfu/cell to 0.001 pfu/cell. A resazurin-based metabolic assay was performed at 72 h.p.i. to assess cell viability. Cells were mock-infected with PBS as a positive control for viability. Cell viability is shown as percent fluorescence emission compared to PBS (mock)-infected cells. Results shown are the means \pm S.E.M. of three independent experiments. No difference in cytotoxicity was seen at any experimental MOI (t-test, $p > 0.05$).

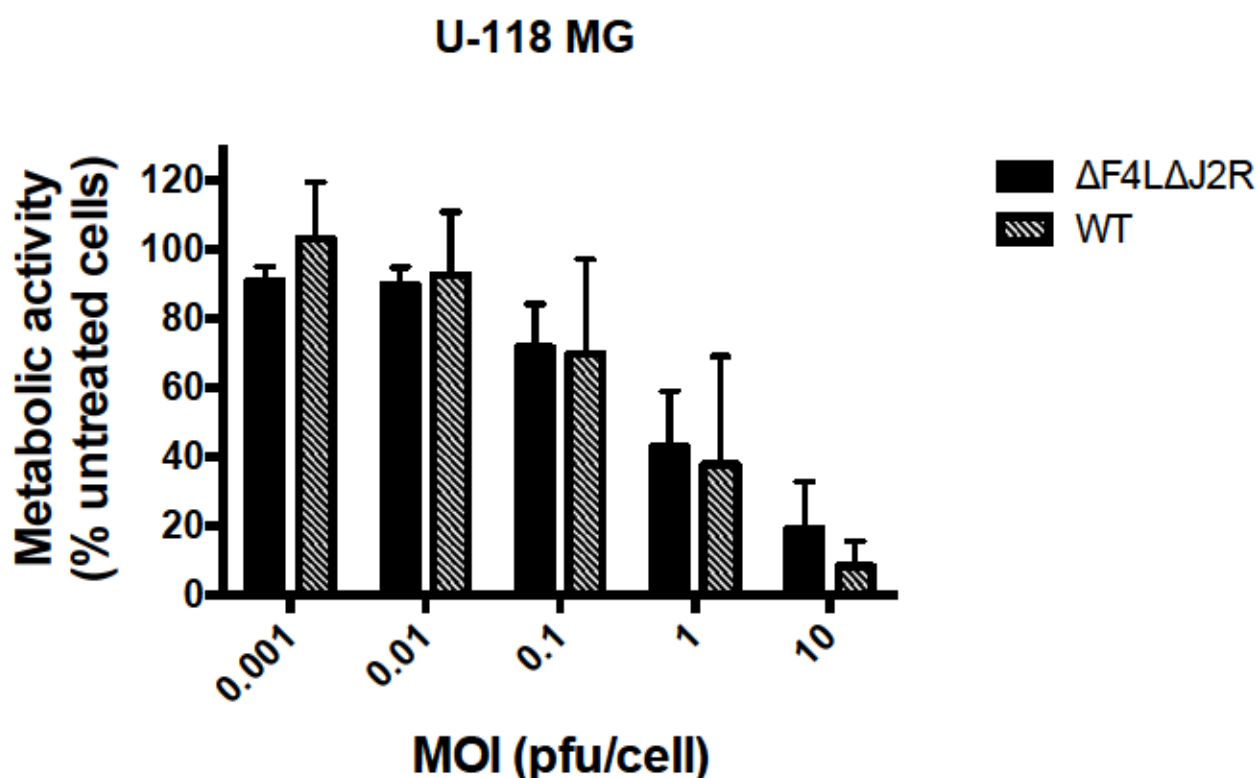


Figure 2.5. $\Delta F4L\Delta J2R$ VACV induces comparable cytotoxicity to wild-type VACV in U-118 glioma cells.

U-118 glioma cells seeded in 96-well plates were infected in triplicate with $\Delta F4L\Delta J2R$ or wild-type VACV at serial dilutions of 10 pfu/cell to 0.001 pfu/cell. A resazurin-based metabolic assay was performed at 72 h.p.i. to assess cell viability. Cells were mock-infected with PBS as a positive control for viability. Cell viability is shown as percent fluorescence emission compared to PBS- (mock-) infected cells. Results shown are the means \pm S.E.M. of three independent experiments. No difference in cytotoxicity was seen at any experimental MOI (t-test, $p > 0.05$).

2.2.3. U-87 MG and U-118 MG cells resistance to 8 Gy IR

Before we began combining our viruses with radiation therapy, we first wanted to determine the susceptibility of our human glioma cells to radiation-mediated death. For our *in vitro* radiation assays, we used a dose of 8 Gy radiation. This dose was chosen as representation of a lethal dose, which was seen to have a cytotoxic effect in human tumour cells in a paper by Mirzayans *et al.* (2007) [88]. To assess the reduction in cell viability induced by 8 Gy radiation exposure alone, a resazurin-based metabolic viability assay was carried out on cells that had been treated with 8 Gy radiation at 72 hours prior to the assay (or mock-irradiated as a no-killing control). Cells were irradiated at subconfluence, and had reached confluence by the time of the addition of resazurin. U-87 MG cells showed metabolic activity at 75% +/- 4% (n=3) of that of non-irradiated cells at 72 h.p.ir. while U-118 MG cells showed metabolic activity at 61% +/- 6% (n=3) that of non-irradiated cells at 72 h.p.ir. (Figure 2.6), suggesting that both U-87 and U-118 cells are relatively resistant to IR. It must be noted, however, that the assay detects metabolism and not cell death, and there may be a discrepancy in the % reduction in metabolism versus % cell death, as cells that had entered senescence would still be metabolically active, albeit at a lower rate than actively proliferation cells.

2.2.4. Radiation increases ribonucleotide reductase small subunit expression in U87 MG (p53-wild-type) and U118 MG (p53-mutant) cell lines

As deleting the small subunit of ribonucleotide reductase (R2) in $\Delta F4L\Delta J2R$ VACV renders the virus dependent on cellular levels of R2, and evidence has suggested that radiation can increase ribonucleotide reductase levels in order to produce dNTPs to

facilitate DNA repair [67, 69] [68], we assessed changes in R2 and p53-R2 expression following exposure to 8 Gy IR. A Western blot analysis of protein expression was used to determine changes in the levels of R2 and p53-R2, as well as in the levels of p21 when cells had been irradiated with 8 Gy IR (Figure 2.7). Whole cell lysates were collected up to 96 h.p.ir. In both U-118 MG and U-87 MG cell lines, R2 levels decreased following irradiation, with the decreased expression seen up to 96 h.p.ir., while levels of p53-R2 increased in both cell lines compared to levels seen at 0 h.p.ir. Expression of p21 increased up to 24 h.p.ir. before again decreasing in U-87 MG cells, which have wild-type p53. P21 levels were nearly undetectable at all time points in the mutant-p53 U-118 MG cell line. As p21 expression is mediated by p53, upregulation of p21 was not expected in a mutant-p53 cell line.

2.2.5. Exposure to IR did not reduce $\Delta F4L\Delta J2R$ or wild-type VACV growth in human GBM cells.

As we had observed that exposure to IR had an effect on cellular ribonucleotide reductase subunit levels, with a decrease in R2 expression and an increase in p53-R2 expression, we next sought to determine whether pre-treatment with IR affected wild-type or $\Delta F4L\Delta J2R$ VACV growth in U-87 and U-118 MG cells. Cells were infected with 0.03 pfu/cell of virus 24 hours following exposure to 5 Gy or 8 Gy IR. A low MOI was used to assess multiple rounds of replication within the 96-hour growth curve time period. In U-87 MG cells, virus yield at 96 h.p.ir. in cells exposed to 5 Gy or 8 Gy IR were not reduced when compared to a non-irradiated control when cells were infected with either $\Delta F4L\Delta J2R$ VACV (Figure 2.8) or wild-type VACV (Figure 2.9). Similarly, in U-118 MG cells there was also no reduction in virus yield at 96 h.p.ir. seen following exposure

to 5 Gy or 8 Gy radiation (Figure 2.10, 2.11). Also of note, the final yields of both $\Delta F4L\Delta J2R$ and wild-type VACV in both irradiated and non-irradiated cells were lower in U-118 MG cells compared to U-87 MG cells, which was consistent with the reduced virus growth in U-118 MG cells seen in initial growth curve studies (Figure 2.2, Figure 2.3). These results indicate that the ability of U-87 MG and U-118 MG cells to support virus growth is not affected by pre-treatment with up to 8 Gy IR.

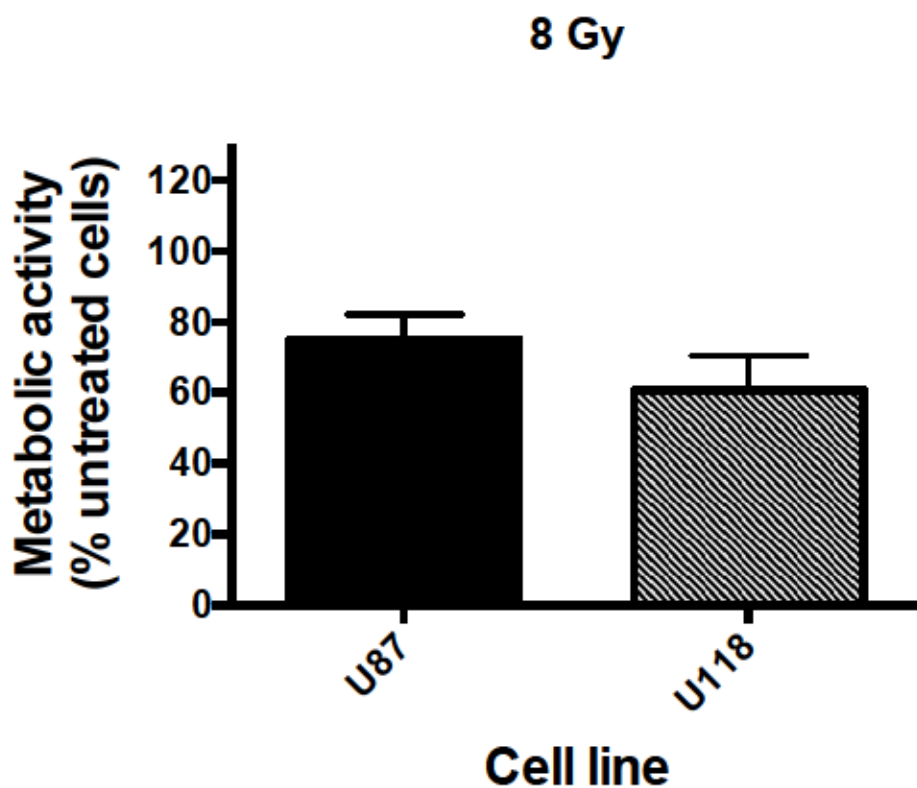


Figure 2.6. Resistance of U-87 and U-118 MG cells to treatment with 8 Gy IR.

U-87 and U-118 cells seeded in 48-well plates were irradiated or mock-irradiated in triplicate with 8 Gy IR. At 72 h.p.ir., a resazurin-based metabolic assay was performed to assess cell number. Triton X-100 was used as a control to simulate complete killing. Cell survival is shown as percent fluorescence compared to non-irradiated cells. Results shown are the means \pm S.E.M. of three independent experiments. There was no significant difference between metabolic activity of U-87 versus U-118 cells exposed to 8 Gy radiation (t-test, $p=0.70$).

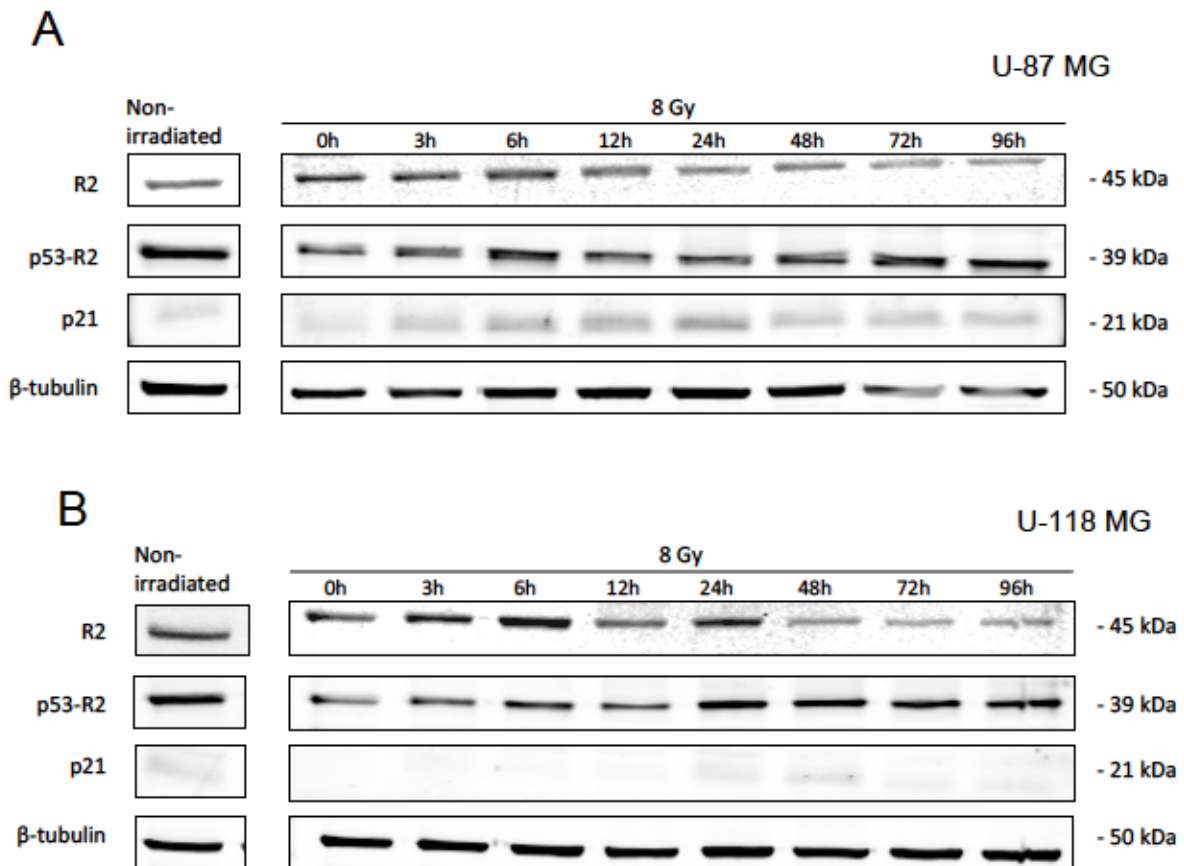
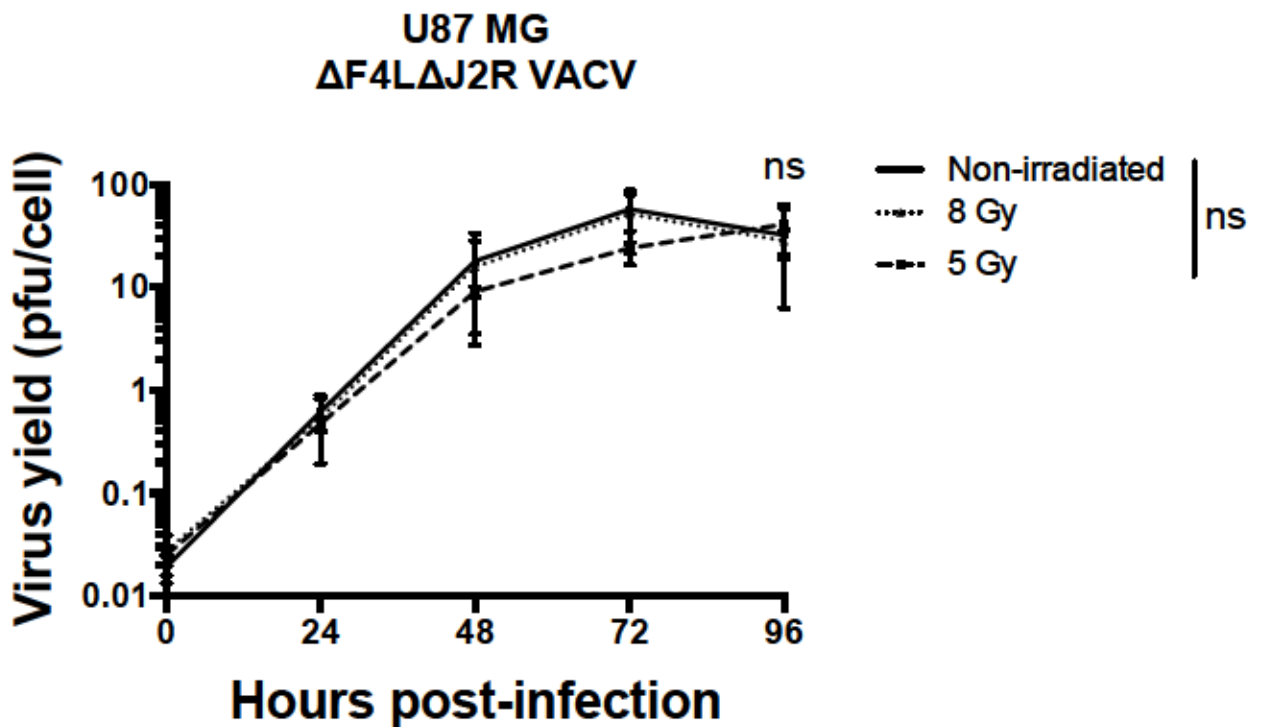


Figure 2.7. Radiation effects on R2/p53-R2 levels in U-87 MG and U-118 MG glioma cells.

U-87 or U-118 cells were mock-irradiated or irradiated with 8 Gy IR. Whole cell lysates were collected at the indicated time points. Protein concentration was determined using a BCA protein assay. 20 μ g of protein for each sample were separated on a 12% acrylamide/SDS-PAGE gel and stained for R2, p53-R2, and p21. β -tubulin was used as a loading control.

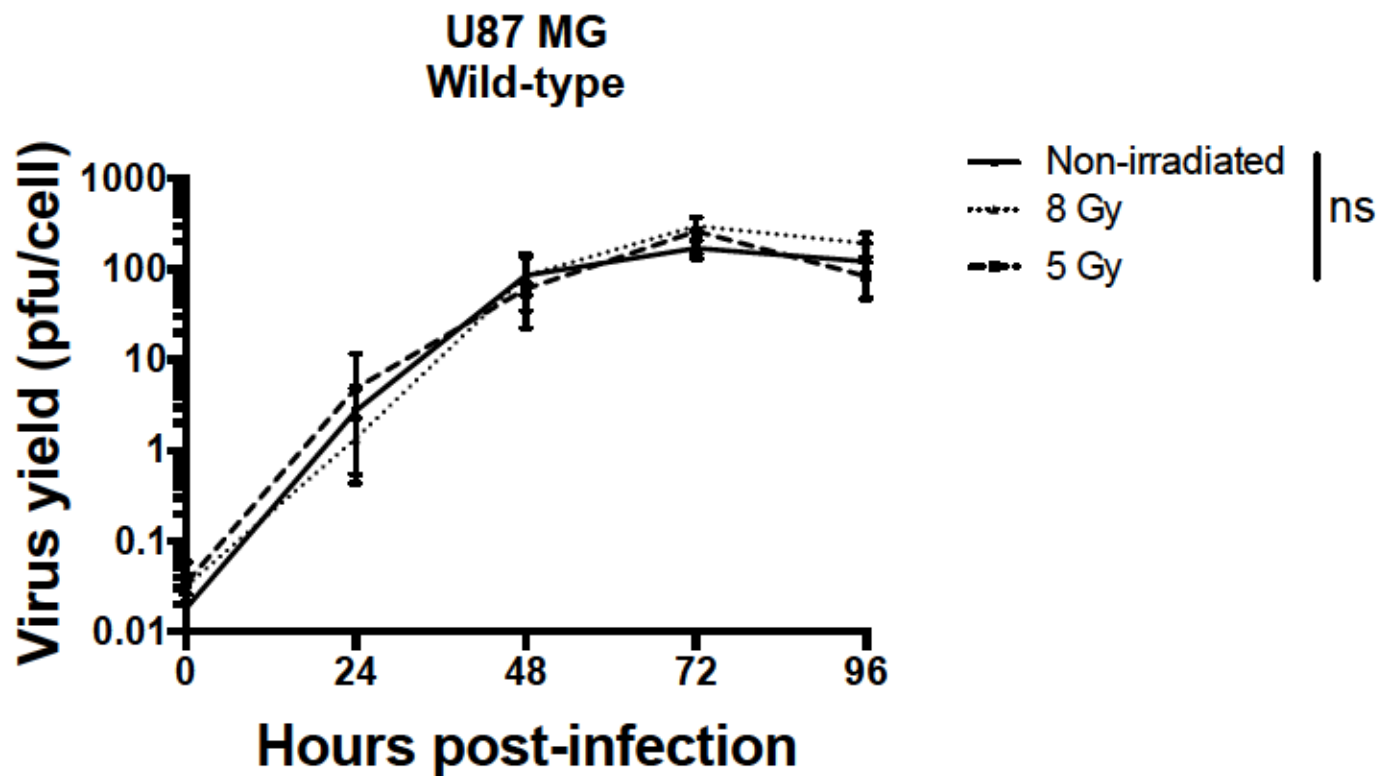


At 96 hours post-infection:

	Non-irradiated	5 Gy	8 Gy
Mean (pfu/cell)	32	41	28
P-Value (compared to non-irradiated)	N/A	0.68	0.81

Figure 2.8. Exposure to IR does not reduce ΔF4LΔJ2R VACV yield in U-87 MG cells.

Subconfluent U87 cells were irradiated with 5 Grays (Gy) or 8 Gy IR or mock-irradiated. Cells were infected with ΔF4LΔJ2R VACV at 24 h.p.ir. at an MOI of 0.03 pfu/cell. Cells were harvested at the indicated time points and tited on BSC40 cells. Points plotted represent mean titres +/- S.E.M. from three independent experiments. Virus yield at 96 h.p.ir. was not reduced in irradiated cells compared to non-irradiated (t-test, $p > 0.05$).



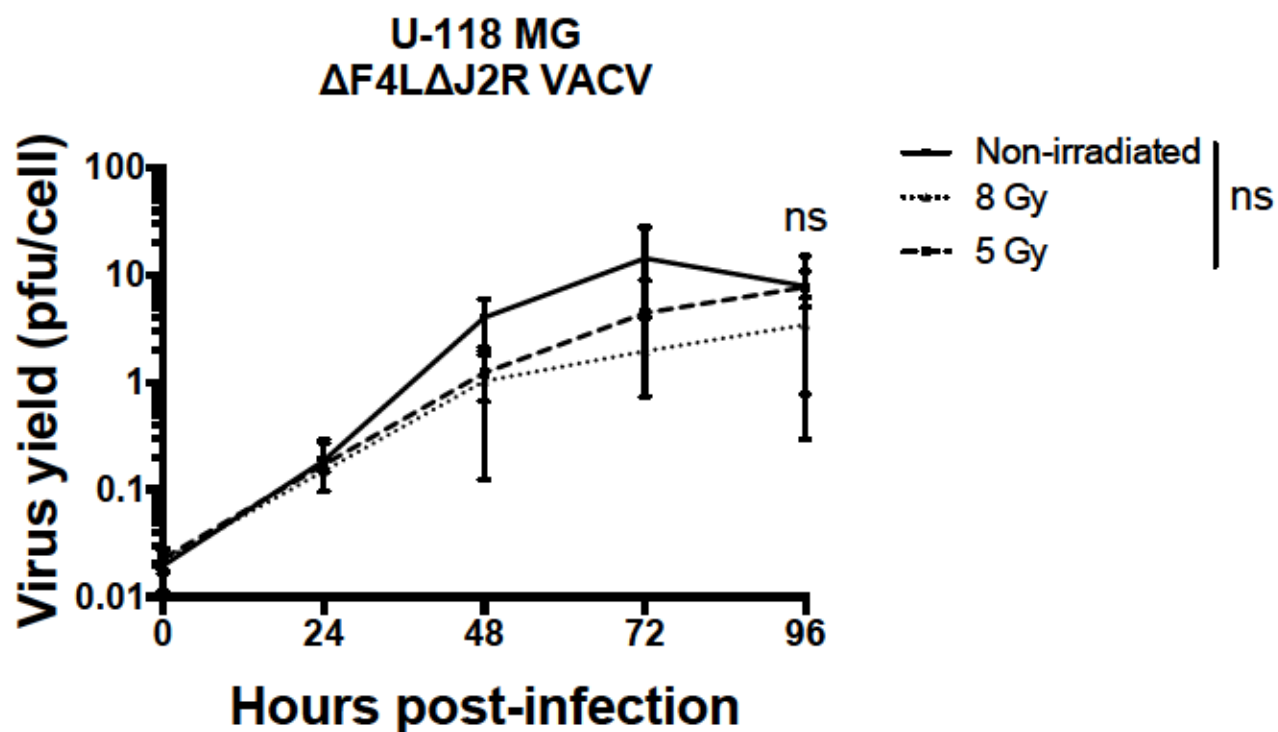
At 96 hours post-infection:

	Non-irradiated	5 Gy	8 Gy
Mean (pfu/cell)	121	84	193
P-Value (compared to non-irradiated)	N/A	0.47	0.25

Figure 2.9. Exposure to IR does not reduce wild-type VACV yield in U-87 MG cells.

Subconfluent U87 cells were irradiated with 5 Grays (Gy) or 8 Gy IR or mock-irradiated.

Cells were infected with wild-type VACV at 24 h.p.ir. at an MOI of 0.03 pfu/cell. Cells were harvested at the indicated time points and titered on BSC40 cells. Points plotted represent mean titres +/- S.E.M. from three independent experiments. Virus yield at 96 h.p.ir. was not reduced in irradiated cells compared to non-irradiated (t-test, $p > 0.05$).

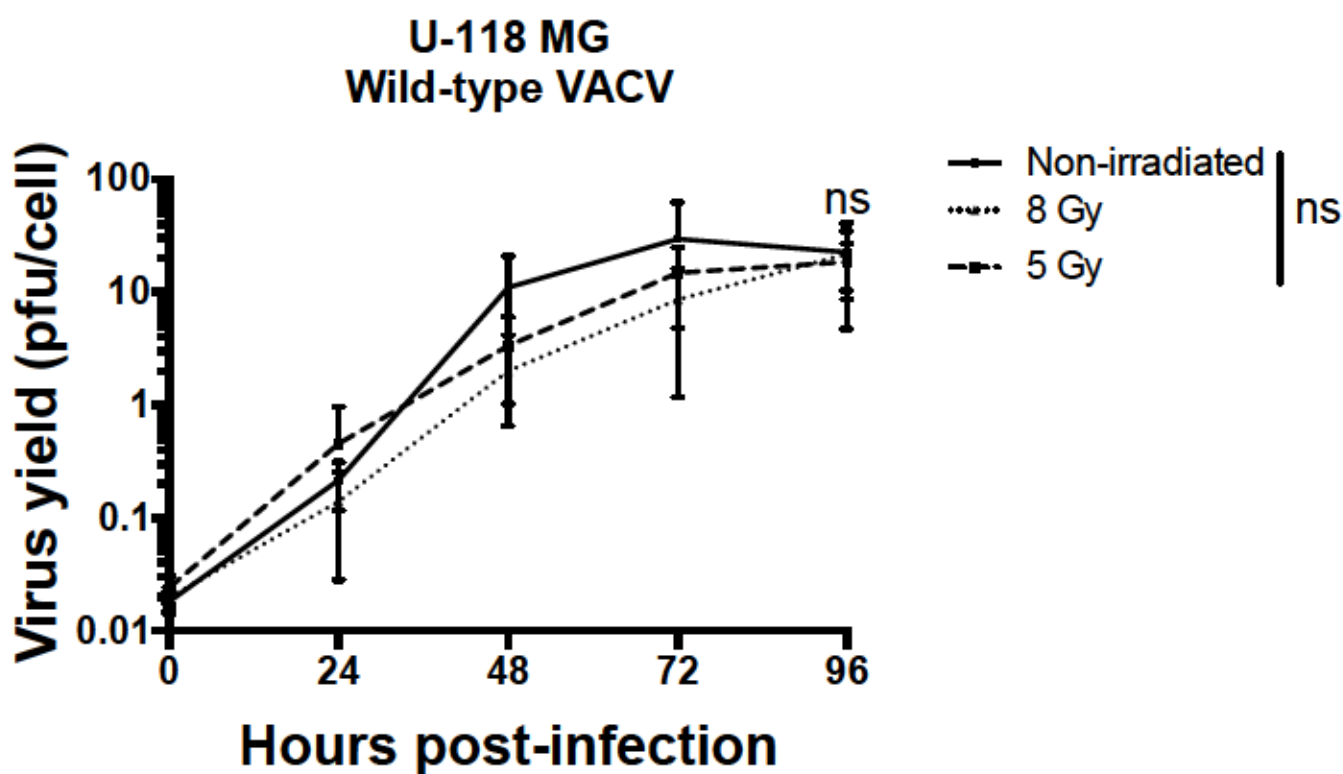


At 96 hours post-infection:

	Non-irradiated	5 Gy	8 Gy
Mean (pfu/cell)	7.9	7.7	3.6
P-Value (compared to non-irradiated)	N/A	0.97	0.19

Figure 2.10. Exposure to IR does not reduce ΔF4LΔJ2R VACV yield in U-118 MG cells.

Subconfluent U-118 MG cells were irradiated with 8 Gy IR or mock-irradiated. Cells were infected with ΔF4LΔJ2R VACV at 24 h.p.ir. at an MOI of 0.03 pfu/cell. Cells were harvested at the indicated time points and titered on BSC40 cells. Points plotted represent mean titres +/- S.E.M. from three independent experiments. Virus yield at 96 h.p.ir. was not reduced in irradiated cells compared to non-irradiated (t-test, $p > 0.05$).



At 96 hours post-infection:

	Non-irradiated	5 Gy	8 Gy
Mean (pfu/cell)	23	19	22
P-Value (compared to non-irradiated)	N/A	0.74	0.94

Figure 2.11. Exposure to IR does not reduce wild-type VACV yield in U-118 MG cells.

Subconfluent U-118 MG cells were irradiated with 8 Gy IR or mock-irradiated. Cells were infected with $\Delta F4L\Delta J2R$ VACV at 24 h.p.ir. at an MOI of 0.03 pfu/cell. Cells were harvested at the indicated time points and titered on BSC40 cells. Points plotted represent mean titres \pm S.E.M. from three independent experiments. Virus yield at 96 h.p.ir. was not reduced in irradiated cells compared to non-irradiated (t-test, $p > 0.05$).

2.2.6. Combining IR with $\Delta F4L\Delta J2R$ VACV infection increased cell killing in human GBM cells.

As virus growth was not reduced in irradiated cells, we then assessed whether treating cells with both IR and $\Delta F4L\Delta J2R$ or wild-type virus affected treatment-induced cytotoxicity relative to non-irradiated, virus-infected cells. A resazurin-based metabolic viability assay was used as a measure of cell viability in cells treated with 8 Gy radiation and infected with serial dilutions of either $\Delta F4L\Delta J2R$ VACV or wild-type VACV, with a mock (PBS)-infected control used as a positive control for viability.

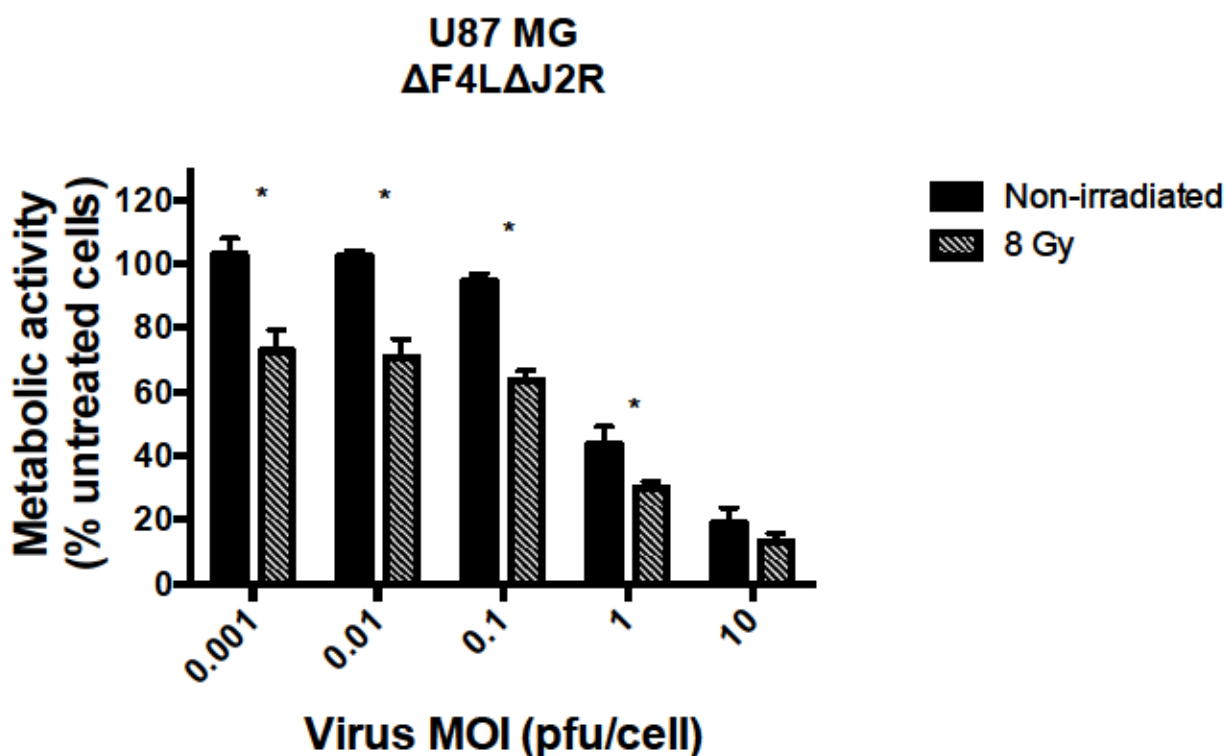
In $\Delta F4L\Delta J2R$ VACV-infected U-87 MG cells, exposure to 8 Gy IR increased cell killing to a fairly small extent at virus MOIs of 0.001 pfu/cell to 1 pfu/cell, as seen by the reduced metabolic activity of cells in the combination treated groups (Figure 2.12). Similarly, U-118 MG cells showed increased cell killing in the combination 8 Gy/ $\Delta F4L\Delta J2R$ VACV group at all virus MOIs compared to non-irradiated (Figure 2.13). Additionally, U-118 MG cells treated with the combination of IR and $\Delta F4L\Delta J2R$ VACV were killed to a slightly greater extent than U-87 MG cells treated with the combination (40%-60% vs. 65-70% cell viability at MOIs of 0.1 pfu/cell or less).

In both cell lines, there was no statistically significant reduction in metabolic activity in 8 Gy/wild-type VACV treated groups compared to non-irradiated, wild-type VACV infected cells, except at the lowest MOI (0.001 pfu/cell) in U-118 cells (Figure 2.14, Figure 2.15); however, this could be in part due to greater variability between replicate experiments using the wild-type virus. Altogether, these results indicate that combining $\Delta F4L\Delta J2R$ VACV with IR could result in increased cytotoxicity to human GBM cells compared to

$\Delta F4L\Delta J2R$ VACV infection alone, while additionally demonstrating that cytotoxicity induced by $\Delta F4L\Delta J2R$ VACV is not significantly worse than that induced by wild-type VACV in irradiated cells.

2.2.7. Single-replication round yield of $\Delta F4L\Delta J2R$ and wild-type VACV is not reduced by increasing time to infection post-irradiation in U-87 MG cells

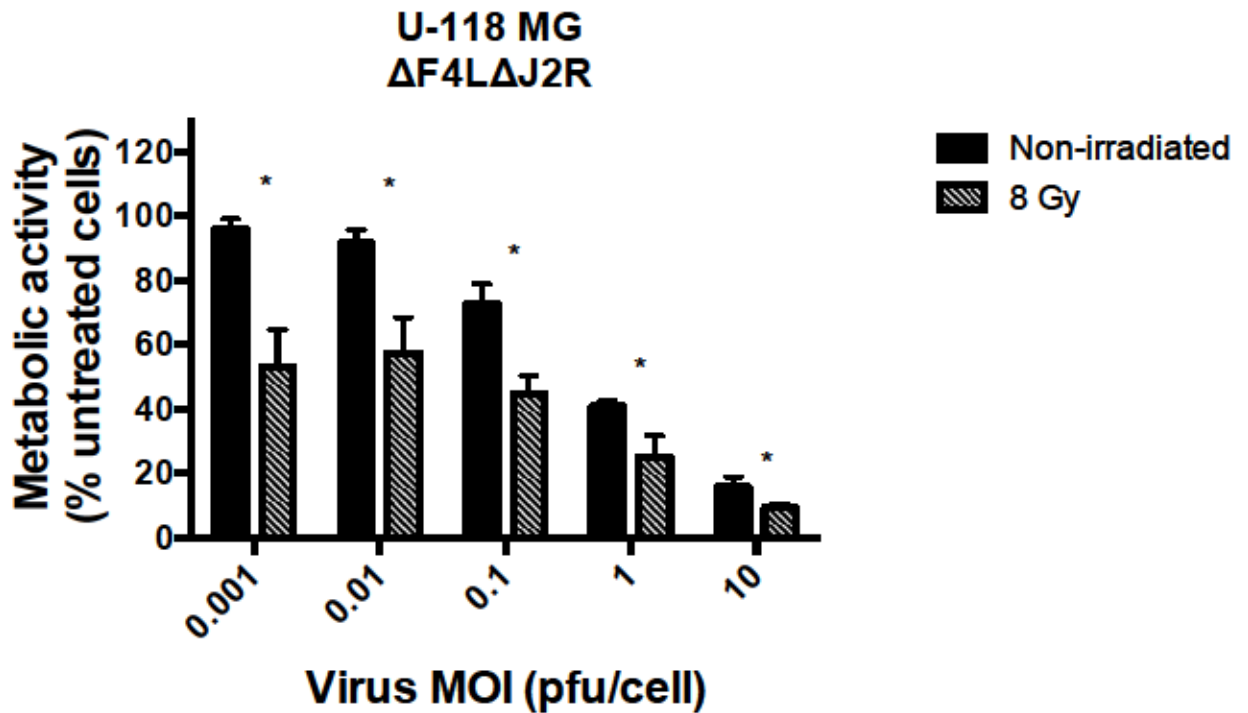
In our initial growth curves of $\Delta F4L\Delta J2R$ and wild-type VACV in irradiated cells, we began virus infection at 24 h.p.ir., as increasing time to infection post-irradiation would have resulted in over-confluent cells by the 96-hour post-infection time point. However, as our next step was to assess the combination therapy in an animal model, we wished to determine whether there was an optimal time of infection post-irradiation for maximum virus yield. A single round of virus replication was assessed by infecting cells with an MOI of 3 pfu/cell and harvesting cells and virus at 24 h.p.i.; this was to more precisely quantify the differences in virus yield on a per cell basis with varying the time to infection. Cells were treated with 8 Gy IR or mock-irradiated and infected with $\Delta F4L\Delta J2R$ or wild-type VACV at time points of 24 h.p.ir., 48 h.p.ir., and 72 h.p.ir. Our results showed that with both $\Delta F4L\Delta J2R$ and wild-type VACV infections, increasing the time to infection post-irradiation did not affect the virus yield (Figure 2.16), suggesting that radiation-induced cellular changes up to 72 h.p.i. do not reduce the growth potential of either virus.



MOI (pfu/cell)	0.001	0.01	0.1	1	10
P-value (non-irradiated versus 8 Gy)	0.003	0.0008	0.0002	0.01	0.13

Figure 2.12. Combination IR with ΔF4LΔJ2R VACV infection increased cell killing of U87 cells.

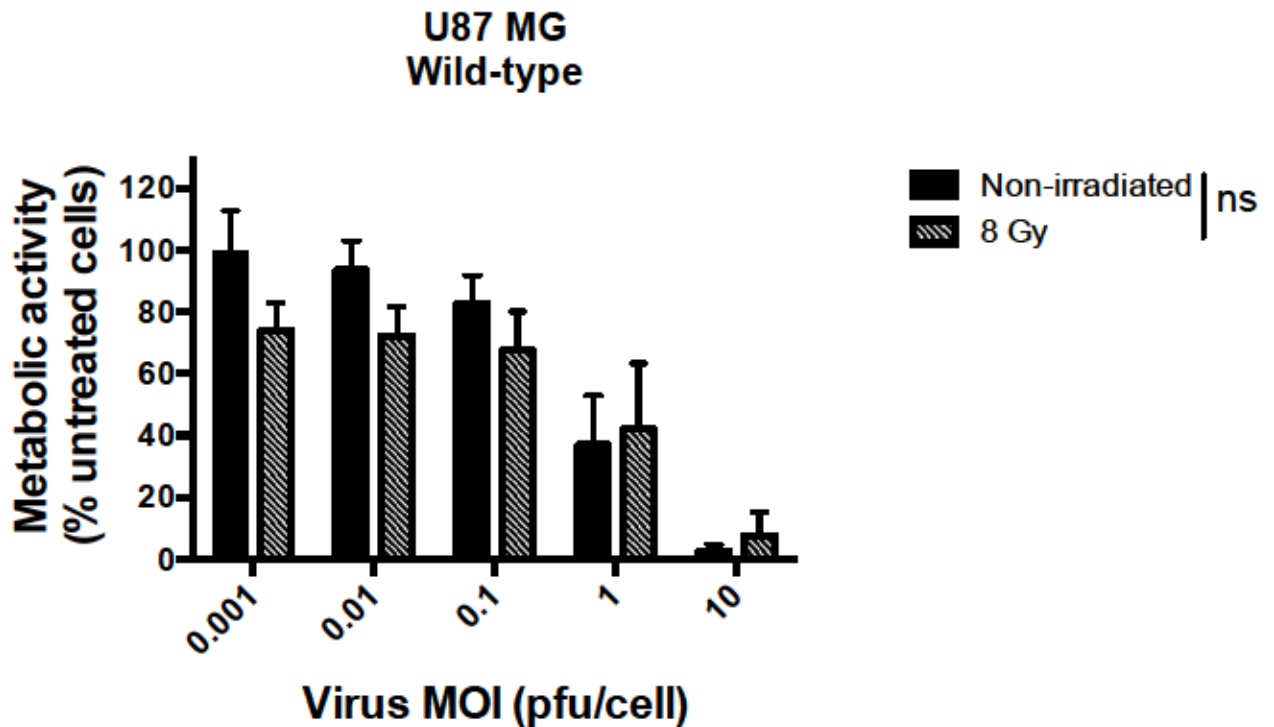
Subconfluent U87 cells were irradiated with 8 Gy or mock-irradiated. Cells were infected in triplicate with ΔF4LΔJ2R VACV or mock- (PBS-) infected at 6 h.p.ir. with serial dilutions of virus at MOIs of 10 pfu/cell to 0.001 pfu/cell. A resazurin-based metabolic assay was performed 72 h.p.i.. Cell viability is shown as percent fluorescence compared to mock (PBS)- infected, non-irradiated cells. Points plotted represent mean titres +/- S.E.M. from three independent experiments. Increased cell killing was seen in combination treated groups at virus MOIs of 0.001 pfu/cell to 1 pfu/cell (t-test, $p < 0.05$).



MOI (pfu/cell)	0.001	0.01	0.1	1	10
P-value (non-irradiated versus 8 Gy)	0.004	0.007	0.005	0.02	0.03

Figure 2.13. Combination IR with ΔF4LΔJ2R VACV infection increased cell killing of U-118 MG cells.

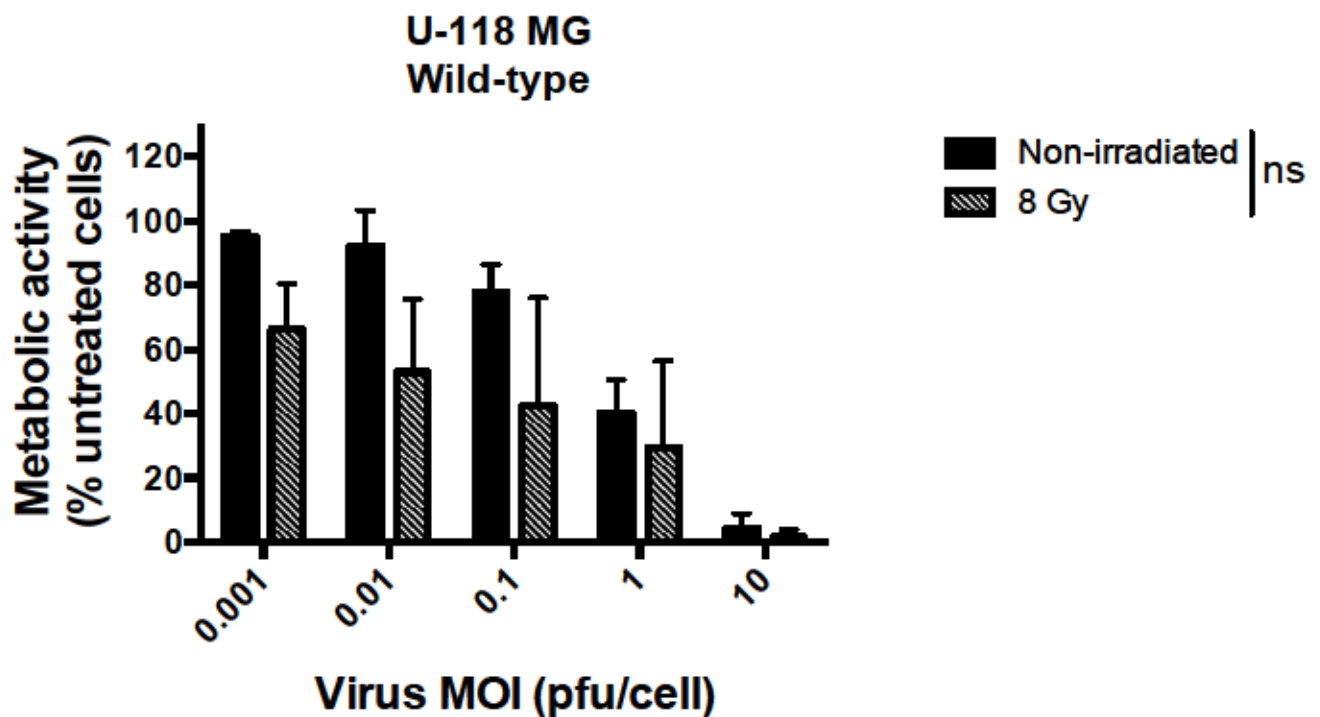
Subconfluent U-118 MG cells were irradiated with 8 Gy or mock-irradiated. Cells were infected in triplicate with ΔF4LΔJ2R VACV or mock (PBS)-infected at 6 h.p.ir. with serial dilutions of virus at MOIs of 10 pfu/cell to 0.001 pfu/cell. A resazurin-based metabolic assay was performed 72 h.p.i. Cell viability is shown as percent fluorescence compared to mock (PBS)-infected, unirradiated cells. Points plotted represent mean titres +/- S.E.M. from three independent experiments. Increased cell killing was seen in all combination treated groups (t-test, $p < 0.05$).



MOI (pfu/cell)	0.001	0.01	0.1	1	10
P-value (wild-type versus $\Delta F4L\Delta J2R$)	0.06	0.05	0.17	0.75	0.33

Figure 2.14. Combining IR with wild-type VACV infection did not significantly increase cell killing in U-87 MG cells.

Subconfluent U87 cells were irradiated with 8 Gy or mock-irradiated. Cells were infected in triplicate with wild-type VACV or mock (PBS)-infected at 6 h.p.i. with serial dilutions of virus at MOIs of 10 pfu/cell to 0.001 pfu/cell. A resazurin-based metabolic assay was performed 72 h.p.i. Cell viability is shown as percent fluorescence compared to mock (PBS)-infected, unirradiated cells. Points plotted represent mean titres \pm S.E.M. from three independent experiments. No increased cell killing was seen in combination treated groups compared to non-irradiated, wild-type VACV-infected cells (t-test, $p > 0.05$).



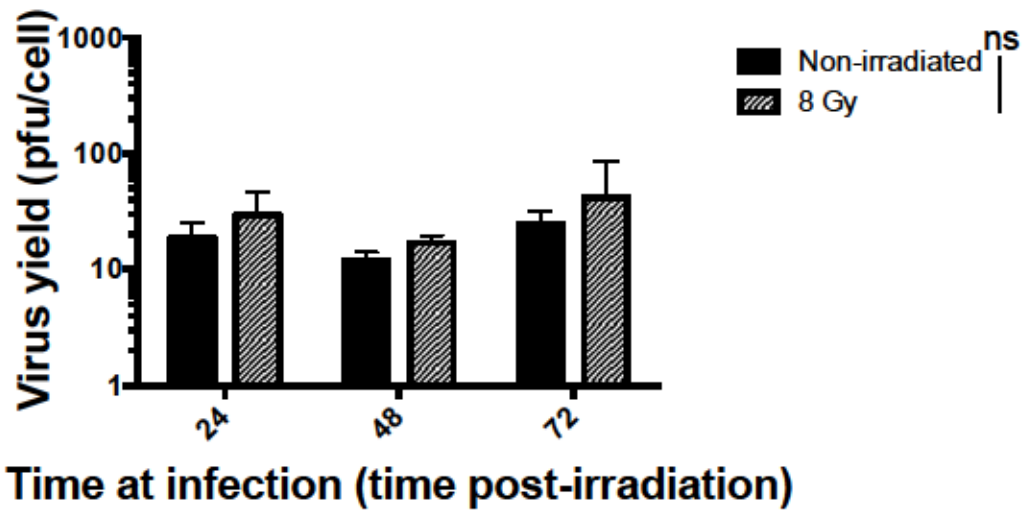
MOI (pfu/cell)	0.001	0.01	0.1	1	10
P-value (wild-type versus $\Delta F4L\Delta J2R$)	0.02	0.05	0.15	0.55	0.37

Figure 2.15. Combination IR with $\Delta F4L\Delta J2R$ VACV infection did not significantly increase cell killing of U-118 MG cells, except at the lowest MOI.

Subconfluent U-118 MG cells were irradiated with 8 Gy or mock-irradiated. Cells were infected in triplicate with wild-type VACV or mock (PBS)-infected at 6 h.p.i. with serial dilutions of virus at MOIs of 10 pfu/cell to 0.001 pfu/cell. A resazurin-based metabolic assay was performed 72 h.p.i. Cell viability is shown as percent fluorescence compared to mock (PBS)-infected cells. Points plotted represent mean titres \pm S.E.M. from three independent experiments. No increased cell killing was seen in combination treated groups compared to non-irradiated, wild-type VACV-infected cells, except at the lowest MOI (t-test, $p < 0.05$).

A

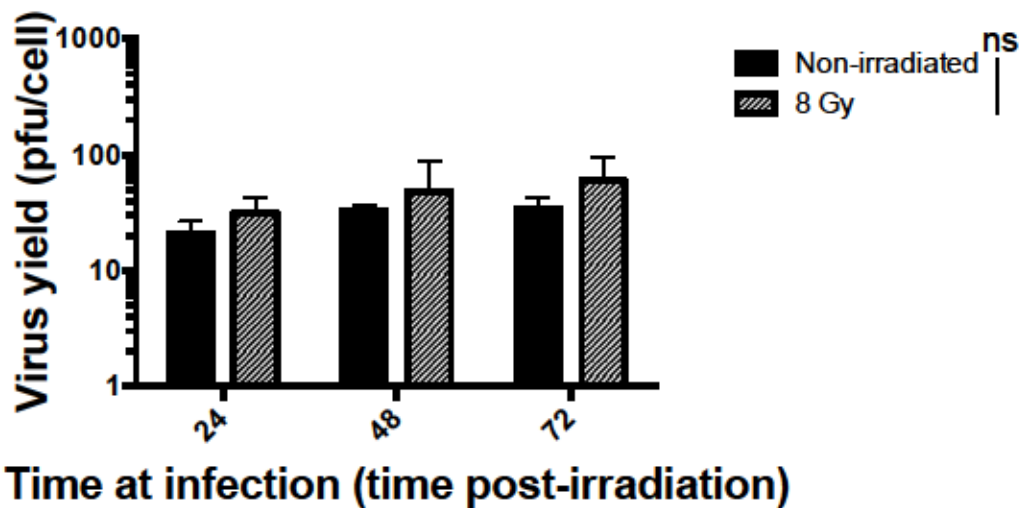
**U87 MG
ΔF4LΔJ2R**



	24 hour		48 hour		72 hour	
	Non-irradiated	8 Gy	Non-irradiated	8 Gy	Non-irradiated	8 Gy
Mean (pfu/cell)	19	30	12	17	24	41
P-Value (non-irradiated versus 8 Gy)	0.34		0.07		0.55	

B

**U87 MG
Wild-type**



	24 hour		48 hour		72 hour	
	Non-irradiated	8 Gy	Non-irradiated	8 Gy	Non-irradiated	8 Gy
Mean (pfu/cell)	21	31	33	48	35	60
P-Value (non-irradiated versus 8 Gy)	0.22		0.54		0.28	

Figure 2.2. Increasing time to infection post-irradiation does not reduce

Δ F4L Δ J2R or wild-type virus yield in U-87 MG cells

Subconfluent U-87 cells were exposed to 8 Gy or mock-irradiated, and infected with Δ F4L Δ J2R (A) or wild-type (B) VACV at time points of 24h, 48h, and 72h post-irradiation.

An MOI of 3 pfu/cell was used and infected cells were harvested at 24 h.p.i. to assess virus yield following a single round of replication. Virus was titred on BSC40 cells.

Results plotted represent means +/- S.E.M. of three independent experiments.

**CHAPTER 3. ESTABLISHING PLATFORM FOR
COMBINATION THERAPY USING VACV AND EXTERNAL
BEAM RADIATION**

3.1. MATERIALS/METHODS

All animal work was approved by the University of Alberta Health Sciences Animal Care and Use Committee or the Cross Cancer Institute Animal Care Committee in accordance with the guidelines from the Canadian Council on Animal Care (CCAC).

3.1.1. Cell preparation for *in vivo* injection

U-87 MG cells (gift of Dr. Roseline Godbout, University of Alberta) at low passage number were cultured in DMEM supplemented with 10%, 2 mM L-glutamine, 0.1 mg/mL penicillin, 100 U/mL streptomycin, and 250 µg/mL Amphotericin B. Cells were trypsinized, pooled, pelleted by centrifugation, and washed twice in cold 1X PBS. Resuspended cells were counted, centrifuged, and resuspended in required volume of 1X PBS for a final cell density of 1×10^6 cells/50 µl PBS.

3.1.2. *In vivo* U-87 MG subcutaneous radiation marker study

Female NIH III mice were obtained from Charles River at 6-8 weeks old and acclimatized for one week. Mice were anesthetized with isoflurane and injected bilaterally into each flank with 2.5×10^6 U-87 MG cells in 100 µl PBS (8 mice) or 1.25×10^6 cells in 50 µl PBS (4 mice). Tumour growth was monitored using twice weekly caliper measurements. When tumours reached sizes of $\sim 1000 \text{ mm}^3$, they were treated with 2 Gy or 10 Gy image-guided targeted radiation using the X-Strahl Small Animal Radiation Research Platform (SARRP) (details of irradiation are described in the results section). At time points of 1h, 6h, 12h, 24h, 48h, and 7 days (d) post-irradiation, mice were sacrificed by CO₂ euthanasia and tumours removed and fixed in 10% neutral-buffered formalin for 24-48 hours. Formalin-fixed tumours were

embedded in paraffin blocks by Dr. Kathryn Graham at the Alberta Cancer Research Biobank at the Cross Cancer Institute.

3.1.3. Immunohistochemical staining of U-87 MG radiation markers

Formalin-fixed and paraffin-embedded (FFPE) tumours were cut into 5 micron sections and mounted onto slides by the Alberta Diabetes Institute Histocore. Sections were deparaffinized and rehydrated using xylene/ethanol washes. Heat-mediated antigen retrieval was performed using a pressure cooker and 10 mM sodium citrate in ddH₂O (pH 6.0) buffer or Tris base (10 mM)/Ethylenediaminetetraacetic acid (EDTA) (1 mM) in ddH₂O (pH 9.0) buffer. Slides were rinsed with Tris-buffered saline (TBS) with 0.025% Triton X-100 and blocked with Dako Antibody Diluent with Background Reducing Component (Dako No. S3022). Slides were probed overnight at 4°C with primary antibodies to histone H2A.X (phosphor-ser139) (Abcam, ab-81299) diluted 1/100, p21 (Abcam, ab-109199) diluted to a concentration of 5 µg/mL, p53-R2 (Abcam, ab-8105) diluted to a concentration of 1 µg/mL, and R2 (Santa Cruz Biotech, sc-10846) diluted to 1/150 in Dako antibody diluent. Slides were rinsed in 1X TBS, 0.025% Triton X-100, and endogenous peroxidase activity was blocked with 0.03% hydrogen peroxide. Slides were probed with a horseradish peroxidase (HRP)-conjugated anti-rabbit secondary antibody (Abcam, ab-6721) or anti-goat secondary antibody (Abcam, diluted in 1:3000 in Dako antibody diluent and counterstained with methyl green added directly to the slide and incubated for three minutes. Slides were dehydrated using ethanol/xylene washes and mounted with coverslips for imaging using an AxioSkop Colour Camera.

3.1.4. *In vivo* subcutaneous radiation and Δ F4L Δ J2R VACV survival

Male NOD.Cg-Prkdc^{scid} Il2rg^{tm1Wjl}/SzJ (NSG) mice (lacking functional T and B lymphocytes) were obtained from the breeding colonies of Dr. Lynne Postovit (Department of Oncology, University of Alberta) and transferred to the Cross Cancer Institute vivarium at 7 weeks of age. Mice were given one week for acclimatization. Mice were injected subcutaneously in the flank with 1×10^6 U-87 MG cells in 50 μ l of PBS. Tumour growth was monitored using twice-weekly caliper measurements of length and width of tumour volume, calculated as $V = \frac{4}{3}\pi(\text{length})(\text{width})^2$. Two mice did not develop tumours and were not included in this study. When tumour diameter reached ~7-8 mm (day 24 post-injection), six tumours were treated with 10 Gy radiation using the X-Strahl Small Animal Radiation Research Platform (SARRP) while mice were under isoflurane anesthesia. Treatment protocol was as follows: using a target dose of 10 Gy: 40% dose with gantry at 80°C, 40% dose with gantry at -90°C, 20% dose with gantry at 0°C, such that 85%-90% tumour volume received 10 Gy radiation. All radiation was delivered using a 5mm x 5mm collimator. The following day, all mice were transported to Health Sciences Laboratory Animal Services (HSLAS) in the Katz Group Centre. At 48 h.p.i.r., tumours were injected with 50 μ l of Δ F4LJ2R VACV (or with a UV-inactivated Δ F4L Δ J2R VACV as a control) in PBS in the following treatment groups: 10 Gy + 1×10^6 pfu mCherry-tagged Δ F4L Δ J2R VACV (3 mice); 10 Gy + F4L Δ J2R (UV- Δ F4L Δ J2R) (3 mice); Δ F4L Δ J2R (3 mice); and UV- Δ F4L Δ J2R (2 mice). Virus injections were repeated at 4 days (d) and 7d post-irradiation. Tumour progression was monitored using twice-weekly caliper measurements and weekly body weight measurements. VACV activity was monitored using fluorescence imaging of mCherry on an IVIS Spectrum In Vivo Imaging System (PerkinElmer) with excitation and emission wavelengths of 587 nm and 610 nm, respectively. Mice were sacrificed by CO₂ euthanasia at tumour volume endpoint (~2500 mm³ or 10% of body weight) or if mice experienced a >20% loss in body weight.

3.2. RESULTS

3.2.1. Bilateral subcutaneous U-87 MG glioma flank model in immunocompromised NIH III mice

A pilot study of subcutaneous U-87 MG tumours in immunocompromised mice was first carried out to establish parameters for the xenograft tumour model, as well as to assess tumour protein expression in response to image-guided radiation therapy (IGRT), delivered using the X-Strahl Small Animal Radiation Research Platform. A mouse model in female NIH III mice (lacking functional T and B lymphocytes) was established, where U-87 MG cells were injected bilaterally into each flank and tumour growth was monitored (Figure 3.1). Body weight was also monitored following tumour injections, as the CCAC dictates that mice must be euthanized if they experience a greater than 20% drop in body weight (Figure 3.1C). As one of the purposes of this study was to establish a subcutaneous flank model of glioma, two different doses of cells were used (2.5×10^6 and 1.25×10^6) to assess whether there was an optimal dose for future animal studies. When tracking tumour growth (tumour volume) post-injection, we saw that there were some tumours with an initial dose of 2.5×10^6 cells that became palpable at an earlier time than those that had an initial dose of 1.25×10^6 cells (~15 days post-injection versus 20 days post-injection) (Figure 3.1A and 3.1B). It appeared, however, that for the most part similar tumour growth kinetics were seen in animals treated with both doses, with comparable growth rates once tumours had become palpable, and most tumours approaching $\sim 1000 \text{ mm}^3$ on or before 30 days post-injection (Figure 3.1A and 3.1B). We therefore concluded that the subcutaneous flank model of U-87 MG tumour was an efficient model, with rapid tumour growth and easily measurable tumours. We did observe, however, that bilateral tumours did not always grow at the same

rate on each flank; as such we opted to use a unilateral flank model with a cell dose of 1×10^6 cells in future animal studies testing survival.

3.2.2. SARRP-mediated image-guided radiation therapy (IGRT) of bilateral subcutaneous U-87 MG tumours in immunocompromised NIH III mice

Once tumours were established in our NIH III animals (3.2) and had approached a tumour size near endpoint ($\sim 1000 \text{ mm}^3$), the tumours were treated with 2 Gy or 10 Gy IGRT; these doses were chosen as 2 Gy is the dose given in a standard clinical fraction, while 10 Gy is the cumulative clinical dose typically given in one week (5 x 2 Gy fractions). Treatment planning (number of isocentres, dose at isocentre) can be seen in Table 3.1; radiation was delivered in an arc, with a gantry rotation from -90° to 90° . The number of isocentres varied based on the size and shape of the tumour at time of treatment; this ensured that radiation was delivered to the maximal tumour volume. The dose per isocentre was determined as the dose required for $\sim 80\%$ of the tumour to receive the target dose of 2 Gy or 10 Gy (as per MuriPlan-generated dose volume histogram; Figure 1.7E). At the indicated time points mice were euthanized (see schematic in Figure 3.2, and experimental plan in Table 3.1) and tumours excised, then formalin-fixed and paraffin-embedded (FFPE). Sections were stained immunohistochemically for markers of radiation damage.

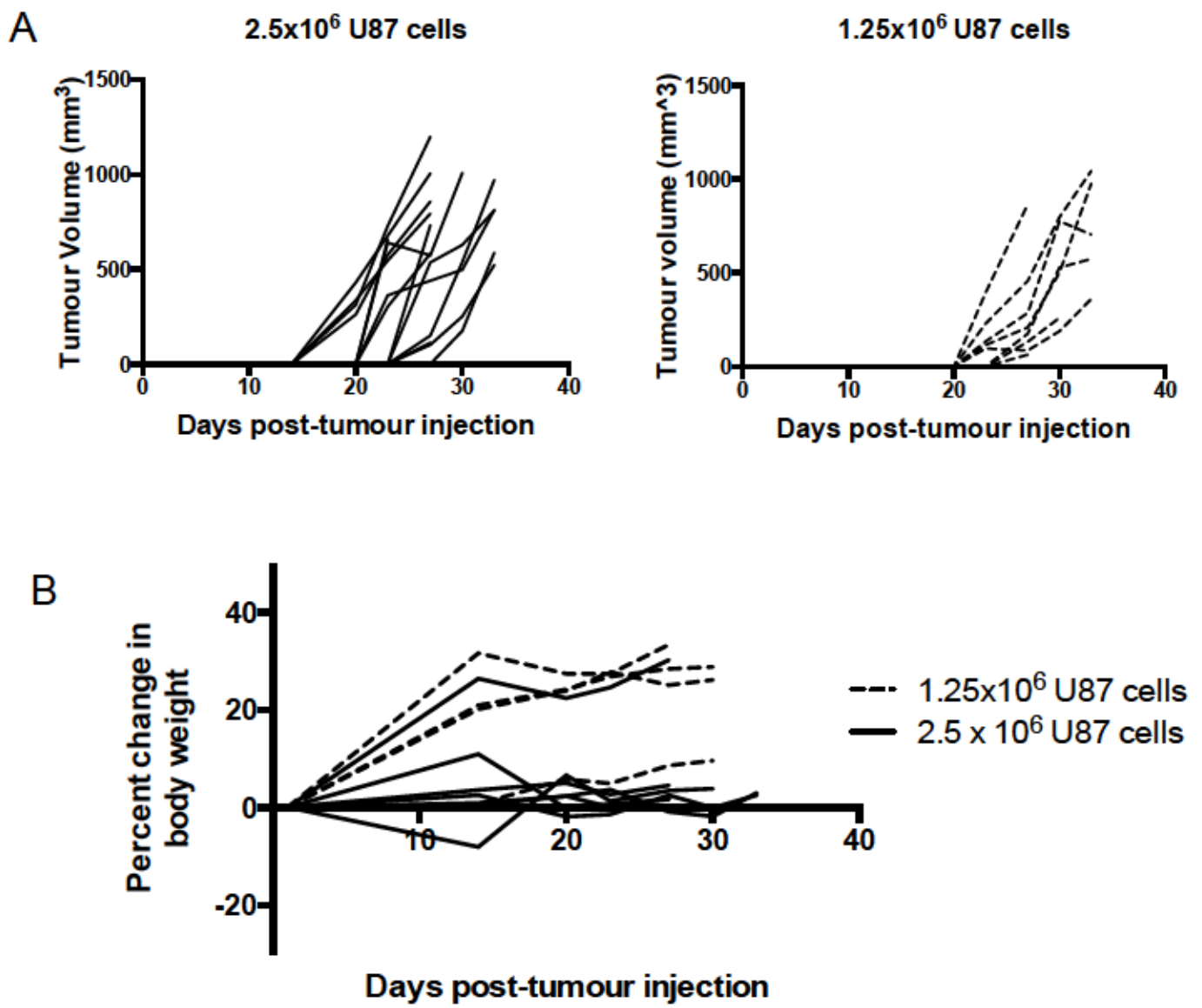
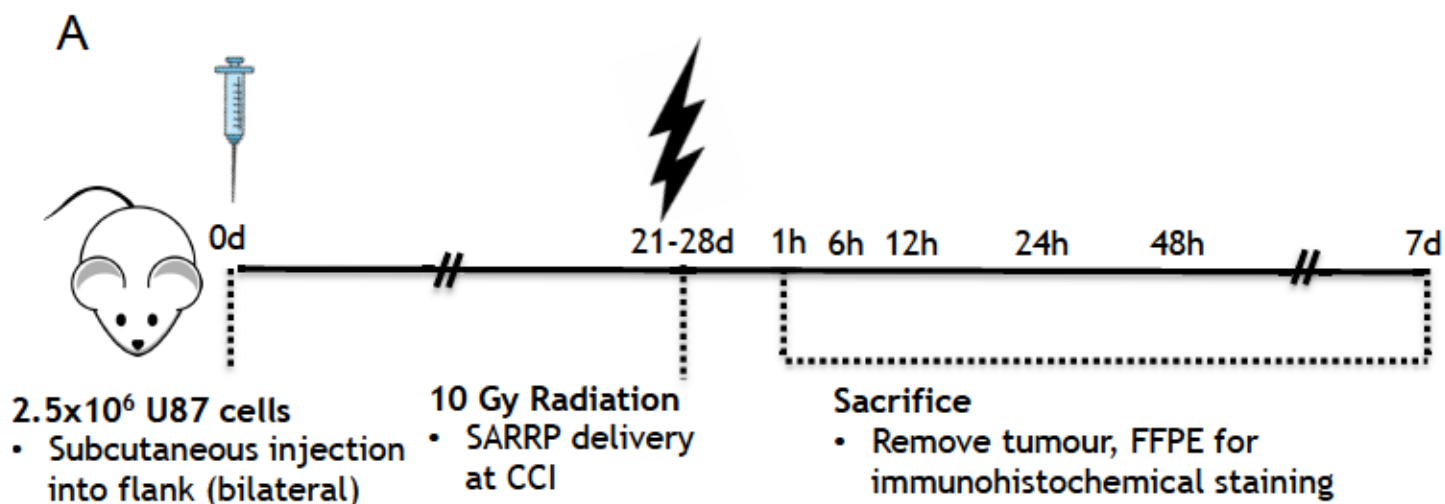


Figure 3.1. Growth kinetics of untreated subcutaneous bilateral U87 xenograft tumours in NIH III mice.

Immunocompromised NIH III mice (6–8 weeks old) were injected bilaterally into each flank with 2.5×10^6 (8 mice) or 1.25×10^6 (4 mice) U-87 MG cells in PBS. (A) Tumour growth (measured using calipers) and (B) body weight was assessed twice weekly, up to time of radiation treatment (Figure 3.2).



B

Table 3.1. Small Animal Radiation Research Platform (SARRP) treatment plans of U-87 MG bilateral flank tumours.

Timepoint*	Target dose (Gy)	Mouse nomenclature**	Flank	Number of isocentres	Dose per isocentre (cGy)
Untreated control	0	1.2	Right	N/A	N/A
1 hr	2	2.1	Right	2	150
	10	1.4	Left	1	1000
6 hr	2	1.1	Left	3	140
	10	2.4	Right	2	800
12 hr	2	2.2	Left	2	150
	10	2.2	Right	2	750
24 hr	2	1.3	Right	2	175
	10	1.3	Left	2	750
48 hr	2	3.4	Left	2	160
	10	3.2	Right	2	750
7 days	2	3.3	Right	1	200
	10	3.1	Right	2	750

* Time to euthanasia relative to time at irradiation

** Mouse #3.1, 3.2, 3.3, 3.4 received 1.25x10⁶ cells bilaterally. All others received 2.5x10⁶ cells at tumour injection

Figure 3.2. SARRP treatment planning in subcutaneous bilateral flank model of human GBM.

(A,B) Timeline for radiation treatment. Immunocompromised female NIH III mice with bilateral U-87 MG tumours in the flank were monitored for tumour growth. Once tumours approached sizes of $\sim 1000 \text{ mm}^3$, selected tumours were treated with either 2 Gy or 10 Gy targeted IR using the X-Strahl Small Animal Research Radiation Platform (SARRP). (B) Mice were sacrificed at time points of 1h, 6h, 12h, 24h, 48h, and 7d post-irradiation, and tumours were removed and formalin-fixed/paraffin-embedded (FFPE) for immunohistochemical analysis.

3.2.3. DNA damage and radiation response in subcutaneous U-87 MG tumours treated with SARRP image-guided radiation therapy (IGRT)

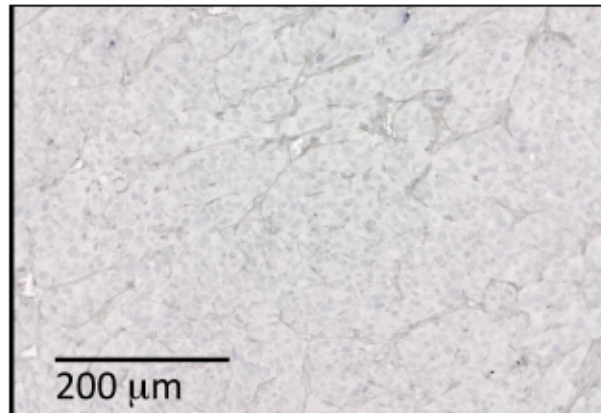
We first assessed γ H2AX expression at 1 hour following exposure to IR. γ H2AX is a sensitive sensor of double-strand DNA breaks (DSBs) and allowed us to monitor DNA damage in tumours treated with 2 Gy or 10 Gy IGRT at 1 h.p.ir. This was used to validate our approach for SARRP-mediated IGRT delivery, as well as to assess the DNA damage inflicted by up to 10 Gy IR. As γ H2AX is a rapid sensor of DNA damage, with γ H2AX clusters forming within 10-30 minutes post-irradiation, γ H2AX expression was only assessed at the 1-hour time point. When compared to a non-irradiated control, γ H2AX expression was seen to be elevated with 2 Gy IGRT, and even further elevated with 10 Gy IGRT (Figure 3.3), indicating an induction of DNA damage following SARRP-mediated radiation delivery. Expression of p21, a p53-mediated marker of senescence, was used as a marker of cellular response to radiation-induced damage. Our results showed that following delivery of 10 Gy IGRT, p21 levels increased at 6 h.p.ir. up to 48 h.p.ir., with the greatest increase in p21 expression seen at 12 h.p.ir (Figure 3.4). Together, these results indicate that the SARRP-delivered dose of 10 Gy was sufficient to induce both DNA damage and radiation response in the subcutaneous U-87 tumours.

P53-R2 is another protein with expression regulated by p53, and is upregulated in response to DNA damage as a means of providing the cell with dNTPs to enable repair of radiation-induced DNA damage. In U-87 tumour sections treated with 10 Gy IGRT, probing for p53-R2 revealed an upregulation of expression at 24 h.p.ir., with expression remaining upregulated compared to the non-irradiated tumour at 48 h.p.ir. (Figure 3.5). Analysis of the protein expression of R2, the non-p53-regulated small ribonucleotide reductase subunit, also revealed increased expression following exposure to 10 Gy IR: increased R2

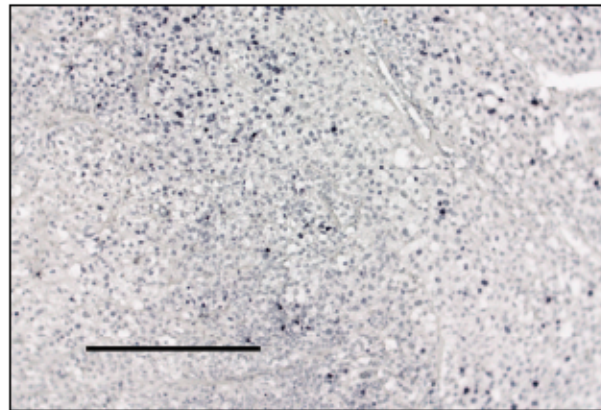
expression was first seen at 6 h.p.ir., with increase in expression peaking at 24 h.p.ir. to 48 h.p.ir., and levels remaining elevated relative to the non-irradiated tumour up to 7 days post-irradiation (d.p.ir.) (Figure 3.6). These results indicate that in addition to the DNA damage and damage response induced by the IGRT, there is also an increase in the expression of the ribonucleotide reductase small subunit, and likely a consequent increase in cellular dNTP synthesis and possibly dNTP pools. This increased dNTP synthesis would facilitate DNA repair, however we propose that increased dNTPs could also provide a cellular environment conducive to the growth of our $\Delta F4L\Delta J2R$ VACV, which relies on cellular R2 and cellular dNTP levels for viral replication.

γ -H2A.X

Non-irradiated



2 Gy, 1 h.p.ir.



10 Gy, 1 h.p.ir.

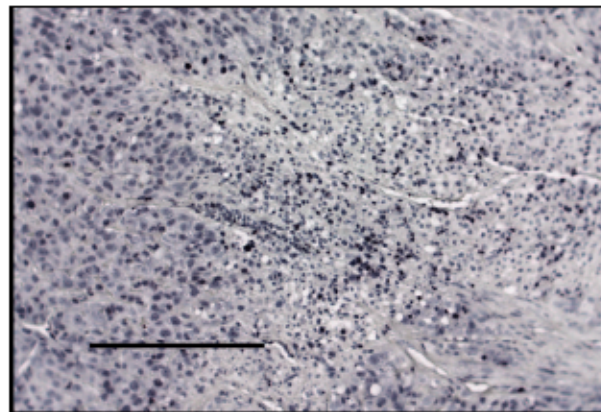
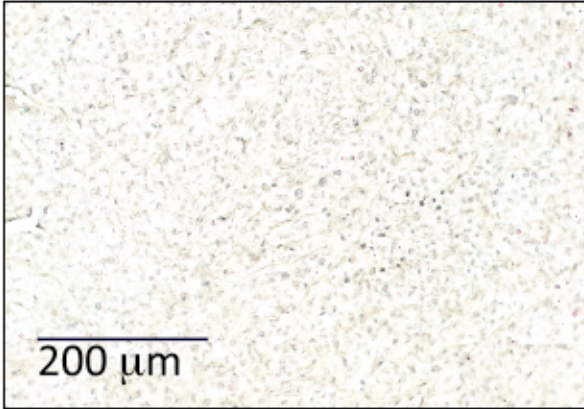


Figure 3.3. γ -H2AX expression *in vivo* increased at 1 hour post-irradiation following treatment with 2 Gy or 10 Gy targeted IR.

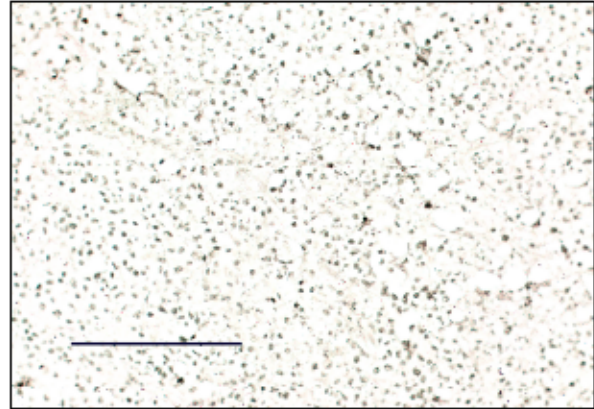
U-87 MG tumours (Figure 3.2) were treated with 2 Gy or 10 Gy IR and excised from the animal one hour later. FFPE sections from these tumours were stained using an α -histone H2AX (phosphor-S139) antibody and HRP-conjugated secondary antibody, with colour developed using 3'3'-Diaminobenzadine tetrahydrochloride (DAB) with cobalt metal enhancer. Positive cells are stained black.

p21

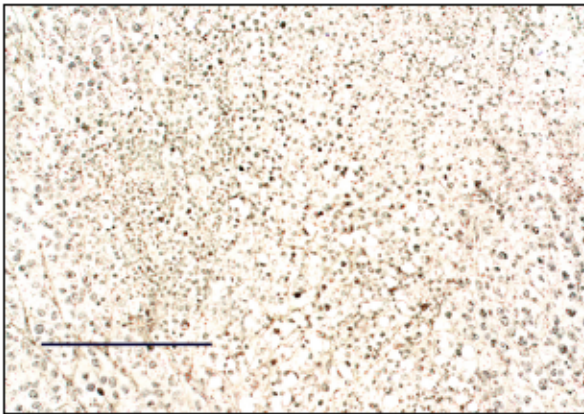
10 Gy, 1 h.p.ir.



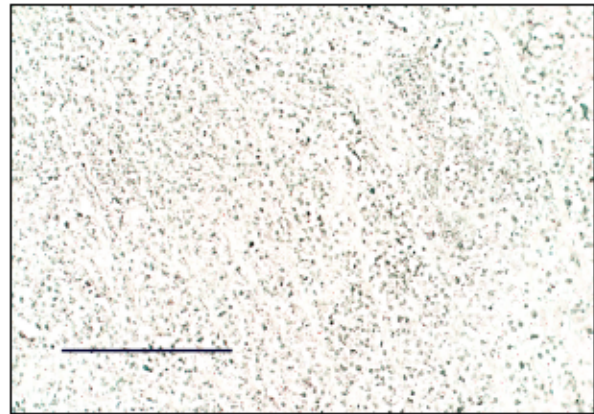
10 Gy, 6 h.p.ir.



10 Gy, 12 h.p.ir.



10 Gy, 48 h.p.ir.



Non-irradiated

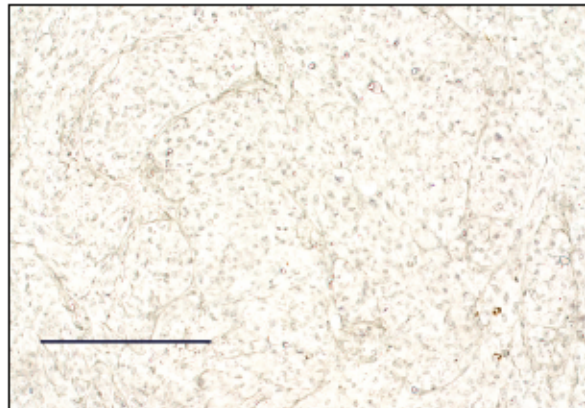
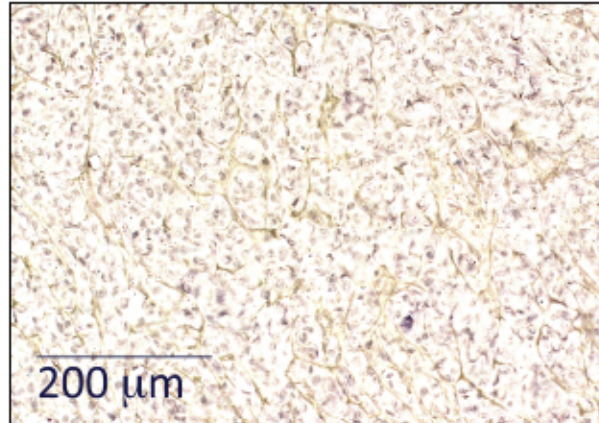


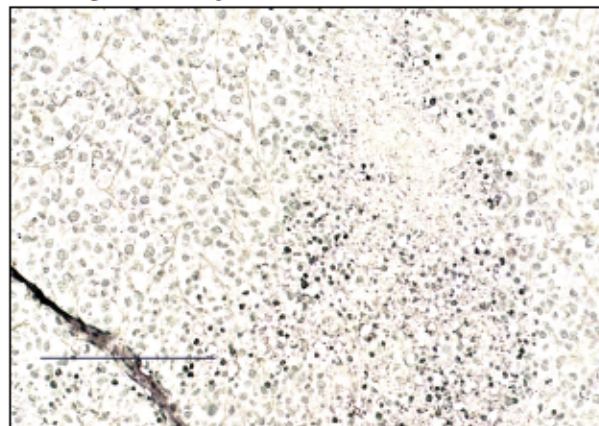
Figure 3.4. p21 expression *in vivo* increased relative to non-irradiated tumour at 6 to 48 hours following treatment with 10 Gy radiation.

U-87 MG tumours (Figure 3.2) were treated with 10 Gy IR and FFPE at 6 hours to 48 h.p.ir. Tumours were sectioned and stained using an α -p21 antibody and HRP-conjugated secondary antibody, with colour developed using DAB cobalt metal enhancer. Sections were counter-stained with methyl green. Field of view shown is representative of whole section. Positive cells are stained dark brown/blue.

Non-irradiated



10 Gy, 24 h.p.ir.



10 Gy, 48 h.p.ir.

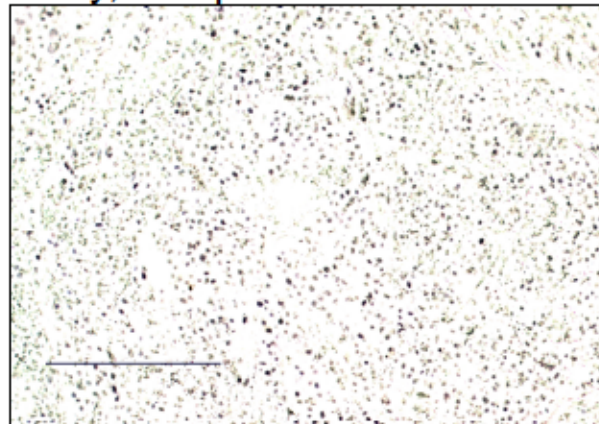
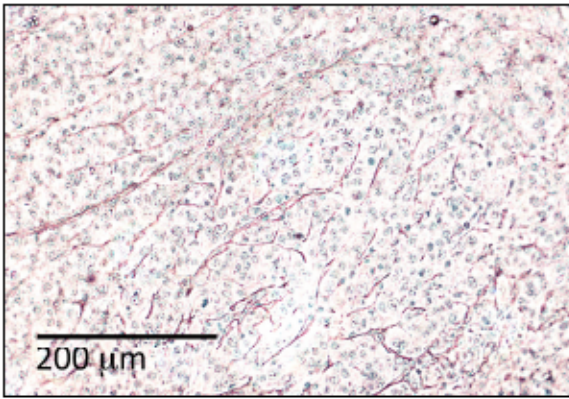


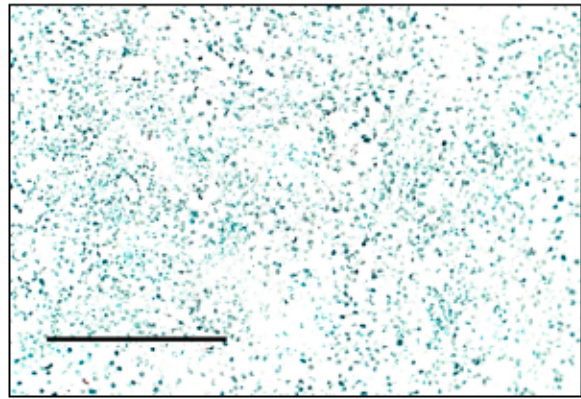
Figure 3.5. p53-R2 expression *in vivo* increased relative to non-irradiated tumour up to 48 hours following treatment with 10 Gy radiation.

U-87 MG tumours (Figure 3.2) were treated with 10 Gy IR then at 24 hours and 48 h.p.ir, tumours were excised and FFPE. Sections were prepared and stained with an α -p53R2 antibody and HRP-conjugated secondary antibody, with colour developed using DAB with cobalt metal enhancer. Sections were counter-stained with methyl green. Field of view is representative of whole section. Positive cells are stained dark brown/blue.

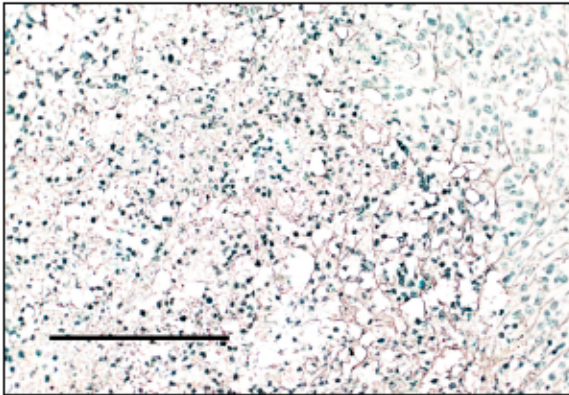
Non-irradiated



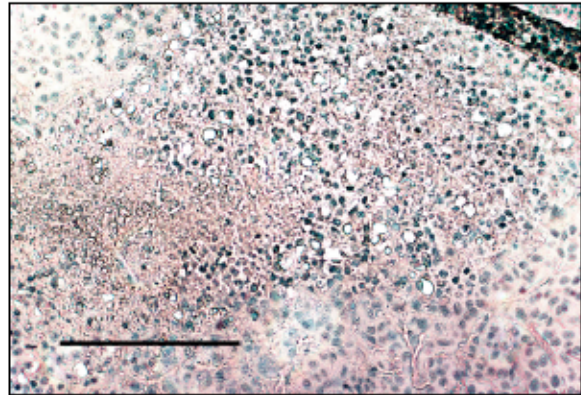
10 Gy, 6 h.p.ir.



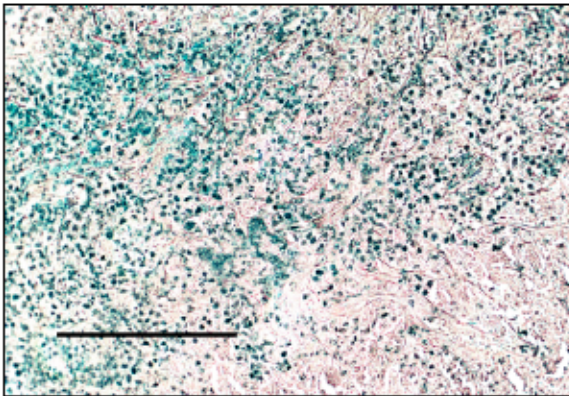
10 Gy, 12 h.p.ir.



10 Gy, 24 h.p.ir.



10 Gy, 48 h.p.ir.



10 Gy, 7 d.p.ir.

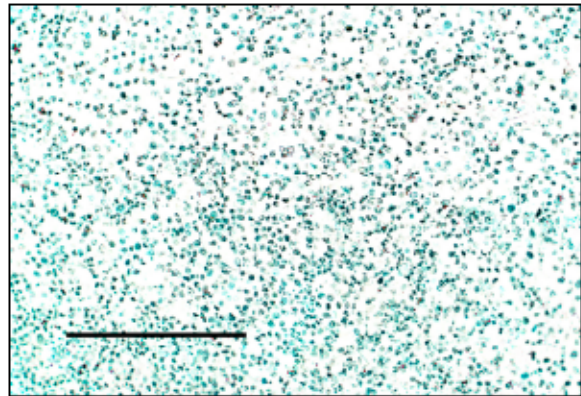


Figure 3.6. R2 expression *in vivo* following 10 Gy radiation compared to non-irradiated control.

U-87 MG tumours (Figure 3.2) irradiated with 10 Gy IR were excised at 1 hour to 7 days post-irradiation, then FFPE sections were prepared and stained using an α -R2 antibody and HRP-conjugated secondary antibody. Colour was developed using a DAB cobalt metal enhancer. Sections were counter-stained with methyl green. Field of view is representative of whole section. Positive cells are stained dark brown/blue. There were some discrepancies in colour of imaged sections despite uniform treatment through the staining protocol - these discrepancies may be due to differential pH exposure throughout handling of the FFPE blocks and sectioning.

3.2.4. Combination 10 Gy IGRT and Δ F4L Δ J2R VACV increased survival and time to tumour progression in pilot study of U-87 MG subcutaneous mouse model

As our U-87 MG marker study suggested that irradiation of tumours may induce an environment supportive of Δ F4L Δ J2R VACV infection, we then undertook a pilot study to assess survival and time to tumour progression of combination 10 Gy/ Δ F4L Δ J2R VACV treated tumours compared to either treatment alone in an immunocompromised, subcutaneous U-87 MG model (Figure 3.7). A dose of 10 Gy was given as it is a non-curative dose that also has clinical relevance, as it is typically the cumulative dose given in one week to patients. Both treatment with Δ F4L Δ J2R VACV alone, as well as the combination of 10 Gy IR with Δ F4L Δ J2R VACV, increased time to tumour progression when compared to 10 Gy alone or non-treated tumours in this experiment (Figure 3.8 A). We also saw improved survival of mice treated with Δ F4L Δ J2R VACV (median survival of 51 days) compared to 10 Gy only (median survival of 35 days) or control mice (median survival of 21 days). A further improved survival was seen in 10 Gy/ Δ F4L Δ J2R VACV treated mice, with a median survival of 80 days (Figure 3.9 A). Taken together, these results suggest that treating U-87 MG tumours with either Δ F4L Δ J2R VACV alone, or with the combination of 10 Gy and Δ F4L Δ J2R VACV may resulted in enhanced tumour regression compared to irradiation alone. However, it should be noted that this was a small pilot experiment that was not designed to achieve statistically significant survival data.

Of note, four mice (1/3 in the 10 Gy group and 3/3 in the combination group) developed radiation-related lesions around 3 weeks post-irradiation (Figure 3.9 B). All lesions cleared on their own within 1-2 weeks with the exception of mouse 1.2 in the combination group, which acquired an infection at the site of the lesion and was euthanized at the advice of Dr. Daina Domahidi, Clinical Veterinarian, HSLAS. Additionally, another mouse (mouse 1.1) in

the combination treatment group experienced a >20% loss of body weight (Figure 3.8 B), and upon euthanasia was found to have tumour spread to the abdominal cavity and the spine. Of note, the mice in the UV- Δ F4L Δ J2R only group also experienced a drop in body weight, however these mice were also experiencing rapid tumour growth. This suggests that weight loss is not a specific indicator of treatment toxicity, but rather of overall health status; stress-related weight loss may also be a result of tumour burden and/or rapid tumour growth.

3.2.5. Δ F4L Δ J2R VACV replication in tumours is maintained up to 150 days post-injection

As our Δ F4L Δ J2R viruses are tagged with fluorescent mCherry, we have the ability to follow replication of the virus by performing *in vivo* and *ex vivo* fluorescence imaging of Δ F4L Δ J2R VACV treated tumours using the Spectrum 200 In Vivo Imaging System (IVIS, Xenogen). In the pilot experiment, mCherry signal was detectable from time of first imaging (9 days after the first virus injection (d.p.i.), 4 days after last virus injection) up to 90 d.p.i. in live mice (Figure 3.10 A). Notably, there was less signal seen in Mouse 1.1 and 1.3 (both treated with combination 10 Gy/ Δ F4L Δ J2R VACV) than in the Δ F4L Δ J2R VACV treated mice at the same time point; this is likely due to the smaller tumour sizes in the combination treated group, although it could also be due to quenching of fluorescence because of the depth of the tumour. At the end of the experiment (150 d.p.i.), the 2 remaining mice were euthanized and their tumours were *ex vivo* imaged. mCherry fluorescence was still detectable in both the Δ F4L Δ J2R VACV-treated tumour and the 10 Gy/ Δ F4L Δ J2R VACV-treated tumour (Figure 3.10 B). This prolonged mCherry signaling indicates that, in addition to the prolonged survival and increased time to tumour progression, the virus may still be actively

replicating and could be maintaining tumour control. Additionally, mCherry signaling in irradiated tumours throughout the experiment suggests robust virus replication even in irradiated tumours, suggesting that virus replication is not inhibited by pre-treatment with radiation.

It should also be noted that there was some mCherry signal detected outside of the tumour, especially at 9 d.p.i. One possible explanation is that there was some autofluorescence beyond that subtracted as background fluorescence. As the non-tumour specific signal was not seen at the same tissue site on subsequent days; and as at this time point it had been only 4 days since the final virus injection; another explanation is that the signal seen at 9 d.p.i. was due to non-tumour-specific virus infection. This may have occurred due to some systemic spread of the virus following virus injections. As mCherry is under the control of a synthetic early/late promoter and its expression is independent of virus replication, the mCherry signal may indicate a non-productive infection of normal tissues.

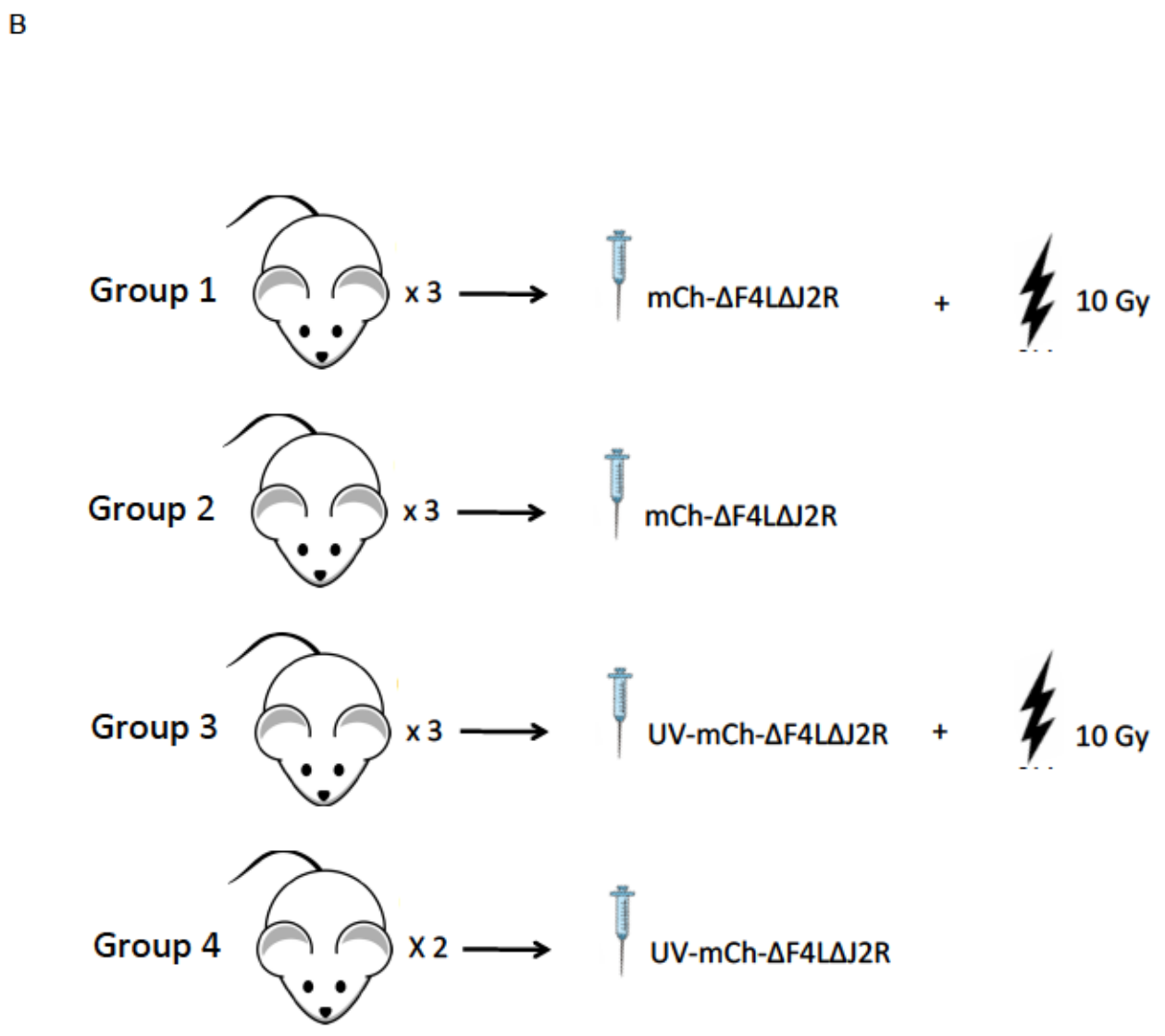
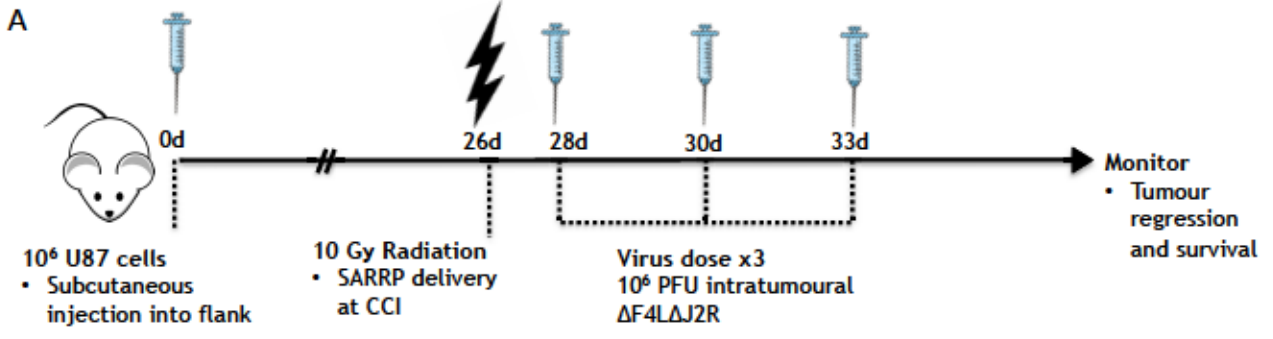
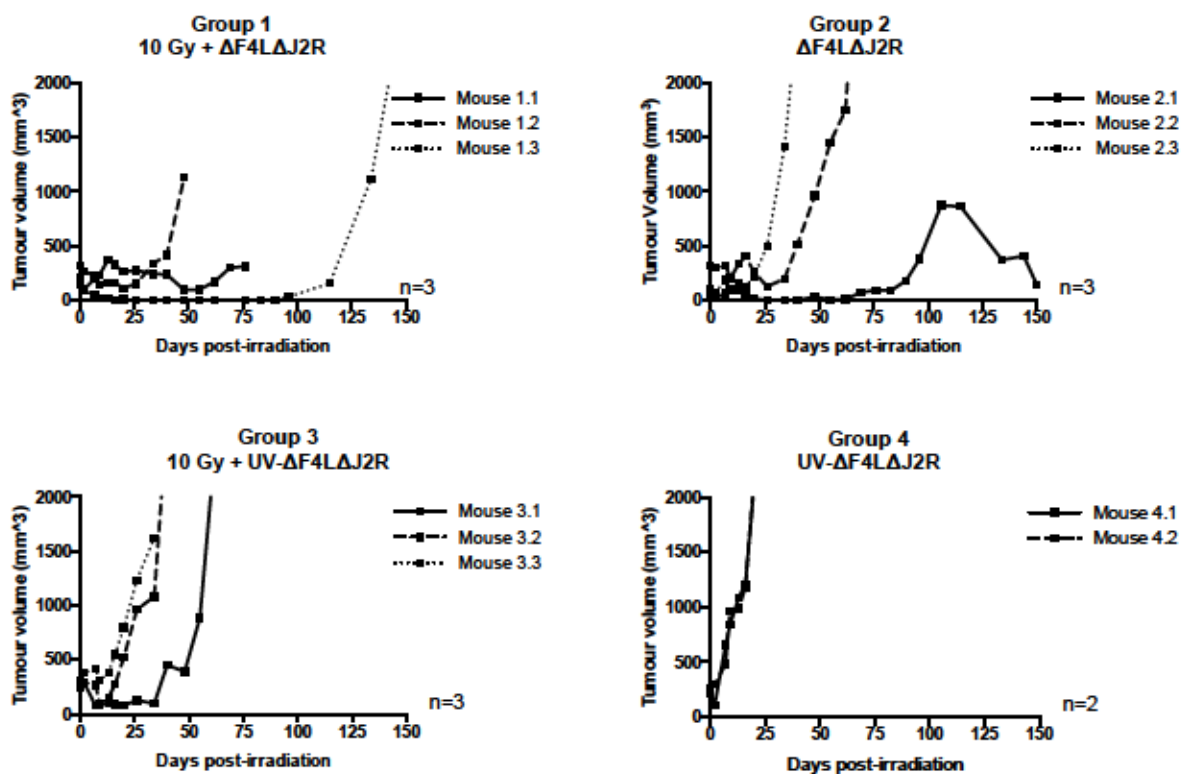


Figure 3.7. Flow chart for combination image-guided radiation therapy (IGRT) and $\Delta F4L\Delta J2R$ VACV therapy of U-87 subcutaneous flank model.

(A) Immunocompromised NSG mice (8 weeks old) were injected in the left flank with 1×10^6 U-87 MG cells. Tumour growth was monitored using calipers. Once tumours approached sizes of ~7-8 mm in diameter, half the mice were treated with 10 Gy IR targeted to the tumour using the X-Strahl SARRP. Treatment planning was standardized as per a plan developed by Kim Rans (University of Alberta, Department of Oncology) with Brittany Umer (graduate student with Dr. David Evans, Department of Medical Microbiology and Immunology, University of Alberta) for the treatment of orthotopic breast tumours in an immunocompromised mouse model. For each irradiated tumour, 85%-90% of tumour volume received a dose of at least 10 Gy as per the DVH (not shown). At 48 h.p.ir., mice received the first of 3 doses of 1×10^8 plaque-forming units (pfu) of mCherry-tagged $\Delta F4L\Delta J2R$ VACV or UV-inactivated $\Delta F4L\Delta J2R$ VACV (UV- $\Delta F4L\Delta J2R$). Virus injections were repeated at 4 days and 7 days post-irradiation for a total of three doses of 1×10^8 pfu. (B) Treatment groups for survival study of subcutaneous U-87 MG model of combination IGRT and $\Delta F4L\Delta J2R$ VACV therapy.

A

Tumour volumes



B

Body weights

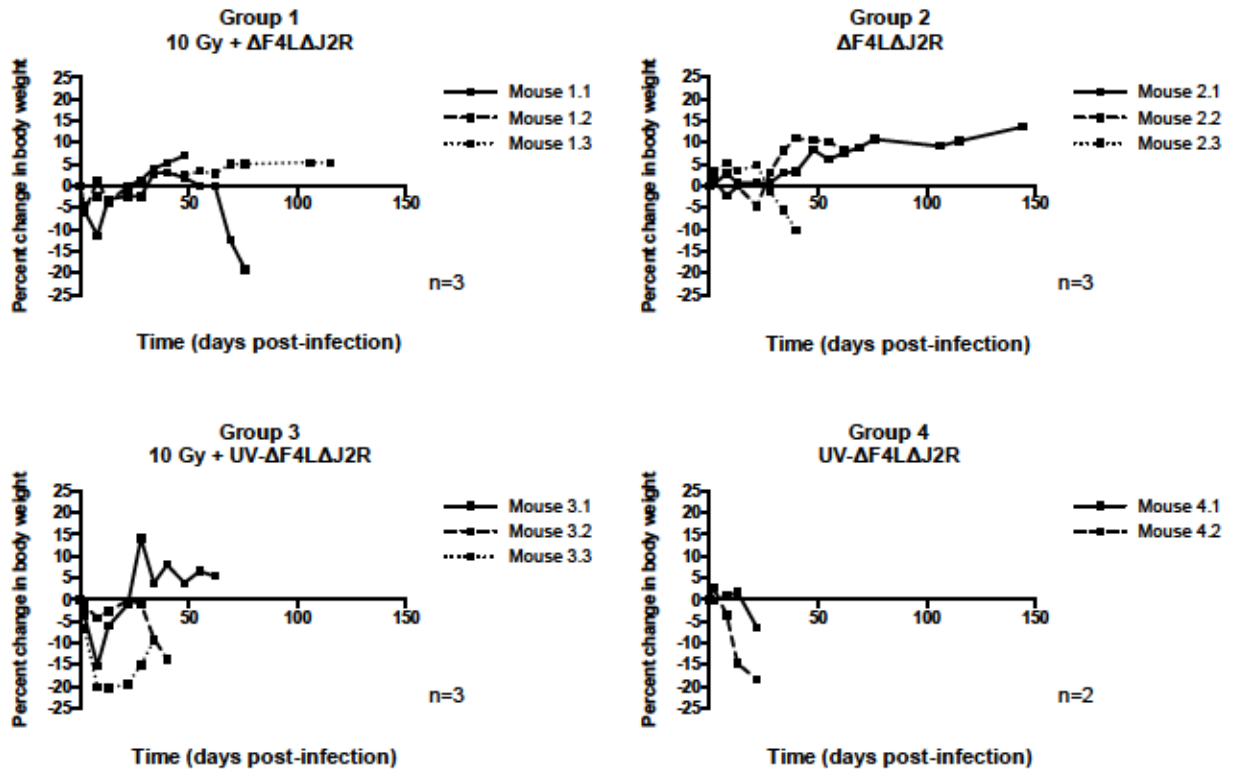
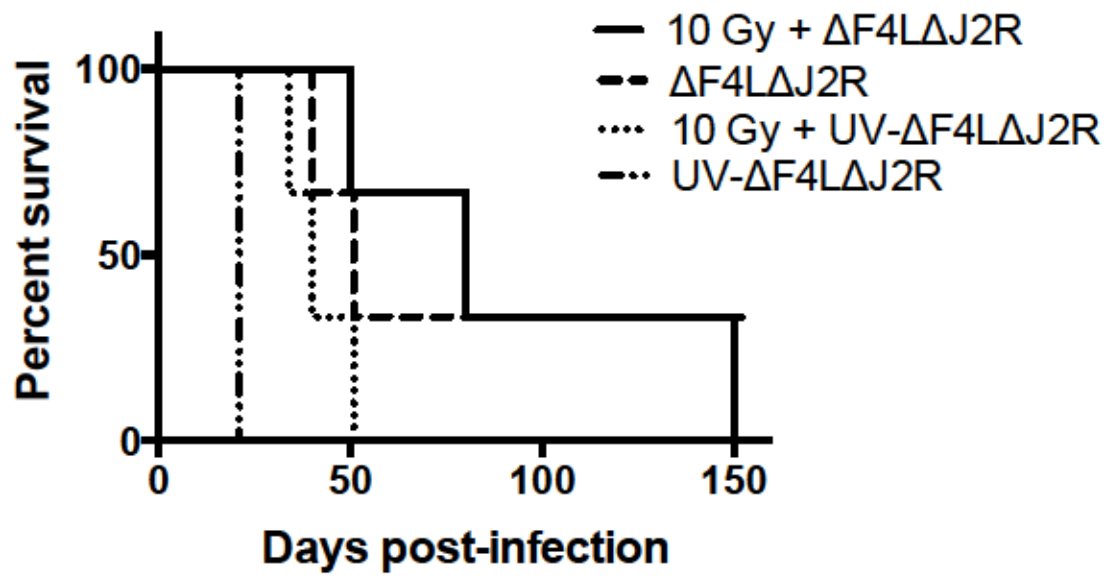


Figure 3.8. Combination 10 Gy IGRT and Δ F4L Δ J2R VACV increased time to tumour progression *in vivo* in pilot study.

NSG mice bearing U-87 MG xenografts were irradiated (or not) with 10 Gy using IGRT (SARRP), then two days later infected with Δ F4L Δ J2R VACV or UV-inactivated Δ F4L Δ J2R VACV (Figure 3.7). (A). Tumour growth was estimated by measuring tumour volumes with calipers twice weekly. Each line represents a different animal. (B) Body weight was measured weekly. Each line represents a different animal. Mice were euthanized (secondary to tumour burden) if a >20% decrease in body weight was observed.

A



B

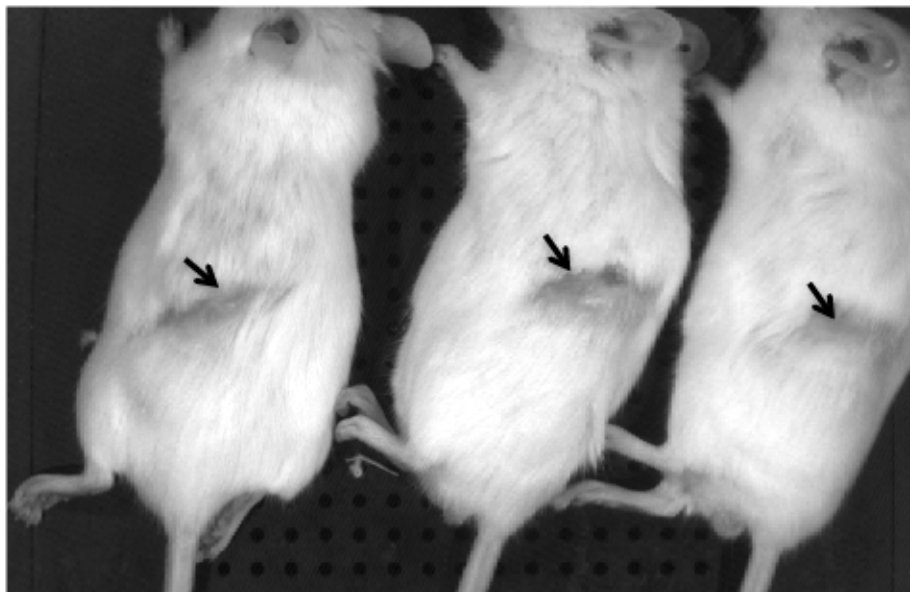


Figure 3.9. Combination treatment with 10 Gy IGRT and Δ F4L Δ J2R VACV

increased overall survival *in vivo* in pilot study of immunocompromised subcutaneous human GBM model.

NSG mice bearing U-87 MG xenografts were irradiated (or not) with 10 Gy using IGRT (SARRP), then two days later infected with Δ F4L Δ J2R VACV or UV- Δ F4L Δ J2R VACV; tumour volumes and animal body weight was monitored with twice-weekly (tumour volume) or weekly (body weight) measurements (Figure 3.7, Figure 3.8). (A) Survival (time to tumour burden endpoint from day of first virus injection, or d.p.i.) was assessed. Endpoint was defined as tumour volume that was greater than 20% of the animal's body weight (as estimated in Figure 3.8). Two mice (mouse 1.1 and mouse 1.2) were sacrificed for reasons secondary to tumour burden at days 50 and 80, respectively. Median survival for each group was as follows: 10 Gy/ Δ F4L Δ J2R = 80 d.p.i (n=3).; Δ F4L Δ J2R = 51 d.p.i (n=3).; 10 Gy/UV- Δ F4L Δ J2R = 40 d.p.i. (n=3); UV- Δ F4L Δ J2R = 21 d.p.i. (n=2). (B) 3/3 mice in the 10 Gy/ Δ F4L Δ J2R VACV group (pictured) and 1/3 mice in the 10 Gy/UV- Δ F4L Δ J2R VACV group (not pictured) developed radiation-induced lesions at 3 weeks post-irradiation, which cleared within 1-2 weeks.

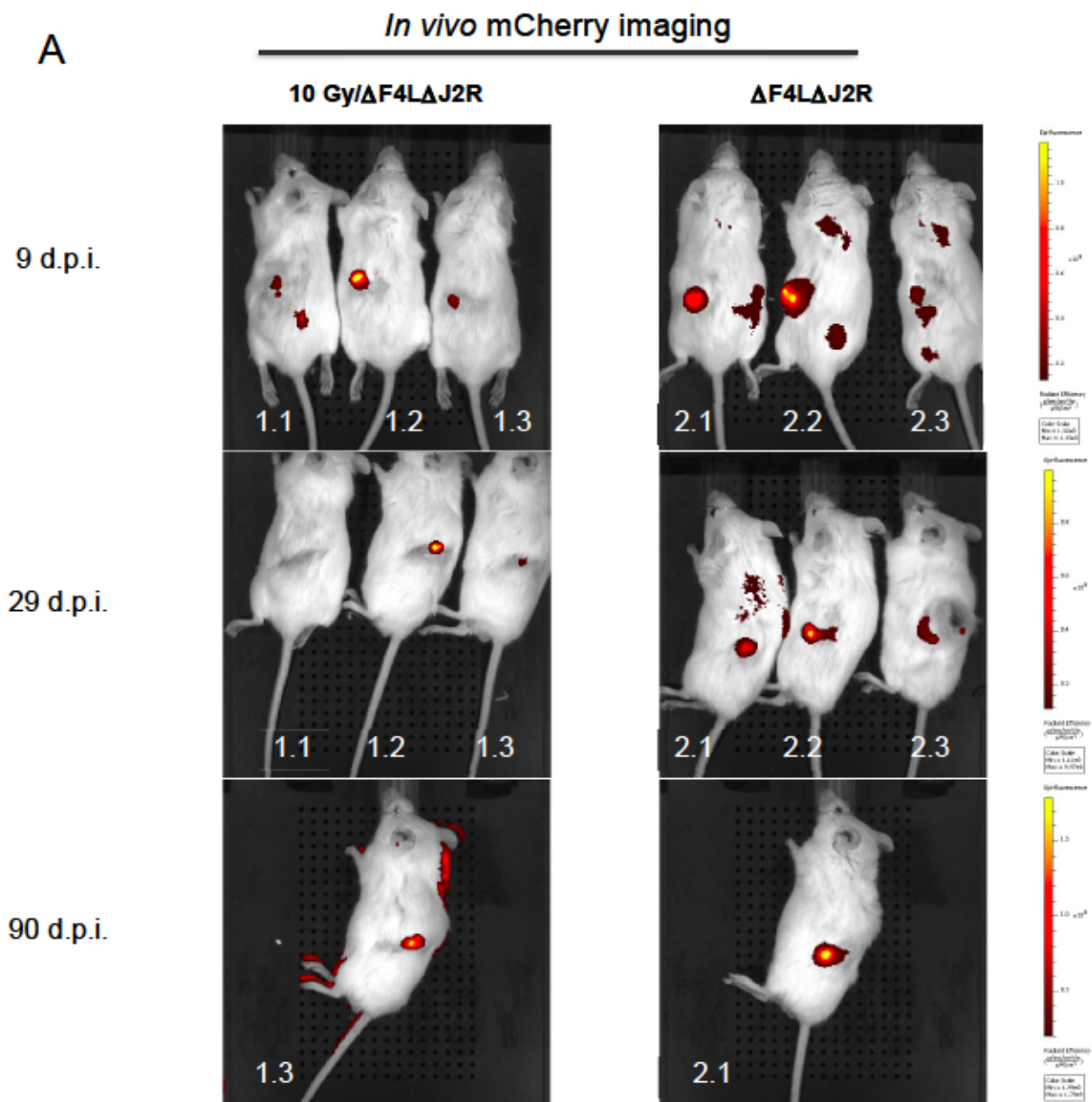


Figure 3.10. mCherry-fluorescence in mCh- Δ F4L Δ J2R VACV-treated animals was visible in tumours up to 150 days post-infection.

Fluorescence of mCherry in Δ F4L Δ J2R VACV-infected cells was imaged using the In Vivo Imaging System (IVIS) Spectrum (Xenogen). All images are to the same scale. (A) *In vivo* mCherry imaging. F4L Δ J2R VACV replication was visible in tumours from 9 days post-initial VACV injection (d.p.i.) up to 90 d.p.i.. No signal above autofluorescence was seen in UV-F4L Δ J2R treated mice (not pictured). (B) *Ex vivo* imaging. Mouse 2.1 (Δ F4L Δ J2R VACV) and mouse 1.3 (10 Gy/ Δ F4L Δ J2R VACV) were euthanized at the end of the experiment (150 d.p.i.), opened, and the tumours were imaged.

CHAPTER 4. DISCUSSION

4.1. DISCUSSION

According to the Canadian Cancer Statistics Report (2015), half of all Canadians will be diagnosed with cancer in their lifetime; of these, 1.7% of men and 1.3% of women will suffer from cancer of the brain/central nervous system [13]. In adults, malignant gliomas are the most common primary brain tumour, while also being characterized by their poor prognosis [6]. GBMs (GBMs), the most aggressive form of malignant glioma, are particularly deadly; while a general cancer diagnosis in Canada has a 5-year survival rate of 63%, the 5-year survival rate of GBMs is under 5% in adults over 45 years of age [13]. The standard of care for malignant glioma has remained much the same for the past decade, wherein maximal tumour volume is surgically excised, followed by post-operative radiotherapy, given in 1.8 Gy - 2 Gy fractions to a total cumulative dose of 58-60 Gy, with TMZ (TMZ) administered concurrent and adjuvant to radiotherapy [9]. The largely unchanged poor prognosis for malignant glioma, however, combined with the relative resistance of many malignant gliomas to the first line treatments of radiation and TMZ, necessitates the need for more and better therapeutic options in the treatment of gliomas [9, 13].

One of the major ways in which curative glioma therapies fail is related to the invasiveness of the tumour, with tumour infiltrations extending well beyond visible tumour margins rendering complete surgical resection impossible [6]. Conditionally replicative oncolytic viruses are a new and promising field of cancer therapeutics that could prove particularly beneficial in the elimination of these micro-extensions to improve malignant prognosis. In 2015 the FDA approved the first oncolytic virus for clinical use, and there are additionally over 30 oncolytic viruses currently undergoing clinical trials. Several of those oncolytic viruses are being tested as treatments for malignant glioma, thought to be a promising target due to the tumour tropism and relatively high safety profile of oncolytic viruses, in contrast to the current standards of radiotherapy and TMZ, which are both limited

in their efficacy by adverse effects [89]. In many of the early clinical trials of oncolytic virotherapy for the treatment of malignant glioma, however, there has been a failure to live up to preclinical expectations [89]. As malignant gliomas are highly heterogeneous and notoriously difficult to treat tumours, it therefore stands to reason that perhaps the more promising approach lies in combination therapies [89] [52]. In order to maximize the potential for combination therapies, there should be the possibility for additivity, synergy, or spatial cooperation of the two therapeutic approaches. Additionally, in gliomas, the most likely approach would be to combine an experimental therapy, in our case oncolytic virotherapy, with radiotherapy, which has been a staple of clinical glioma treatment for decades [9]. Combining these two treatment modalities has the potential for additivity or synergy from the upregulation of cellular nucleotide synthesis for DNA repair following radiation. Our oncolytic VACVs, deleted in the gene encoding the small ribonucleotide reductase subunit (R2), become dependent on cellular R2 levels and may therefore have increased replication and oncolysis in irradiated cells that have increased their dNTP biogenesis. Furthermore, it is possible that, as both surgery and radiation require visualization of tumour borders, the active replication of the virus may allow for spread through and elimination of tumour microextensions, providing a potential reduction in recurrence and survival benefit.

4.1.1 Oncolytic activity of F4L-deleted VACV in human GBM cells

Ribonucleotide reductase is an enzyme required for *de novo* nucleotide biogenesis, with homologs found in a wide range of organisms, from mammals to microorganisms to viruses [90]. There are three different classes of ribonucleotide reductases; in mammals, which encode a class I ribonucleotide reductase, the enzyme is composed of two subunits, a large

subunit (R1) and small subunit (R2) which form tetrameric complexes [47]. The small subunit, R2, in particular is cell cycle dependent: while both subunits are synthesized in S-phase, the R1 subunit remains relatively stable for constitutive protein levels, whereas R2 has a short half-life and is present only in actively dividing cells [47]. Mammalian cells additionally encode a p53-inducible form of the small subunit (p53-R2), which is activated by p53 in response to genomic stress, allowing for dNTP synthesis to facilitate DNA repair [47] [90]. Interestingly, while nearly all poxviruses encode their own small subunit of ribonucleotide reductase, there are only two families, the Suipox- and Orthopoxviruses, that encode both the small and large subunit [47]. This led a group, led by David Evans (University of Alberta), to explore the role of the large and small subunits in the replication of VACV, of the family *Orthopoxvirus* [47]. They found that, while deletion of the large subunit R1 (I4L in VACV) did not attenuate virus replication compared to wild-type in immunocompetent mice, deletion of the small subunit R2 (F4L in VACV) resulted in a high level of attenuation of the virus [47]. Moreover, they found that in cancer cell lines that naturally produce high levels of cellular R2, likely due to dysregulated cellular DNA replication resulting in continuous R2 synthesis as the cell enters S-phase, replication of the F4L-deleted viruses was restored to a level that neared wild-type replication [47]. Further studies by Kyle Potts (Graduate student supervised by Dr. Mary Hitt, Department of Oncology, University of Alberta) and Shyam Chaurasiya (Graduate student also supervised by Dr. Hitt) have confirmed that these F4L-deleted VACV mutants can maintain a level of viral replication and cytotoxicity comparable to that of wild-type VACV *in vitro* in bladder and breast tumour cells while demonstrating a greatly reduced replicative capacity in the N-60 normal fibroblast cell line and in normal tissues in immune-compromised mice and rats. When the same viruses were compared to F4L-containing VACV *in vivo* in mice and rats, they found that tumour control was comparable in F4L-deleted and F4L-retaining viruses, with both demonstrating increased survival of tumour-bearing mice compared to control

animals treated with inactivated virus. Notably, while the F4L-retaining virus showed some development of poxvirus lesions and evidence of virus spread to some organs, the F4L-deleted viruses showed no development of poxvirus lesions and no evidence of virus spread outside the tumour, suggesting an increased safety profile of our mutant viruses.

Our first step was therefore to assess the oncolytic activity of our F4L-deleted viruses (Δ F4L VACV and Δ F4L Δ J2R VACV, encoding an additional inactivation at the J2R locus encoding thymidine kinase) in two human GBM cell lines, U-87 MG and U-118 MG. As was seen in the studies of bladder cancer and breast cancer mentioned above, we found that Δ F4L Δ J2R VACV replication was not reduced compared to wild-type or Δ J2R VACV in either cell line, while we did see a moderate reduction in Δ F4L VACV replication in U-118 MG cells compared to wild-type VACV. Similarly, Δ F4L Δ J2R VACV induced comparable cytotoxicity to wild-type in both cell lines, though it should be noted that U-118 MG cells were less permissive to virus growth than U-87 MG, producing virus titres \sim 1 log lower than in U-87 MG cells for all mutant and wild-type viruses. This effect has also been observed in JX-594 infection of the same cell lines [91]. Notably lacking from this study, however, was use of a primary normal cell type control. As mentioned above, previous studies have demonstrated that F4L-deleted VACV replication is attenuated in the N60 fibroblast cell line, however a control more relevant to glioma would be preferable. Toward this end, primary astrocytes were cultured from an untreated rat brain, however the astrocytes did not grow to sufficient numbers to set up an assay for virus growth. Future studies are required to assess the safety profile of our F4L-mutant viruses in a suitable normal control for gliomas.

A group led by Lun *et al.* has tested a double-deleted VACV (vvDD) deleted in *J2R* and the vaccinia growth factor (*VGF*) genes in models of malignant glioma. [92]. Their initial studies with U-87 xenografts in nude mice showed results similar to those seen in Chapter 3 of this thesis, *i.e.*, treatment with vvDD provided long-term control of the U-87 subcutaneous

tumours (no tumour growth up to experimental endpoint of 60 days post-infection) compared to rapid growth of untreated tumours, but also failed to completely cure mice of tumours [92]. Interestingly, when they used orthotopic U-87 glioma models in immune-competent mice, they found that their vvDD was safe when delivered systemically, but demonstrated toxicity when administered intracranially, which they attributed to rapid oncolysis and subsequent intracranial inflammation. Additionally, they found that following systemic delivery there was rapid clearance of the virus, with no detectable fluorescence of EGFP-tagged vvDD 7 days post-infection. Immune suppression with cyclophosphamide or rapamycin significantly prolonged virus replication, [92]. Taken together, this may suggest that a more attenuated virus such as our $\Delta F4L\Delta J2R$ VACV may allow for intracranial administration without rapid oncolysis leading to toxicity, as the *in vitro* viability assays of vvDD suggested increased cell killing at an MOI of 1 pfu/cell compared to our $\Delta F4L\Delta J2R$ VACV (~35% cell viability compared to ~50%-60% cell viability at 72 h.p.i, respectively). As the brain is an immune-privileged site, systemic anti-viral immune responses and immune-mediated virus clearance could be reduced compared to that following vvDD, prolonging virus replication and increasing tumour clearance and mouse survival.

Currently, the oncolytic VACV that has been tested the most extensively in clinical trials is Pexa-Vec (JX-594), which is in Phase III trials for the treatment of unresectable hepatocellular carcinoma [26]. Pexa-Vec is a genetically engineered VACV encoding a thymidine kinase (J2R) deletion in a Wyeth-strain backbone [26]. In a Phase I trial of systemically administered Pexa-Vec for the treatment of colorectal cancer, however, there were some virus-related adverse effects seen: 7 of 9 patients developed virus-related skin lesions, while others developed some hypotension or a cough [45]. In a separate case study, a man treated with Pexa-Vec for hepatocellular carcinoma developed poxvirus-related skin lesions following intravenous virus administration [46]. Although the adverse

effects resolved in these patients, these observations suggest that, despite the relative success of the J2R-mutant VACV in clinical trials, an oncolytic VACV with an improved safety profile may be beneficial.

4.1.2 R2/p53R2 upregulation in irradiated glioma cells: implication for Δ F4L Δ J2R VACV infection

As mentioned previously, while there has been some success with oncolytic viruses as standalone treatments in clinical trials [21] [45] [24], it is likely that oncolytic viruses will be most efficacious as a combination treatment; especially when used against a highly heterogeneous tumour such as malignant glioma [52]. For the purpose of my thesis, I pursued the combination of our oncolytic VACV, deleted in F4L (R2) and J2R (thymidine kinase) genes, with radiotherapy. One of the reasons we chose to combine our Δ F4L Δ J2R VACV with radiotherapy was due to possible additive or synergistic effects. IR acts through DNA damage – in order for DNA repair to occur, there must be an increase in nucleotides through *de novo* dNTP synthesis [67]. P53 is a protein that responds to DNA damage to activate a variety of radiation response pathways. One of the ways in which p53 acts is to induce transcription of p53R2, which is then able to complex with cellular R1 to form an active ribonucleotide reductase enzyme [47]. In Chapter 2 of this thesis, we demonstrated that p53R2 levels were maintained following irradiation of both U-87 MG and U-118 MG cells, accompanied by a decrease in R2 levels. These observations correspond with that of a similar study examining R2 and p53R2 levels following irradiation in a panel of colorectal, breast, and fibroblast cell lines, wherein p53R2 levels increased and R2 levels decreased following exposure to 14 Gy radiation [93]. The decrease in cell-cycle-regulated R2 may be more complicated, as R2 has also been shown to increase following irradiation [69]. Interestingly, when we assessed levels of those same proteins following irradiation of U-87

MG tumours *in vivo* in Chapter 3, we saw that both R2 and p53R2 levels increased following radiation. Both the western blots of R2/p53-R2 protein expression and the immunohistochemical analysis of R2/p53-R2 expression *in vivo* following radiation were only performed once, however, with some concerns raised over the use of that antibody for IHC.. It would be beneficial to repeat both the western blot analysis of *in vitro* irradiated cell cultures, as well as the immunohistochemical staining of irradiated tumour sections, with a second, verified antibody. Despite this, however, the observed increase in p53R2 (and possibly in R2 in the immunohistochemical analysis) could have broader implications for the efficacy of a combination with $\Delta F4L\Delta J2R$ VACV. As $\Delta F4L\Delta J2R$ VACV is dependent on cellular dNTP pools and cellular dNTP synthesis for viral replication, upregulation of R2/p53R2 following exposure to radiation could increase viral replication compared to that in non-irradiated tumours.

The possible increased susceptibility to our virus of irradiated cells expressing higher levels of R2 could also provide a means of eliminating radioresistant cell populations. A study by Kuo *et al.* examining the role of R2 levels in radiosensitivity found that cells with higher levels of R2/p53R2 following exposure to IR were more likely to have reduced radiosensitivity. This was thought to be due to the increased ability to repair DNA damage caused by radiation through the increased activity of ribonucleotide reductase [94]. Interestingly, Gammon *et al.* demonstrated enhanced viral replication of F4L-deleted vaccinia mutants in a pancreatic cancer cell line with high R2 expression (PANC-1) versus a pancreatic cancer cell line with low R2 expression (CAPAN-2) [47]. This suggests that there may be two different but cooperative fates for cells treated with the combination of radiotherapy and F4L-deleted VACV: (1) the cells may be directly induced to undergo cell death by IR (although malignant gliomas are known to be relatively radioresistant) [95]; or (2) the cells that prove to be radioresistant through efficient DNA repair will be susceptible to virus-mediated cell death through the increased dNTP synthesis accompanying DNA repair.

4.1.3 thCombination radiotherapy and oncolytic VACV in *in vitro* and *in vivo* glioma models

Combining radiotherapy with our F4L-deleted oncolytic VACV could potentially increase tumour cell killing through both spatial cooperation and additive effects. Tumour microextensions are often missed by both surgical excision and radiotherapy, frequently leading to the failure of glioma therapeutics and eventual death [4]. We propose that radiation could be used to target the bulk of the tumour, while our replicative oncolytic virus could spread through the tumour margins and microextensions to eliminate the remnants of the tumour not targeted by radiation. Additionally, we propose that the DNA repair response to radiation could provide a cellular environment conducive to growth of our F4L-deleted mutant VACV. In fact, a similar response has been seen in a study combining G207 (an oncolytic herpes simplex virus type 1 containing a deletion of the large subunit of ribonucleotide reductase) with radiotherapy [82]. These authors demonstrated increased ribonucleotide reductase activity in irradiated cells compared to non-irradiated cells which correlated with increased virus production per surviving cell and increased virus-induced killing.

When we combined IR with $\Delta F4L\Delta J2R$ VACV *in vitro* (Chapter 2), we found that pre-treatment with IR had no significant impact on overall virus yields compared to non-irradiated cells. However, there were fewer cells present in irradiated cultures compared to non-irradiated cultures at the time they were harvested to assess virus production, so it is possible, that there could have been an increase in virus replication per surviving cell, without increasing the overall yield. In that case, a more accurate representation of virus growth in irradiated vs. non-irradiated cells may be revealed in future experiments by calculating the number of plaque-forming units per cell using daily cell counts as opposed to initial cell counts. Our data suggest that, despite the reduction in R2 expression following

irradiation of glioma cells, the ability of the virus to replicate in and induce killing of irradiated cells remained robust.

An important note to address, however, is that metabolic assays of cell viability are difficult to interpret because 3 cell fates are possible following irradiation: (1) cells are proliferation-competent (high metabolism, signal increasing with time in culture due to increase in cell number); (2) cells are senescent (metabolically active, but growth arrested so no increase in signal with time); or (3) cells are dead (complete absence of metabolism and signal) [96]. It may be, then, that cells detected in our assay (at 72 h.p.ir. had undergone growth arrest and lowered metabolism, but not death, as might be concluded from the metabolic assay we used. The complexity of these assays identifies a need for a more accurate determination of radiation-induced cytotoxicity. Clonogenic assays are typically the assay of choice for assessing viability of irradiated cells. This approach, however, is problematic for assessing survival following the combination of radiotherapy with oncolytic virotherapy, because the virus can potentially spread from one colony to another during the course of the assay. In order to compare to survival following virus infection, survival of irradiated U-87 MG and U-118 MG was assessed using the resazurin-based metabolic assay. Despite the flaws in this approach, the radiation-induced cytotoxicity of our human malignant glioma cell lines was similar to that seen in other studies of malignant glioma radioresistance – particularly the relative resistance of our cell lines to 8 Gy IR. A study by Jiguet Jiglaire *et al.* compared cytotoxic response of various glioma cell lines to several doses of IR and found that at 96 hours following a dose of 8 Gy there was an approximately 25% decrease in U-87 cell viability; this is comparable to the ~20% decrease we saw 72 h.p.ir. [97]. Interestingly, when clonogenic survival assays are used to assess post-irradiation viability, the surviving fraction of U-87 cells exposed to 8 Gy radiation decreases to under 10% [98-100]. It therefore may be beneficial to use clonogenic assays, modified to prevent virus spread, for measuring radioresistance in the future.

It would also be beneficial to determine the proportion of irradiated cells that are senescent, as well as to assess the ability of the virus to infect and induce cytotoxicity in senescent cells. Most common assays of senescence utilize the senescence-associated β -galactosidase (SA- β -gal) biomarker, which converts substrates such as X-gal or C₁₂FDG (5-Dodecanoylamino fluorescein Di- β -D-Galactopyranoside) to a colorimetric or fluorescent form, respectively, for identification of senescent cells [101]. Our Δ F4L Δ J2R VACV, however, encodes the *lacZ* gene inserted in the *J2R* locus. As *lacZ* is a protein that acts on the same substrates as SA- β -gal, it therefore isn't possible to identify virus-infected senescent cells using typical senescence assays. As a possible indirect approach, cells exposed to irradiation and infected with Δ F4L Δ J2R could be fixed and probed with a fluorescent anti-p21 antibody; immunofluorescence of p21 and mCherry could then be visualized for co-localization of senescence markers and virus infection. Alternatively, a study by Althubiti *et al.* identified novel markers of senescence for use with flow cytometry as a means of senescence detection [102]. A flow cytometric assay for dual fluorescence of Δ F4L Δ J2R mCherry and these novel senescence markers (DEP1 and B2MG plasma membrane-associated proteins, although their role in senescence is unknown) could therefore be used to assess virus infectivity of irradiated, senescent cell populations, although further validation of DEP1 and B2MG as senescence biomarkers would likely be necessary.

As we had determined that irradiated glioma cells were capable of supporting Δ F4L Δ J2R VACV infection, and that the combination of radiation and virus perhaps even increased cell killing, it was appropriate to examine the combination in an animal model. A pilot animal study was carried out both to establish a platform for treating subcutaneous glioma xenografts with combination image-guided radiotherapy and oncolytic VACV therapy, as well as to assess the potential tumour control and survival benefits of a combination

approach (Chapter 3). Our results suggested that radiotherapy alone at our dose of 10 Gy failed to provide long-term control of tumour growth, as was expected based on the fact that clinically radiation is given to a cumulative dose of 58-60 Gy [9]. This non-curative dose was chosen to better assess the potential additive or synergistic effects of a combination oncolytic VACV and radiotherapy approach. Promisingly, our results suggested that both $\Delta F4L\Delta J2R$ VACV alone, as well as the combination of $\Delta F4L\Delta J2R$ VACV with 10 Gy IR may provide a survival benefit and improved tumour control relative to radiation alone. In the $\Delta F4L\Delta J2R$ VACV/10 Gy IR treated group, however, one animal appeared to have undergone a cure, with no detectable tumour for several weeks, following which it appeared that virus control of the tumour failed and the mouse eventually reached tumour burden endpoint. There was persistent virus-encoded mCherry signal throughout the experiment, with an increase in signal as tumour size increased to tumour burden endpoint. A similar growth trend was seen in one mouse in the $\Delta F4L\Delta J2R$ VACV treated group, wherein tumour control failed after several weeks; in this case, however, it appeared that the virus was able to effectively control the tumour again. It is unclear, therefore, why control of the $\Delta F4L\Delta J2R$ treated tumour would again be possible but the $\Delta F4L\Delta J2R/10Gy$ treated tumour would not. This difference may be attributable to experimental variability, since so few animals were tested. However, the recurrence of both tumours, as well as the persistent virus signal, suggests that the tumour had remained at undetectable levels, perhaps under the control of the virus, and that at some point the virus control failed and led to regrowth.

The late recurrence of the tumour poses the question of whether a small number of tumour cells were resistant to virus-mediated oncolysis. This resistance may have been due to a lower level of proliferation, or perhaps no proliferation, such as that seen in the core of many GBM tumours [103]. With the absence of proliferation, there would be a reduction of cellular R2 expression, which may reduce viral replication and increase the cell's resistance

to $\Delta F4L\Delta J2R$ VACV. Fluorescence imaging of tumours, however, revealed that mCherry signal, and therefore virus, persisted throughout the experiment. This would suggest that, if the tumour cells were resistant to oncolysis, there must have been some reservoir of virus that persisted. One possibility is that, due to the $\Delta F4L\Delta J2R$ VACV tropism for endothelial cells (as demonstrated by Shyam Chaurasiya, graduate student supervised by Dr. Mary Hitt, Department of Oncology, University of Alberta), the virus was maintained in tumour vasculature that remained despite the collapse of the initial tumour.

Alternatively, it is possible that the remaining cells were not completely resistant to the virus, but rather that there was a low turnover of tumour cells due to a persistent low level of oncolysis. It is possible that, due to tumour architecture, wherein the core of the tumour has low to no proliferation and the outer edges are proliferative, the virus was able to continue replication and oncolysis of edges but the inner core remained resistant to virus. If true, the presence of a non-replicative core may suggest the presence of a virus-resistant, lowly proliferative stem cell-like population, which then gives rise to virus-susceptible progeny that are continually eliminated through viral oncolysis and repopulated by the stem cell-like population. As there would be a constant selective pressure for cells that are resistant to either viral infection or virus-mediated oncolysis, the recurrence of the tumour would likely indicate a rise of the resistant cell population. Interestingly, however, there was still a strong mCherry signal present even at tumour burden endpoint – this would suggest that the virus was still replicating, but was not able to kill the bulk of the cancer cells. A possible test for virus resistance would be to re-inject tumours with virus to determine whether the virus could shrink the tumour. Alternatively, subcutaneous tumours could be removed and dissociated to establish U-87 neurospheres which are then infected with $\Delta F4L\Delta J2R$ VACV, to assess whether there is indeed a population of virus-resistant cells that may continue to re-populate the tumour [104].

4.2. FUTURE DIRECTIONS

4.2.1 Δ F4L Δ J2R VACV kinetics in the brain

Our studies have demonstrated that deletion of the F4L gene encoding ribonucleotide reductase subunit R2 does not impair virus replication in human GBM cells compared to wild-type. However, it remains to be seen whether this deletion attenuates the F4L-deleted vaccinia mutants in the brain in the absence of tumour. While N60 fibroblasts have been used previously in our lab as the non-tumour control, they are not truly representative of normal brain tissue. A more appropriate normal control for brain would be primary rodent astrocytes [105]. In our early studies of culturing primary astrocytes from adult rats, however, we observed relatively rapid proliferation, while astrocytes in a mature brain are generally non-proliferative [106]. As an important mechanism of tumour-selectivity of Δ F4L Δ J2R VACV relies on the differential growth of cancer cells (highly replicative and therefore high R2) versus normal, differentiated cells (low to no replication, low R2), the rapid growth of primary astrocyte cultures would need to be addressed to render the experiment more clinically applicable. To address this, growth of primary astrocytes could potentially be reduced by serum-starvation, using 0.1% FBS instead of 10% FBS is commonly in the medium. Human GBM cells grown in the same FBS concentration would maintain their exponential growth, mimicking *in vivo* conditions. Alternatively, primary astrocytes could be grown to confluency such that they became contact-inhibited. Once primary astrocyte growth had been slowed, virus growth curves in primary astrocytes versus U-87 MG or U-118 MG cells could be compared to assess whether Δ F4L Δ J2R VACV is truly tumour selective in the brain.

4.2.2 Radiation-mediated induction of senescence and susceptibility to vaccinia infection

We observed (Chapter 2) that combination radiation therapy and $\Delta F4L\Delta J2R$ VACV appeared to decrease cell survival compared to $\Delta F4L\Delta J2R$ VACV alone, using a metabolic activity assay as a readout. It remains to be seen whether the observed results were due to cell death, transient cell cycle arrest, or induction of cellular senescence. Of particular relevance would be the induction of transient cell cycle arrest or senescence. Originally senescence was thought to be a permanent growth arrest, however recent evidence suggests that cells are able to overcome stress-induced premature senescence (SIPS) and regain proliferative capacity, leading to tumour recurrence [107]. Additionally, studies have shown that some GBM cell lines (including U-87 MG), when exposed to doses of up to 10 Gy radiation, undergo transient growth arrest for up to 96 hours, following which they regain their proliferative capacity [108]. Both the induction of senescence or a transient growth arrest pose an interesting opportunity for the $\Delta F4L\Delta J2R$ VACV: if the virus is able to replicate in and induce cytotoxicity in these cell populations due to IR-induced ribonucleotide reductase activity, then there is the possibility of eliminating these populations that may contribute to radioresistance.

Traditionally, senescence has been identified by the marker SA- β -gal, which can be detected cytochemically or fluorescently. Unfortunately, due to the *lacZ* insertion in the J2R locus of our mutant VACV, these assays cannot be used in virus-infected cells. A better means of assessing virus infectivity of senescent cell populations would be to first isolate the senescent cell population using fluorescence-activated cell sorting (FACS) [102]. These senescent cell populations could then be infected with $\Delta F4L\Delta J2R$ VACV, and virus growth kinetics and cytotoxicity assessed. Alternatively, an indirect method of assessing whether

$\Delta F4L\Delta J2R$ VACV can infect senescent cells in a non-sorted population would be through co-localization of p21 and $\Delta F4L\Delta J2R$ VACV, which could be detected fluorescently through antibody-mediated fluorescent labeling of p21, a well-known marker of senescence, and mCherry signal from the mutant virus [66]. Assessing virus infection of radiation-induced senescent cell populations could provide important insights into the ability of the virus to complement radiotherapy, in that the virus could enable elimination of those cells that contribute to radioresistance to enhance the efficacy of a combination therapy approach.

4.2.3 Vaccinia virus and combination therapy kinetics in glioma stem cell populations

An important and emerging topic in all cancer therapeutics is the role of cancer stem cells (CSCs) in tumour propagation and resistance to therapies. In GBMs, which are notoriously radioresistant cancers, it is thought that cancer stem cells (CSCs) play a large role in both radioresistance and chemoresistance. CSCs are largely unaffected by traditional clinical radiation dosing schedules, enabling rapid regrowth of tumours [109]. The potential for our $\Delta F4L\Delta J2R$ VACV to infect and eliminate these stem cells could therefore prove to play an important role in improving malignant glioma prognosis. A study by Pistollato *et al.* examined the structure of GBMs, wherein they found that the tumours are comprised of distinct layers, the core of which is anoxic and highly chemoresistant, with the majority of cells bearing stem cell markers [103]. This is promising for our virus therapy as previous studies in our lab have demonstrated that $\Delta F4L\Delta J2R$ VACV is able to propagate even in hypoxic tumour environments, which are known to contribute to radioresistance [95] [110]. Additionally, it is thought that one of the contributing factors to radioresistance of glioma stem cells is their high propensity for DNA repair. As DNA repair requires dNTP synthesis,

this suggests that irradiated glioma stem cells may support $\Delta F4L\Delta J2R$ VACV infection [111]. In our lab, previous studies on breast cancer stem cells have showed susceptibility of F4L-deleted VACV infection at levels comparable to that of non-stem cell breast cancer cell lines (Shyam Chaurasiya, graduate student of Dr. Mary Hitt, Department of Oncology, University of Alberta). Despite this, in the pilot animal study described in this thesis, the failure of the virus to control tumours permanently suggests that the residual cells may have been resistant to virus-mediated cell death. Further studies into the role of glioma stem cells in tumour propagation, and their response to radiation and virus infection, must therefore be explored.

In vitro studies of glioma stem cells may be undertaken through the use of neurospheres, in which GBM tumour samples are first established as a monolayer culture, then manipulated to form neurospheres [112]. The stem cell population (defined as CD133+) can then be enriched from the neurospheres through CD133+ microbead purification and re-seeded to form CD133+ tumour subspheres, for a population that is up to 90% CD133+ [112]. These neurospheres could then be infected with $\Delta F4L\Delta J2R$ VACV, with virus replication in the CD133+ population assessed through confocal microscopy of the spheres, using viral-encoded mCherry fluorescence as a marker. It would also be beneficial to assess the R2 expression levels in these stem cell populations, both before and following exposure to radiation. If upregulation of R2 is seen following radiation, then assessing virus infectivity of these irradiated stem cells could provide some insight into the efficacy of combination treatment on the elusive glioma stem cell populations. This approach could also be extended to mouse models, wherein CD133+ cell cultures would be implanted subcutaneously or orthotopically into mouse brains [111], and the efficacy of radiation and $\Delta F4L\Delta J2R$ VACV in controlling these CD133+ enriched tumours would be compared to

efficacy in controlling a non-enriched (patient-derived primary GBM) xenograft or U-87 MG xenograft.

4.2.4 Furthering animal studies: xenograft and orthotopic models of combination therapy

Though our pilot animal study combining radiation therapy and $\Delta F4L\Delta J2R$ VACV infection (Chapter 3) provided some insights into the possible efficacy of a combination treatment, there is much that remains to be done before this study is conclusive. The first step would be expanding the original study, such that conclusions of statistical significance may be drawn. Our next step would be to extend our combination therapy study to an orthotopic glioma model, using a stereotactic implantation device for intracranial injection of U-87 MG cells. One difficulty with this approach is that there is insufficient contrast for high resolution SARRP CT imaging to guide RT and to monitor tumour growth. In most studies using orthotopic glioma models, tumour imaging is performed through (MRI) [113]. A validation study of SARRP-mediated irradiation of an intracranial glioma (rat) model also used MRI imaging of tumours, using a multi-modality bed that allowed for transport of the animal in a fixed position from the MRI scanner to the SARRP [76]. Alternatively, a luciferase-tagged U-87 MG cell line could be used as a means of monitoring tumour growth through bioluminescence. However, it is likely that MRI may still be necessary for SARRP-mediated IGRT of the tumour, as MRI would provide the highest resolution imaging, which is necessary in order to define the tumour area as precisely as possible for increased accuracy of IGRT targeting.

One important mechanism of VACV-mediated oncolysis is through stimulation of anti-tumour immunity, providing resistance to secondary tumour challenge following primary

tumour clearance [38]. The role of vaccinia-mediated anti-tumour immunity may be less clear, however, in an immune-distinct site such as the brain [17]. As such, an important future direction is to assess the combination radiation and $\Delta F4L\Delta J2R$ VACV treatment in an immune-competent, syngeneic animal model. There are several options for syngeneic mouse models of glioma, the major ones of which are listed in a review published by Oh *et al.* (2014) [114]; of these, perhaps the most applicable and accessible model is the GL261;C57BL/6 model, which re-capitulates many characteristics of GBM and is widely used for testing immunogenic therapies [115]. As an added benefit, this model has also been demonstrated to be enriched for CD133+ stem cells [116]. A syngeneic, immunocompetent model of glioma, especially one used orthotopically, could provide important insights into virus activation of anti-cancer immunity in the brain. Anti-tumour immunity of $\Delta F4L\Delta J2R$ VACV-treated mice (compared to non-virus-treated mice) could be assessed either indirectly by tumour re-challenge, or by examining immune infiltration in tumours excised from treated animals [38]. Additionally, anti-tumour immune activation could be assessed by isolation of splenocytes of treated mice, and testing the ability of the cultured splenocytes to induce cell killing when co-cultured with tumour cells [38].

4.3. CONCLUSIONS

Malignant gliomas are a notoriously high fatality and difficult to treat cancer, with limited therapeutic options for patients. The use of oncolytic virotherapy has shown promise as a means of increasing therapeutic options as well as providing a survival benefit. Due to the highly heterogeneous nature of malignant glioma, it is likely that oncolytic virotherapy will be most effective in combination with other treatment modalities. Here, we assessed the efficacy of combining a genetically engineered oncolytic VACV, deleted in the F4L (R2) and J2R (thymidine kinase) genes, with radiotherapy for the treatment of high-grade malignant. Our results showed that virus infectivity is maintained in irradiated cells, and that, through elevation of R2/p53R2 following radiation, there is the possibility for cooperation through the dependence of our mutant virus on cellular R2 levels and cellular production of dNTPs. Additionally, early pilot studies of an immune-compromised, subcutaneous xenograft model combining image-guided radiation therapy with $\Delta F4L\Delta J2R$ VACV infection have suggested that either $\Delta F4L\Delta J2R$ VACV alone, or the combination of $\Delta F4L\Delta J2R$ VACV and radiotherapy, may provide a means of better controlling tumour growth and may provide a survival benefit. Further studies, using both immune-compromised subcutaneous and orthotopic models as well as an immune-competent syngeneic model of combination therapy, are necessary to better understand the possible therapeutic efficacy of the combination treatment.

REFERENCES

1. Aldape, K.D., Okcu, M.F., Bondy, M.L., and Wrensch, M. (2003). Molecular epidemiology of glioblastoma. *Cancer J* 9, 99-106.
2. Lee, J.J., Kim, B.C., Park, M.J., Lee, Y.S., Kim, Y.N., Lee, B.L., and Lee, J.S. (2011). PTEN status switches cell fate between premature senescence and apoptosis in glioma exposed to ionizing radiation. *Cell Death Differ* 18, 666-677.
3. Ostrom, Q.T., Bauchet, L., Davis, F.G., Deltour, I., Fisher, J.L., Langer, C.E., Pekmezci, M., Schwartzbaum, J.A., Turner, M.C., Walsh, K.M., et al. (2014). The epidemiology of glioma in adults: a "state of the science" review. *Neuro Oncol* 16, 896-913.
4. Dunn, G.P., Dunn, I.F., and Curry, W.T. (2007). Focus on TILs: Prognostic significance of tumor infiltrating lymphocytes in human glioma. *Cancer Immun* 7, 12.
5. Carlsson, S.K., Brothers, S.P., and Wahlestedt, C. (2014). Emerging treatment strategies for glioblastoma multiforme. *EMBO Mol Med* 6, 1359-1370.
6. Juratli, T.A., Schackert, G., and Krex, D. (2013). Current status of local therapy in malignant gliomas—a clinical review of three selected approaches. *Pharmacol Ther* 139, 341-358.
7. Network, C.G.A.R. (2008). Comprehensive genomic characterization defines human glioblastoma genes and core pathways. *Nature* 455, 1061-1068.
8. Furnari, F.B., Fenton, T., Bachoo, R.M., Mukasa, A., Stommel, J.M., Stegh, A., Hahn, W.C., Ligon, K.L., Louis, D.N., Brennan, C., et al. (2007). Malignant astrocytic glioma: genetics, biology, and paths to treatment. *Genes Dev* 21, 2683-2710.
9. Stupp, R., Mason, W.P., van den Bent, M.J., Weller, M., Fisher, B., Taphoorn, M.J., Belanger, K., Brandes, A.A., Marosi, C., Bogdahn, U., et al. (2005). Radiotherapy plus concomitant and adjuvant temozolomide for glioblastoma. *N Engl J Med* 352, 987-996.
10. Reagan, T.J., Bisel, H.F., Childs, D.S., Layton, D.D., Rhoton, A.L., and Taylor, W.F. (1976). Controlled study of CCNU and radiation therapy in malignant astrocytoma. *J Neurosurg* 44, 186-190.
11. Walker, M.D., Alexander, E., Hunt, W.E., MacCarty, C.S., Mahaley, M.S., Mealey, J., Norrell, H.A., Owens, G., Ransohoff, J., Wilson, C.B., et al. (1978). Evaluation of BCNU and/or radiotherapy in the treatment of anaplastic gliomas. A cooperative clinical trial. *J Neurosurg* 49, 333-343.

12. Mrugala, M.M., Kesari, S., Ramakrishna, N., and Wen, P.Y. (2004). Therapy for recurrent malignant glioma in adults. *Expert Rev Anticancer Ther* 4, 759-782.
13. (2015). Canadian Cancer Society's Advisory Committee on Cancer Statistics. (Canadian Cancer Statistics 2015: Canadian Cancer Society).
14. Desjardins, A., Vlahovic, G., and Friedman, H.S. (2016). Vaccine Therapy, Oncolytic Viruses, and Gliomas. *Oncology (Williston Park)* 30, 211-218.
15. Westphal, M., Hilt, D.C., Bortey, E., Delavault, P., Olivares, R., Warnke, P.C., Whittle, I.R., Jääskeläinen, J., and Ram, Z. (2003). A phase 3 trial of local chemotherapy with biodegradable carmustine (BCNU) wafers (Gliadel wafers) in patients with primary malignant glioma. *Neuro Oncol* 5, 79-88.
16. Li, S., Tokuyama, T., Yamamoto, J., Koide, M., Yokota, N., and Namba, H. (2005). Potent bystander effect in suicide gene therapy using neural stem cells transduced with herpes simplex virus thymidine kinase gene. *Oncology* 69, 503-508.
17. Dunn, G.P., Fecci, P.E., and Curry, W.T. (2012). Cancer immunoediting in malignant glioma. *Neurosurgery* 71, 201-222; discussion 222-203.
18. Pallasch, C.P., Struss, A.K., Munnia, A., König, J., Steudel, W.I., Fischer, U., and Meese, E. (2005). Autoantibodies against GLEA2 and PHF3 in glioblastoma: tumor-associated autoantibodies correlated with prolonged survival. *Int J Cancer* 117, 456-459.
19. Sawamura, Y., Hosokawa, M., Kuppner, M.C., Kobayashi, H., Aida, T., Abe, H., and de Tribolet, N. (1989). Antitumor activity and surface phenotypes of human glioma-infiltrating lymphocytes after in vitro expansion in the presence of interleukin 2. *Cancer Res* 49, 1843-1849.
20. Fadul, C.E., Fisher, J.L., Hampton, T.H., Lallana, E.C., Li, Z., Gui, J., Szczepiorkowski, Z.M., Tosteson, T.D., Rhodes, C.H., Wishart, H.A., et al. (2011). Immune response in patients with newly diagnosed glioblastoma multiforme treated with intranodal autologous tumor lysate-dendritic cell vaccination after radiation chemotherapy. *J Immunother* 34, 382-389.
21. Pol, J., Buqué, A., Aranda, F., Bloy, N., Cremer, I., Eggermont, A., Erbs, P., Fucikova, J., Galon, J., Limacher, J.M., et al. (2016). Trial Watch-Oncolytic viruses and cancer therapy. *Oncoimmunology* 5, e1117740.
22. Andtbacka, R.H., Kaufman, H.L., Collichio, F., Amatruda, T., Senzer, N., Chesney, J., Delman, K.A., Spittle, L.E., Puzanov, I., Agarwala, S.S., et al. (2015). Talimogene Laherparepvec Improves Durable Response Rate in Patients With Advanced Melanoma. *J Clin Oncol* 33, 2780-2788.

23. Andtbacka, R.H., Ross, M., Puzanov, I., Milhem, M., Collichio, F., Delman, K.A., Amatruda, T., Zager, J.S., Cranmer, L., Hsueh, E., et al. (2016). Patterns of Clinical Response with Talimogene Laherparepvec (T-VEC) in Patients with Melanoma Treated in the OPTiM Phase III Clinical Trial. *Ann Surg Oncol*.
24. Noonan, A.M., Farren, M.R., Geyer, S.M., Huang, Y., Tahiri, S., Ahn, D., Mikhail, S., Ciombor, K.K., Pant, S., Aparo, S., et al. (2016). Randomized Phase 2 Trial of the Oncolytic Virus Pelareorep (Reolysin) in Upfront Treatment of Metastatic Pancreatic Adenocarcinoma. *Mol Ther* 24, 1150-1158.
25. Ranki, T., Pesonen, S., Hemminki, A., Partanen, K., Kairemo, K., Alanko, T., Lundin, J., Linder, N., Turkki, R., Ristimäki, A., et al. (2016). Phase I study with ONCOS-102 for the treatment of solid tumors - an evaluation of clinical response and exploratory analyses of immune markers. *J Immunother Cancer* 4, 17.
26. Breitbach, C.J., Moon, A., Burke, J., Hwang, T.H., and Kim, D.H. (2015). A Phase 2, Open-Label, Randomized Study of Pexa-Vec (JX-594) Administered by Intratumoral Injection in Patients with Unresectable Primary Hepatocellular Carcinoma. *Methods Mol Biol* 1317, 343-357.
27. Pugalenthi, A., Mojica, K., Ady, J.W., Johnsen, C., Love, D., Chen, N.G., Aguilar, R.J., Szalay, A.A., and Fong, Y. (2015). Recombinant vaccinia virus GLV-1h68 is a promising oncolytic vector in the treatment of cholangiocarcinoma. *Cancer Gene Ther* 22, 591-596.
28. Jiang, H., Clise-Dwyer, K., Ruisaard, K.E., Fan, X., Tian, W., Gumin, J., Lamfers, M.L., Kleijn, A., Lang, F.F., Yung, W.K., et al. (2014). Delta-24-RGD oncolytic adenovirus elicits anti-glioma immunity in an immunocompetent mouse model. *PLoS One* 9, e97407.
29. Markert, J.M., Razdan, S.N., Kuo, H.C., Cantor, A., Knoll, A., Karrasch, M., Nabors, L.B., Markiewicz, M., Agee, B.S., Coleman, J.M., et al. (2014). A phase 1 trial of oncolytic HSV-1, G207, given in combination with radiation for recurrent GBM demonstrates safety and radiographic responses. *Mol Ther* 22, 1048-1055.
30. Geletneky, K., Kiprianova, I., Ayache, A., Koch, R., Herrero Y Calle, M., Deleu, L., Sommer, C., Thomas, N., Rommelaere, J., and Schlehofer, J.R. (2010). Regression of advanced rat and human gliomas by local or systemic treatment with oncolytic parvovirus H-1 in rat models. *Neuro Oncol* 12, 804-814.
31. Geletneky, K., Huesing, J., Rommelaere, J., Schlehofer, J.R., Leuchs, B., Dahm, M., Krebs, O., von Knebel Doeberitz, M., Huber, B., and Hajda, J. (2012). Phase I/IIa study of intratumoral/intracerebral or intravenous/intracerebral administration of Parvovirus H-1 (ParvOryx) in patients with progressive primary or recurrent glioblastoma multiforme: ParvOryx01 protocol. *BMC Cancer* 12, 99.

32. Goetz, C., and Gromeier, M. (2010). Preparing an oncolytic poliovirus recombinant for clinical application against glioblastoma multiforme. *Cytokine Growth Factor Rev* 21, 197-203.
33. Levitan, D. (2016). Polio-Rhinovirus Conjugate Receives Breakthrough Therapy Designation for Glioblastoma. (*Oncology*).
34. Kim, M. (2015). Replicating poxviruses for human cancer therapy. *J Microbiol* 53, 209-218.
35. Beaud, G. (1995). Vaccinia virus DNA replication: a short review. *Biochimie* 77, 774-779.
36. Thorne, S.H. (2014). Immunotherapeutic potential of oncolytic vaccinia virus. *Front Oncol* 4, 155.
37. Zeh, H.J., Downs-Canner, S., McCart, J.A., Guo, Z.S., Rao, U.N., Ramalingam, L., Thorne, S.H., Jones, H.L., Kalinski, P., Wieckowski, E., et al. (2015). First-in-man study of western reserve strain oncolytic vaccinia virus: safety, systemic spread, and antitumor activity. *Mol Ther* 23, 202-214.
38. Parviainen, S., Ahonen, M., Diaconu, I., Kipar, A., Siurala, M., Vähä-Koskela, M., Kanerva, A., Cerullo, V., and Hemminki, A. (2015). GMCSF-armed vaccinia virus induces an antitumor immune response. *Int J Cancer* 136, 1065-1072.
39. Ichihashi, Y. (1996). Extracellular enveloped vaccinia virus escapes neutralization. *Virology* 217, 478-485.
40. Leite, F., and Way, M. (2015). The role of signalling and the cytoskeleton during Vaccinia Virus egress. *Virus Res* 209, 87-99.
41. Cudmore, S., Cossart, P., Griffiths, G., and Way, M. (1995). Actin-based motility of vaccinia virus. *Nature* 378, 636-638.
42. Doceul, V., Hollinshead, M., van der Linden, L., and Smith, G.L. (2010). Repulsion of superinfecting virions: a mechanism for rapid virus spread. *Science* 327, 873-876.
43. Fend, L., Remy-Ziller, C., Foloppe, J., Kempf, J., Cochin, S., Barraud, L., Accart, N., Erbs, P., Fournel, S., and Prévaille, X. (2016). Oncolytic virotherapy with an armed vaccinia virus in an orthotopic model of renal carcinoma is associated with modification of the tumor microenvironment. *Oncoimmunology* 5, e1080414.
44. Downs-Canner, S., Sheng Guo, Z., Ravindranathan, R., Breitbach, C.J., O'Malley, M.E., Jones, H.L., Moon, A., McCart, J.A., Shuai, Y., Zeh, H.J., et al. (2016). Phase I Study of Intravenous Oncolytic Poxvirus (vvDD) in Patients with Advanced Solid Cancers. *Mol Ther*.

45. Park, S.H., Breitbart, C.J., Lee, J., Park, J.O., Lim, H.Y., Kang, W.K., Moon, A., Mun, J.H., Sommermann, E.M., Maruri Avidal, L., et al. (2015). Phase 1b Trial of Biweekly Intravenous Pexa-Vec (JX-594), an Oncolytic and Immunotherapeutic Vaccinia Virus in Colorectal Cancer. *Mol Ther* 23, 1532-1540.
46. Kung, C.H., Kuo, S.C., Chen, T.L., and Weng, W.S. (2015). Isolation of vaccinia JX594 from pustules following therapy for hepatocellular carcinoma. *BMC Cancer* 15, 704.
47. Gammon, D.B., Gowrishankar, B., Duraffour, S., Andrei, G., Upton, C., and Evans, D.H. (2010). Vaccinia virus-encoded ribonucleotide reductase subunits are differentially required for replication and pathogenesis. *PLoS Pathog* 6, e1000984.
48. Chabes, A., and Thelander, L. (2000). Controlled protein degradation regulates ribonucleotide reductase activity in proliferating mammalian cells during the normal cell cycle and in response to DNA damage and replication blocks. *J Biol Chem* 275, 17747-17753.
49. Xue, L., Zhou, B., Liu, X., Qiu, W., Jin, Z., and Yen, Y. (2003). Wild-type p53 regulates human ribonucleotide reductase by protein-protein interaction with p53R2 as well as hRRM2 subunits. *Cancer Res* 63, 980-986.
50. Yen, Y. (2003). Ribonucleotide reductase subunit one as gene therapy target: commentary re: M-Y. Cao et al., Adenovirus-mediated ribonucleotide reductase R1 gene therapy of human colon adenocarcinoma. *Clin. Cancer Res.*, 9: 4304-4308, 2003. *Clin Cancer Res* 9, 4304-4308.
51. Zhou, B., Liu, X., Mo, X., Xue, L., Darwish, D., Qiu, W., Shih, J., Hwu, E.B., Luh, F., and Yen, Y. (2003). The human ribonucleotide reductase subunit hRRM2 complements p53R2 in response to UV-induced DNA repair in cells with mutant p53. *Cancer Res* 63, 6583-6594.
52. El-Shemi, A.G., Ashshi, A.M., Na, Y., Li, Y., Basalamah, M., Al-Allaf, F.A., Oh, E., Jung, B.K., and Yun, C.O. (2016). Combined therapy with oncolytic adenoviruses encoding TRAIL and IL-12 genes markedly suppressed human hepatocellular carcinoma both in vitro and in an orthotopic transplanted mouse model. *J Exp Clin Cancer Res* 35, 74.
53. Leroi, N., Lallemand, F., Coucke, P., Noel, A., and Martinive, P. (2016). Impacts of Ionizing Radiation on the Different Compartments of the Tumor Microenvironment. *Front Pharmacol* 7, 78.
54. Asaithamby, A., Hu, B., and Chen, D.J. (2011). Unrepaired clustered DNA lesions induce chromosome breakage in human cells. *Proc Natl Acad Sci U S A* 108, 8293-8298.
55. Snider, J.W., and Mehta, M. (2016). Principles of radiation therapy. *Handb Clin Neurol* 134, 131-147.

56. Boonstra, J., and Post, J.A. (2004). Molecular events associated with reactive oxygen species and cell cycle progression in mammalian cells. *Gene* 337, 1-13.
57. Pollycove, M., and Feinendegen, L.E. (2003). Radiation-induced versus endogenous DNA damage: possible effect of inducible protective responses in mitigating endogenous damage. *Hum Exp Toxicol* 22, 290-306; discussion 307, 315-297, 319-223.
58. Kavanagh, J.N., Redmond, K.M., Schettino, G., and Prise, K.M. (2013). DNA double strand break repair: a radiation perspective. *Antioxid Redox Signal* 18, 2458-2472.
59. Havaki, S., Kotsinas, A., Chronopoulos, E., Kletsas, D., Georgakilas, A., and Gorgoulis, V.G. (2015). The role of oxidative DNA damage in radiation induced bystander effect. *Cancer Lett* 356, 43-51.
60. Frankenberg-Schwager, M. (1989). Review of repair kinetics for DNA damage induced in eukaryotic cells in vitro by ionizing radiation. *Radiother Oncol* 14, 307-320.
61. Lavelle, C., and Foray, N. (2014). Chromatin structure and radiation-induced DNA damage: from structural biology to radiobiology. *Int J Biochem Cell Biol* 49, 84-97.
62. PUCK, T.T., and MARCUS, P.I. (1956). Action of x-rays on mammalian cells. *J Exp Med* 103, 653-666.
63. Kim, B.M., Hong, Y., Lee, S., Liu, P., Lim, J.H., Lee, Y.H., Lee, T.H., and Chang, K.T. (2015). Therapeutic Implications for Overcoming Radiation Resistance in Cancer Therapy. *Int J Mol Sci* 16, 26880-26913.
64. Kesari, S., Advani, S.J., Lawson, J.D., Kahle, K.T., Ng, K., Carter, B., and Chen, C.C. (2011). DNA damage response and repair: insights into strategies for radiation sensitization of gliomas. *Future Oncol* 7, 1335-1346.
65. Mirzayans, R., Andrais, B., Scott, A., and Murray, D. (2012). New insights into p53 signaling and cancer cell response to DNA damage: implications for cancer therapy. *J Biomed Biotechnol* 2012, 170325.
66. Mirzayans, R., Andrais, B., Scott, A., Wang, Y.W., and Murray, D. (2013). Ionizing radiation-induced responses in human cells with differing TP53 status. *Int J Mol Sci* 14, 22409-22435.
67. Kunos, C.A., Chiu, S.M., Pink, J., and Kinsella, T.J. (2009). Modulating radiation resistance by inhibiting ribonucleotide reductase in cancers with virally or mutationally silenced p53 protein. *Radiat Res* 172, 666-676.
68. Tanaka, H., Arakawa, H., Yamaguchi, T., Shiraishi, K., Fukuda, S., Matsui, K., Takei, Y., and Nakamura, Y. (2000). A ribonucleotide reductase gene involved in a p53-dependent cell-cycle checkpoint for DNA damage. *Nature* 404, 42-49.

69. Kuo, M.L., and Kinsella, T.J. (1998). Expression of ribonucleotide reductase after ionizing radiation in human cervical carcinoma cells. *Cancer Res* 58, 2245-2252.
70. Cohen, M.H., Johnson, J.R., and Pazdur, R. (2005). Food and Drug Administration Drug approval summary: temozolomide plus radiation therapy for the treatment of newly diagnosed glioblastoma multiforme. *Clin Cancer Res* 11, 6767-6771.
71. Hau, E., Shen, H., Clark, C., Graham, P.H., Koh, E.S., and L McDonald, K. (2016). The evolving roles and controversies of radiotherapy in the treatment of glioblastoma. *J Med Radiat Sci* 63, 114-123.
72. Baumann, B.C., Benci, J.L., Santoiemma, P.P., Chandrasekaran, S., Hollander, A.B., Kao, G.D., and Dorsey, J.F. (2012). An integrated method for reproducible and accurate image-guided stereotactic cranial irradiation of brain tumors using the small animal radiation research platform. *Transl Oncol* 5, 230-237.
73. Matinfar, M., Iordachita, I., Wong, J., and Kazanzides, P. (2010). Robotic Delivery of Complex Radiation Volumes for Small Animal Research. *IEEE Int Conf Robot Autom 2010*, 2056-2061.
74. Eslami, S., Yang, Y., Wong, J., Patterson, M.S., and Iordachita, I. (2013). An Integrated X-Ray/Optical Tomography System for Pre-clinical Radiation Research. *Proc SPIE Int Soc Opt Eng* 8668, 866830.
75. Wong, J., Armour, E., Kazanzides, P., Iordachita, I., Tryggestad, E., Deng, H., Matinfar, M., Kennedy, C., Liu, Z., Chan, T., et al. (2008). High-resolution, small animal radiation research platform with x-ray tomographic guidance capabilities. *Int J Radiat Oncol Biol Phys* 71, 1591-1599.
76. Bolcaen, J., Descamps, B., Deblaere, K., Boterberg, T., Hallaert, G., Van den Broecke, C., Decrock, E., Vral, A., Leybaert, L., Vanhove, C., et al. (2014). MRI-guided 3D conformal arc micro-irradiation of a F98 glioblastoma rat model using the Small Animal Radiation Research Platform (SARRP). *J Neurooncol* 120, 257-266.
77. Zeng, J., See, A.P., Phallen, J., Jackson, C.M., Belcaid, Z., Ruzevick, J., Durham, N., Meyer, C., Harris, T.J., Albesiano, E., et al. (2013). Anti-PD-1 blockade and stereotactic radiation produce long-term survival in mice with intracranial gliomas. *Int J Radiat Oncol Biol Phys* 86, 343-349.
78. Kyula, J.N., Khan, A.A., Wilkinson, M.J., Mansfield, D., and Harrington, K.J. (2013). Radiation lays down covering fire for viral shock troops. *Oncotarget* 4, 1329-1330.
79. Dai, M.H., Liu, S.L., Chen, N.G., Zhang, T.P., You, L., Q Zhang, F., Chou, T.C., Szalay, A.A., Fong, Y., and Zhao, Y.P. (2014). Oncolytic vaccinia virus in combination with radiation shows synergistic antitumor efficacy in pancreatic cancer. *Cancer Lett* 344, 282-290.

80. Mansfield, D., Pencavel, T., Kyula, J.N., Zaidi, S., Roulstone, V., Thway, K., Karapanagiotou, L., Khan, A.A., McLaughlin, M., Touchefeu, Y., et al. (2013). Oncolytic Vaccinia virus and radiotherapy in head and neck cancer. *Oral Oncol* 49, 108-118.
81. McEntee, G., Kyula, J.N., Mansfield, D., Smith, H., Wilkinson, M., Gregory, C., Roulstone, V., Coffey, M., and Harrington, K.J. (2016). Enhanced cytotoxicity of reovirus and radiotherapy in melanoma cells is mediated through increased viral replication and mitochondrial apoptotic signalling. *Oncotarget*.
82. Stanziale, S.F., Petrowsky, H., Joe, J.K., Roberts, G.D., Zager, J.S., Gusani, N.J., Ben-Porat, L., Gonen, M., and Fong, Y. (2002). Ionizing radiation potentiates the antitumor efficacy of oncolytic herpes simplex virus G207 by upregulating ribonucleotide reductase. *Surgery* 132, 353-359.
83. Markert, J.M., Liechty, P.G., Wang, W., Gaston, S., Braz, E., Karrasch, M., Nabors, L.B., Markiewicz, M., Lakeman, A.D., Palmer, C.A., et al. (2009). Phase Ib trial of mutant herpes simplex virus G207 inoculated pre-and post-tumor resection for recurrent GBM. *Mol Ther* 17, 199-207.
84. Wong, E.T., Hess, K.R., Gleason, M.J., Jaeckle, K.A., Kyritsis, A.P., Prados, M.D., Levin, V.A., and Yung, W.K. (1999). Outcomes and prognostic factors in recurrent glioma patients enrolled onto phase II clinical trials. *J Clin Oncol* 17, 2572-2578.
85. Golden, E.B., Pellicciotta, I., Demaria, S., Barcellos-Hoff, M.H., and Formenti, S.C. (2012). The convergence of radiation and immunogenic cell death signaling pathways. *Front Oncol* 2, 88.
86. Bhattacharyya, T., Purushothaman, K., Puthiyottil, S.S., Bhattacharjee, A., and Muttah, G. (2016). Immunological interactions in radiotherapy-opening a new window of opportunity. *Ann Transl Med* 4, 51.
87. Potts, K.G., Irwin, C.W., Favis, N.A., Pink, D.B., Vincent, K.M., Lewis, J.D., Moore, R.B., Hitt, M.M., Evans, D.H. (2016). Oncolytic vaccinia virus F4L (ribonucleotide reductase) mutants promote anti-tumor immunity with superior safety in bladder cancer models.
88. Mirzayans, R., Andrais, B., Scott, A., Tessier, A., and Murray, D. (2007). A sensitive assay for the evaluation of cytotoxicity and its pharmacologic modulation in human solid tumor-derived cell lines exposed to cancer-therapeutic agents. *J Pharm Pharm Sci* 10, 298s-311s.
89. Spencer, D.A., Young, J.S., Kanojia, D., Kim, J.W., Polster, S.P., Murphy, J.P., and Lesniak, M.S. (2015). Unlocking the promise of oncolytic virotherapy in glioma: combination with chemotherapy to enhance efficacy. *Ther Deliv* 6, 453-468.
90. Nordlund, P., and Reichard, P. (2006). Ribonucleotide reductases. *Annu Rev Biochem* 75, 681-706.

91. Lun, X., Chan, J., Zhou, H., Sun, B., Kelly, J.J., Stechishin, O.O., Bell, J.C., Parato, K., Hu, K., Vaillant, D., et al. (2010). Efficacy and safety/toxicity study of recombinant vaccinia virus JX-594 in two immunocompetent animal models of glioma. *Mol Ther* 18, 1927-1936.
92. Lun, X.Q., Jang, J.H., Tang, N., Deng, H., Head, R., Bell, J.C., Stojdl, D.F., Nutt, C.L., Senger, D.L., Forsyth, P.A., et al. (2009). Efficacy of systemically administered oncolytic vaccinia virotherapy for malignant gliomas is enhanced by combination therapy with rapamycin or cyclophosphamide. *Clin Cancer Res* 15, 2777-2788.
93. Yamaguchi, T., Matsuda, K., Sagiya, Y., Iwadate, M., Fujino, M.A., Nakamura, Y., and Arakawa, H. (2001). p53R2-dependent pathway for DNA synthesis in a p53-regulated cell cycle checkpoint. *Cancer Res* 61, 8256-8262.
94. Kuo, M.L., Hwang, H.S., Sosnay, P.R., Kunugi, K.A., and Kinsella, T.J. (2003). Overexpression of the R2 subunit of ribonucleotide reductase in human nasopharyngeal cancer cells reduces radiosensitivity. *Cancer J* 9, 277-285.
95. Fidoamore, A., Cristiano, L., Antonosante, A., d'Angelo, M., Di Giacomo, E., Astarita, C., Giordano, A., Ippoliti, R., Benedetti, E., and Cimini, A. (2016). Glioblastoma Stem Cells Microenvironment: The Paracrine Roles of the Niche in Drug and Radioresistance. *Stem Cells Int* 2016, 6809105.
96. Liao, E.C., Hsu, Y.T., Chuah, Q.Y., Lee, Y.J., Hu, J.Y., Huang, T.C., Yang, P.M., and Chiu, S.J. (2014). Radiation induces senescence and a bystander effect through metabolic alterations. *Cell Death Dis* 5, e1255.
97. Jiguet Jiglaire, C., Baeza-Kallee, N., Denicolaï, E., Baretts, D., Metellus, P., Padovani, L., Chinot, O., Figarella-Branger, D., and Fernandez, C. (2014). Ex vivo cultures of glioblastoma in three-dimensional hydrogel maintain the original tumor growth behavior and are suitable for preclinical drug and radiation sensitivity screening. *Exp Cell Res* 321, 99-108.
98. Naidu, M.D., Mason, J.M., Pica, R.V., Fung, H., and Pena, L.A. (2010). Radiation resistance in glioma cells determined by DNA damage repair activity of Ape1/Ref-1. *J Radiat Res* 51, 393-404.
99. Short, S.C., Mitchell, S.A., Boulton, P., Woodcock, M., and Joiner, M.C. (1999). The response of human glioma cell lines to low-dose radiation exposure. *Int J Radiat Biol* 75, 1341-1348.
100. Oertel, S., Krempien, R., Lindel, K., Zabel, A., Milker-Zabel, S., Bischof, M., Lipson, K.E., Peschke, P., Debus, J., Abdollahi, A., et al. (2006). Human glioblastoma and carcinoma xenograft tumors treated by combined radiation and imatinib (Gleevec). *Strahlenther Onkol* 182, 400-407.

101. Debacq-Chainiaux, F., Erusalimsky, J.D., Campisi, J., and Toussaint, O. (2009). Protocols to detect senescence-associated beta-galactosidase (SA-beta-gal) activity, a biomarker of senescent cells in culture and in vivo. *Nat Protoc* 4, 1798-1806.
102. Althubiti, M., Lezina, L., Carrera, S., Jukes-Jones, R., Giblett, S.M., Antonov, A., Barlev, N., Saldanha, G.S., Pritchard, C.A., Cain, K., et al. (2014). Characterization of novel markers of senescence and their prognostic potential in cancer. *Cell Death Dis* 5, e1528.
103. Pistollato, F., Abbadì, S., Rampazzo, E., Persano, L., Della Puppa, A., Frasson, C., Sarto, E., Scienza, R., D'avella, D., and Basso, G. (2010). Intratumoral hypoxic gradient drives stem cells distribution and MGMT expression in glioblastoma. *Stem Cells* 28, 851-862.
104. Rath, P., Lal, B., Ajala, O., Li, Y., Xia, S., Kim, J., and Lattera, J. (2013). In Vivo c-Met Pathway Inhibition Depletes Human Glioma Xenografts of Tumor-Propagating Stem-Like Cells. *Transl Oncol* 6, 104-111.
105. Kim, H.J., and Magrané, J. (2011). Isolation and culture of neurons and astrocytes from the mouse brain cortex. *Methods Mol Biol* 793, 63-75.
106. Guizzetti, M., Kavanagh, T.J., and Costa, L.G. (2011). Measurements of astrocyte proliferation. *Methods Mol Biol* 758, 349-359.
107. Chakradeo, S., Elmore, L.W., and Gewirtz, D.A. (2016). Is Senescence Reversible? *Curr Drug Targets* 17, 460-466.
108. Quick, Q.A., and Gewirtz, D.A. (2006). An accelerated senescence response to radiation in wild-type p53 glioblastoma multiforme cells. *J Neurosurg* 105, 111-118.
109. Yu, V.Y., Nguyen, D., Pajonk, F., Kupelian, P., Kaprealian, T., Selch, M., Low, D.A., and Sheng, K. (2015). Incorporating cancer stem cells in radiation therapy treatment response modeling and the implication in glioblastoma multiforme treatment resistance. *Int J Radiat Oncol Biol Phys* 91, 866-875.
110. Lathia, J.D., Mack, S.C., Mulkearns-Hubert, E.E., Valentim, C.L., and Rich, J.N. (2015). Cancer stem cells in glioblastoma. *Genes Dev* 29, 1203-1217.
111. Bao, S., Wu, Q., McLendon, R.E., Hao, Y., Shi, Q., Hjelmeland, A.B., Dewhirst, M.W., Bigner, D.D., and Rich, J.N. (2006). Glioma stem cells promote radioresistance by preferential activation of the DNA damage response. *Nature* 444, 756-760.
112. Pavon, L.F., Marti, L.C., Sibov, T.T., Malheiros, S.M., Brandt, R.A., Cavalheiro, S., and Gamarra, L.F. (2014). In vitro Analysis of Neurospheres Derived from Glioblastoma Primary Culture: A Novel Methodology Paradigm. *Front Neurol* 4, 214.

113. El Meskini, R., Iacovelli, A.J., Kulaga, A., Gumprecht, M., Martin, P.L., Baran, M., Householder, D.B., Van Dyke, T., and Weaver Ohler, Z. (2015). A preclinical orthotopic model for glioblastoma recapitulates key features of human tumors and demonstrates sensitivity to a combination of MEK and PI3K pathway inhibitors. *Dis Model Mech* 8, 45-56.
114. Oh, T., Fakurnejad, S., Sayegh, E.T., Clark, A.J., Ivan, M.E., Sun, M.Z., Safaee, M., Bloch, O., James, C.D., and Parsa, A.T. (2014). Immunocompetent murine models for the study of glioblastoma immunotherapy. *J Transl Med* 12, 107.
115. Maes, W., and Van Gool, S.W. (2011). Experimental immunotherapy for malignant glioma: lessons from two decades of research in the GL261 model. *Cancer Immunol Immunother* 60, 153-160.
116. Wu, A., Oh, S., Wiesner, S.M., Ericson, K., Chen, L., Hall, W.A., Champoux, P.E., Low, W.C., and Ohlfest, J.R. (2008). Persistence of CD133+ cells in human and mouse glioma cell lines: detailed characterization of GL261 glioma cells with cancer stem cell-like properties. *Stem Cells Dev* 17, 173-184.